DEVELOPMENT OF NEUROTROPHIC FACTOR ELUTING NERVE ALLOGRAFTS FOR PERIPHERAL NERVE REPAIR

By

Richard B. Boyer

Dissertation

Submitted to the Faculty of the

Graduate School of Vanderbilt University

in partial fulfillment of the requirements

for the degree of

DOCTOR OF PHILOSOPHY

in

Biomedical Engineering

May 2015

Nashville, Tennessee

Approved:

Wesley P. Thayer, M.D., Ph.D.
Mark D. Does, Ph.D.
Lillian B. Nanney, Ph.D.
Craig Duvall, Ph.D.
Richard D. Dortch, Ph.D.

To Emily and Mosby

ACKNOWLEDGEMENTS

This dissertation was only made possible through the support and guidance that has been provided to me over the years by several individuals. First, I would like to give special thanks to my mentor Dr. Wesley Thayer for always being supportive of my work and for being a wonderful teacher and friend. In addition to teaching me the surgical and analytical skills necessary to complete this work, Dr. Thayer has allowed me to gain valuable experience as a lead investigator on several projects.

I would also like to thank Dr. Lillian Nanney, who has been a great source of advice and encouragement since entering the lab. Dr. Nanney's commitment to teaching has helped me to be successful in this work and in my medical school coursework. I would also like to thank several individuals without whom I could not have completed this endeavor, including Alonda Pollins, Nancy Cardwell, Dr. Kevin Sexton, Charlie Rodriguez-Feo, Dr. Ratnam Nookala, Colton Riley, Nathaniel Kelm and Janice Williams. Special thanks are also due to Dr. Bruce Shack who has supported and welcomed me as a member of the Department of Plastic Surgery.

I would also like to thank the members of my committee, including Dr. Mark Does, Dr. Richard Dortch, Dr. Craig Duvall, Dr. Lillian Nanney and Dr. Wesley Thayer, who have all assisted me in completing this work, and Dr. Jeanette Norden whose amazing teaching was my inspiration to enter the field of neuroscience research.

I would like to also acknowledge the Vanderbilt University Medical Scientist Training Program and its leadership, Dr. Terry Dermody, Dr. Michelle Grundy, Dr. Danny Winder and Melissa Krasnove, for funding my training as a physician-scientist and for providing endless support.

Lastly, I could not have succeeded in this work without my wonderful wife, Emily, and our furry children, Mosby and Bean.

TABLE OF CONTENTS

LIST OF TABLES

LIST OF FIGURES

CHAPTER I

BACKGROUND AND SIGNIFICANCE

Introduction

The nervous system is composed of the central nervous system and the peripheral nervous system. The central nervous system controls all voluntary and involuntary activity, executive function and higher order cognitive processes. The peripheral nervous system is a vast network of nerves that relay signals to and from the central nervous system, viscera and peripheral targets, such as motor end plates and sensory mechanoreceptors. Somatic peripheral nerves include spinal motor nerves (and their branches), which contain axons of motor neurons with cell bodies located in the ventral horn of the spinal cord, and sensory nerves, which contain axons of pseudounipolar neurons with cell bodies located in dorsal root ganglia. Although the central and peripheral nervous systems are interconnected and composed of similar anatomical units, differences in cell and environment produce a dichotomy following axon injury: peripheral axons can regenerate, central axons cannot. The mechanism behind this difference remains unknown, but significant progress has been made in identifying contributors to axonal regeneration and growth inhibition. In peripheral nerve injury research we investigate methods of enhancing regeneration of motor and sensory neurons for the improvement of traumatic nerve injury outcomes. However, it would be naïve to discount progress in understanding peripheral nerve regeneration as irrelevant to central nervous system injuries. As I will describe, several experimental therapeutics for peripheral nerve regeneration have also shown promise in spinal cord injury and traumatic brain injury.

Techniques for repairing peripheral nerves have evolved significantly over the last decade. The use of high-morbidity nerve autografts has decreased as other options have become available, including

synthetic nerve guidance conduits and scaffolds, and more recently the advent of acellular nerve allografts. Several experimental therapeutics have been shown to enhance nerve regeneration in animal models, including specific growth factor therapies and extracellular matrix-modifying agents. However, important questions remain in regards to: 1) the effects of these agents in combination with state-of-the-art microsurgical repair modalities and 2) the feasibility of their delivery to nerve injuries following repair. I will address both of these fundamental questions in this dissertation.

Peripheral Nerve Anatomy

The peripheral nerve is composed of several connective tissue layers and supportive glia, or Schwann cells, which form myelin sheaths over individual axons (Figure 1). Each myelinated axon is encapsulated by several Schwann cells that bind to a single axon at their adaxonal membrane and bind to the basal lamina at the their abaxonal membrane. In contrast, multiple unmyelinated axons can be ensheathed by a single Schwann cell, forming a Remak bundle. In myelinated axons, nodes of Ranvier are present between each Schwann cell, which allow for saltatory conduction of nerve action potentials and increased conduction velocity. The basal lamina of neighboring Schwann cells and Type IV collagen fibrils form the endoneurium, or the innermost connective tissue layer of the peripheral nerve that envelops a single axon. The perineurium is the intermediate layer of connective tissue that ensheaths fascicles, or bundles of axons, and consists of lamellae of squamous cells and fibrous collagen. The outermost layer of areolar connective tissue, or epineurium, consists of collagenous fibers that surround nerve fascicles and intraneural blood vessels.

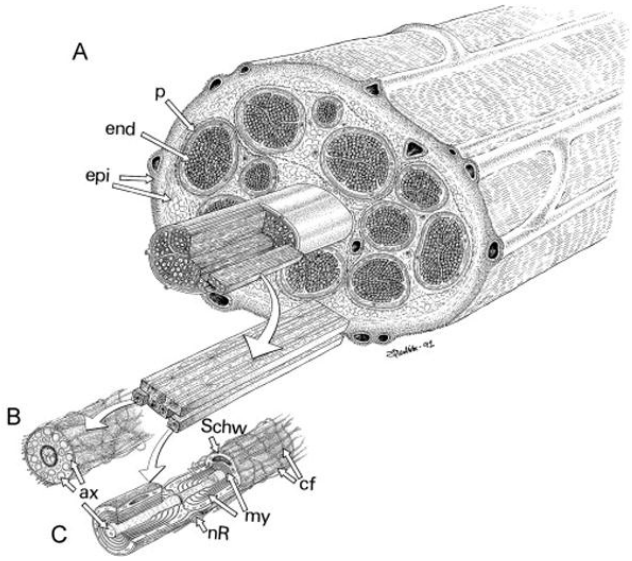

Fig 1. Anatomical diagram of a multi-fascicular peripheral nerve (A) with unmyelinated axons in Remak bundles (B) and myelinated axons with Schwann cells. Epi – epineurium, p – perineurium, end – endoneurium, ax – axon, Schw – Schwann cell, nR – node of Ranvier, my – myelin, cf – collagen fibrils. (Bove 2008 [1], with permission)

The axon is a long process of a neuron that contains axoplasm in continuity with the cytoplasm of the cell body and a variety of organelles that are surrounded by the axolemma, a lipid bilayer membrane specialized for action potential propagation. Axonal structure is supported by a dense cytoskeletal network of neurofilaments and microtubules that are important for anterograde and retrograde transport of molecules between the periphery and the cell body. Depending on the specific nerve and location, the axons contained in a peripheral nerve include those from afferent and efferent neurons from both the somatic and autonomic nervous systems. Although some nerves will have no cutaneous innervation, there are no pure sensory or pure motor nerves. The different types of nerve fibers are described in Table 1.

Table 1. Types of nerve fibers and their anatomical and functional properties.

Fiber Type	Function	Diameter (um)	Conduction Velocity (m/s)	Myelination
Alpha	Motor, Proprioception	12-20	70-120	myelinated
Beta	Fine touch, pressure	5-12	30-70	myelinated
Gamma	Muscle spindles	3-6	15-30	myelinated
Delta	Pain, temperature	2-5	12-30	light myelination
Type B	Autonomic preganglionic	<3	3-15	myelinated
Type C	Pain	0.4-12	0.5-2.3	unmyelinated
Sympathetic	Sympathetic postganglionic	0.3-1.3	0.7-2.3	myelinated

Overview Of Peripheral Nerve Injury

Over 350,000 people are estimated to suffer from peripheral nerve injuries each year in the United States.[2] Although not associated with mortality, many patients experience life-long disability after a peripheral nerve injury.[3] Paralysis, muscle weakness and chronic pain are not uncommon in these patients, often necessitating activity and work restrictions.

The economic burden of peripheral nerve injury in the United States is enormous. Acute upper extremity injuries are responsible for over 32 million days of restricted activity and 10 million days of work absence reported in a single year.[4] Peripheral nerve injuries, which are present in approximately one third of all upper extremity injuries, contribute to lost productivity due to long recovery periods and poor functional prognosis.[4] Particularly high rates of peripheral nerve injuries are found in military personnel. Acute extremity injuries accounted for 54% of combat wounds sustained in Operation Iraqi Freedom and Operation Enduring Freedom.[5], [6] One of the key determinants for lower extremity amputation is concomitant nerve injury, while for upper extremity injuries segmental nerve loss with bone and vascular injury is often an indication for amputation. [7]

Severity of nerve injury is assessed with a grading system, known as the Sunderland scale (Table 2). In Sunderland first-degree nerve injury or neurapraxia, there is local loss of nerve conduction without

physical damage to the axon or connective tissue layers. Since neurapraxic injury has intact neuronal fibers it has excellent prognosis and typically results in complete return of function. However, in higher grades of nerve injury that involve transection of axonal fibers, recovery is dependent on the regenerative capacity of the neuron, intactness of the neural tube and the proximo-distal site of the lesion. Intuitively, the further the lesion is distally, the greater the chance for recovery because of proximity to the innervation target. In severe proximal lesions, such as brachial plexus trauma, target muscles can undergo denervation atrophy prior to reinnervation leading to permanent muscle weakness or paralysis. According to Brushart, ideal reinnervation of target muscles could be expected before 3 months of denervation and functional reinnervation could be expected within 1 year. [7]

Table 2. Clinical grading of peripheral nerve injury.

Seddon	**Sunderland (Degree)**	**Characteristics of Injury**	**Potential for Recovery**
Neurapraxia	I	Local conduction block with no Wallerian degeneration.	Recovery is complete.
Axonotmesis	II	Axonal damage. The endoneurium and perineurium are intact.	Regeneration restores full function.
	III	Damage to the endoneurium.	Recovery is dependent on the degree of endoneurial scarring.
	IV	Damage to axons, endoneurium, and perineurium. The epineurium remains intact; hence, the nerve is in continuity.	Recovery will not occur without surgical intervention.
Neurotmesis	V	The nerve is completely transected.	Recovery will not occur without surgical intervention.
	Mackinnon VI	Mixed pattern injury, combining any of the Sunderland's classification above	Patterns of recovery are mixed.

(Pabari 2010 [8], with permission)

Nerve injury is a time-sensitive medical condition that should be urgently evaluated. Delay in repairing a transected nerve is estimated to induce a loss of achievable function of 1% for every 6 days of delay.[9] This urgency is complicated by our inability to assess injury severity in the early stage of acute nerve injury. Even with electrodiagnostics, such as nerve conduction and electromyographic studies, it can take up to 16 weeks for the injury to be fully characterized.[10]

In the case of a transected nerve, surgical repair is required for any recovery to be possible. In the United States, approximately 56% of nerve injuries can be directly repaired with suture. However, the remaining 44% of nerve injuries cannot be repaired with tension free suture and require nerve gap bridging using a graft, conduit or nerve transfer. The gold standard in these cases is to use autologous nerve graft, but other options have become available and will be discussed later in this chapter.

Pathology Of Peripheral Nerve Injury

Peripheral nervous system neurons undergo a series of events following axon transection that set the stage for regeneration in a process known as Wallerian degeneration. Following injury, cell bodies show characteristic changes of chromatolysis and increased protein synthesis. Chromatolysis, or dissolution of Nissl bodies, occurs during the first 24 hours following injury in conjunction displacement of the nucleus to the periphery of the perikaryon. The proximal segment of the injured axon initially dies back from the zone of injury a short distance (approximately 1-2 millimeters) prior to formation of the growth cone. If the neuron survives, the growth cone directs elongation of the axon by responding to neurotrophic gradients and substrates. Axon elongation is then supported by proliferating Schwann cells that release growth factors and extracellular matrix proteins, but regeneration proceeds slowly at a rate of 2 to 3 mm per day.

In the distal segment of injured axons, myelin and axonal organelles degenerate and are phagocytosed by infiltrating monocytes and macrophages. As cellular debris is cleared, Schwann cells in

the distal nerve segment rapidly proliferate within the endoneurial sheath and form elongated tubes, or Bands of Bungner, that guide nascent neurites to target structures. Nonneuronal cells of the distal nerve stump also increase production of specific growth factors such as Nerve Growth Factor, cytokines, and extracellular matrix proteins. Chondroitin sulfate proteoglycans (CSPGs) are a family of extracellular matrix proteins that have been well characterized as inhibitors of axon elongation in the CNS and PNS. Chondroitin sulfate proteoglycans, such as aggrecan and versican, are upregulated following axon injury and accumulate in both the glial scar in CNS injury and the distal nerve segment in PNS injury. In vivo animal studies have shown improvement in neurite regeneration following enzymatic removal of CSPGs in peripheral nerves, and minor improvement in CNS lesions.

Neurotrophic Factors

Three distinct families of neurotrophic factors have been investigated in peripheral nerve injury and regeneration – neurotrophins, GDNF family of ligands and neuropoeitic cytokynes (Table 3).

Neurotrophins are noncovalent homodimers that mediate effects by binding two classes of receptors, high-affinity tyrosine receptor kinases (TrkA, TrkB, TrkC) and low-affinity TNF-α (p75) receptors. The neurotrophin family has 4 members in mammals, Nerve Growth Factor (NGF), Brain-Derived Neurotrophic Factor (BDNF), Neurotrophin-3 (NT-3) and Neurotrophin-4/5 (NT-4/5). All neurotrophins bind to the p75 receptor with similar affinity, but Trk receptors exhibit more selective binding. NGF binds with high affinity to TrkA, BDNF and NT-4/5 to Trk B and NT-3 to TrkC. The p75 receptor also increases the total amount of Trk binding by serving as a fast-dissociating sink for neurotrophins. The p75 receptor mediates apoptosis and cell survival in all neurons and is upregulated after injury. In contrast, TrkA mediates cell survival in sensory neurons and glial cells, but is not present in motoneurons. Following axonal injury, NGF and BDNF are upregulated in the distal nerve stump to support neurite outgrowth and survival.

The GDNF family of ligands include glial cell line derived neurotrophic factor (GDNF), neurturin, artemin and persephin. These ligands signal through a multicomponent receptor system composed of a receptor tyrosine kinase molecule (RET) and glycosylphosphatidylinositol (GPI)-anchored coreceptor (GFRα1-4). GDNF has been shown to be a potent factor for survival and regeneration of motor neurons *in vitro* and *in vivo*.[11]–[14] Following sciatic nerve transection, GDNF and its receptors are upregulated in the distal nerve stump as well as in the target muscle.[15]

The neuropoeitic cytokines are a family of small proteins that signal through the gp130 receptor complex, including interleukins IL-6, IL-11 and IL-27, leukaemia inhibitory factor (LIF), ciliary neurotrophic factor (CNTF), cardiotrophin 1 (CT-1), neuropoietin and cardiotrophin-like cytokine (CLC).[16] These cytokines are involved in neural development and regulation, and many are upregulated in the peripheral nervous system following nerve injury, including IL-6, IL-11 and LIF, mainly by Schwann cells.[17]

Table 3. Changes in PNS expression of neurotrophic factors after nerve injury. (Boyd and Gordon 2003 [18], with permission)

Location	Peptide phenotype	Neurotrophins	GDNF family	Neuropoetic cytokines
Motoneurons	ChAT ↓ AChE ↓ VANP-1 ↓ neurofilament ↓	BDNF ↑ trkB ↑ p75 ↑	ret ↑ GFR-α1 ↑	IL-6 ↑ LIFR ↑
	CGRP ↑ VAMP-2 ↑ GAP-43 ↑ tubulin ↑ actin ↑	NT-3 ↓ NT-4/5 ↓ trkC ↓		CNTFR ↓ gp130 ↓
Distal nerve stump		NGF ↑ BDNF ↑ p75 ↑ NT-3 ↓ NT-4/5 ↓ trunc. trkB ↓ trunc. trkC ↓	GDNF ↑ GFR-α1 ↑	IL-6 ↑ LIF ↑ gp 130 ↑ CNTFR ↑ IL-6R ↑ CNTF ↓

Peripheral Nerve Repair

The main goal of nerve repair is reestablishing apposition of the proximal and distal nerve stumps without tension and removing barriers to neurite outgrowth. The proximal and distal nerve stumps are trimmed back to identify healthy, well-organized fascicles, because the zone of injury is known to obstruct regenerating neurites. Additionally, the distal nerve stump is dissected to identify correct fascicular alignment prior to coaptation. Incorrect fascicular alignment, particularly with sensory and motor fascicle coaptation can result in poor functional outcomes and synkinesis.

The violence of injury is the key determinant of a primary or secondary nerve repair. In a sharp injury, such as a nerve laceration with a knife or a surgeon's scalpel, immediate primary direct suture is the preferred nerve repair. However, in a blunt injury, such as a penetrating missile injury or closed traction injury, secondary nerve repair should be performed after the soft tissue bed has settled and the zone of injury is apparent.

Anesthesia and/or weakness develop immediately following transection of a nerve due to loss of impulse conduction across the injured segment. While these patient symptoms are obvious, the specific diagnosis of the type of nerve injury can be equivocal. Neurapraxia is characterized by conduction block in the absence of physical nerve injury, but it can present with symptoms similar to the more severe axonotmesis or neurotmesis. The patient history and clinical exam are essential to diagnosing nerve injury. Although not always accurate, dermatomal sensory loss and weakness or paralysis after physical trauma should be diagnosed as nerve transection until proven otherwise. Tinel's sign, or pain when percussing over the nerve, is also used to assess the level and severity of nerve injury. Additional neurodiagnostics, such as nerve conduction studies and electromyography, are helpful in diagnosing mixed nerve injuries, but they have difficulty discriminating partial and complete nerve injuries in the acute setting and are most useful 6-12 weeks after injury.

Neurorrhaphy

Direct suturing of proximal and distal nerve endings is preferred in cases where tensionless repair is possible. Epineurium is the primary surgical plane of interest and confers tensile strength and a protective sleeve to the repaired nerve. In immediate nerve repair, fascicular repair should also be performed, as torsion of individual nerve bundles is possible in the fresh wound.

Nerve grafting

Autologous nerve grafts from cutaneous nerves of the injured limb are the preferred graft for bridging small (<3 cm) and large (>3 cm) nerve gaps when enough viable tissue is available for tension-free repair. If ipsilateral nerves are not available for grafting, then specific non-critical nerves of the contralateral limb and trunk can be harvested, such as the medial cutaneous nerve or the sural nerve. Autologous nerve grafts have the advantage of preserved extracellular matrix, Schwann cells and neurotrophic factors. Although several attempts have been made at pedicle grafting of vascularized nerve grafts, there are only a few cases of successful return of function using this technique.

Antigenicity of fresh cadaveric nerve prevents use of allografts in clinical practice and led to the development of acellular nerve allografts. Acellular nerve allografts are detergent processed cadaveric nerves that are non-antigenic and therefore do not require recipient immunosuppression. Detergents used in nerve processing are effective in removing all cellular components of the graft, while preserving extracellular matrix proteins and endoneurial structure.

Nerve transfer

Although the concept of nerve transfers dates back to the 1980's, the use of this technique for repairing proximal nerve injuries has recently become a popular alternative to long nerve grafts. The goal of nerve transfer is to redirect a healthy non-critical nerve to the target of a critical injured nerve that has low

chance for recovery. Although sensory nerves will show collateral sprouting into an end-to-side epineurial window, motor neurons require neurectomy for any growth to occur.

Research Models

The standard *in vivo* model of peripheral nerve injury is the rat sciatic nerve transection model. In this model, the sciatic nerve is dissected and mobilized below the biceps femoris muscle in the lateral thigh. The nerve is ligated with a sharp instrument to produce minimal zone of injury and then microsurgically repaired using epineurial and/or fascicular sutures. For studies of nerve gap injuries, conduits or biologic grafts are sutured tension-free to the proximal and distal nerve stumps.

Outcomes for in-vivo nerve regeneration studies include functional measurements, post-mortem histology and recently, in-vivo neurite imaging, such as two-photon fluorescence imaging of *Thy1*-GFP transgenic rats.[19] Functional measurements of nerve regeneration include sciatic function index, foot fault, tapered beam and nerve and muscle electrophysiology. Sciatic function index (SFI) measures the ability of the rat to perform toe spread, plantar flexion and leg extension – all functions of the sciatic nerve and involved in rat gait. An equation developed by Bain et al [20] quantifies SFI performance of the ipsilateral injured hind leg to the contralateral healthy leg.

Post-mortem histology of the rat sciatic nerve is well described at both the light microscopy and electron microscopy levels. Light microscopy is useful for identifying the overall nerve architecture and axon counts. Toluidine blue is the typical stain used for axon counts due to the robust staining of myelin sheath. However, for early neurite regeneration and neuronal subtyping, immunohistochemistry can be particularly useful. Transmission electron microscopy is useful for identifying neuronal and myelin pathology.

Large nerve gap injuries are particularly problematic to study in the rat sciatic nerve injury model due to the limited accessible length of the sciatic nerve (typically < 2 cm from sciatic notch to bifurcation)

and retraction of nerve stumps after injury. However, nerve conduits and biologic grafts have mainly been investigated with this model due to its wide availability and acceptance.

Experimental Treatments

Neurotrophic factors have been the primary candidates for regenerative nerve therapeutics, because of their prominent roles in neural development and nerve injury. Through binding their cognate cell surface receptors on axonal membranes, they are known to regulate neurite growth and branching as well as protect injured neurons from apoptosis.[18], [21] Two general methods of experimental neurotrophic factor therapy have been explored: 1) delivery of recombinant or purified peptide and 2) seeding the nerve injury or scaffold with cells capable of producing neurotrophic factors, i.e. Schwann cells.

Neurotrophic Factor Delivery

Initial studies of neurotrophic factor therapy involved local injection or continuous subcutaneous delivery of peptide by osmotic pumps.[22] However, rapid degradation and elimination of injected peptide and infection risk with implantable pumps limit the success of these strategies. Instead, several techniques have been investigated for sustained delivery of neurotrophic factors in peripheral nerve injuries. The majority of prior studies have involved diffusion-based methods of peptide delivery. In diffusion-based neurotrophic factor delivery, the specific biomaterial properties (e.g. porosity) of the delivery scaffold are tuned to modulate the diffusion coefficient of the peptide within the matrix.[23] Affinity-based delivery systems are another method of sustained delivery in which the peptide is bound noncovalently to proteins

within the scaffold and its release is controlled by its binding affinity and kinetics. NGF and GDNF have both been investigated with affinity-based delivery using heparin-containing fibrin matrices, and these studies have shown promising results in an *in vivo* rat sciatic nerve model.[14], [24]

Schwann Cell Seeding

Schwann cells, the supportive glial cells of the PNS, produce many of the neurotrophic factors critical for nerve regeneration and are known to upregulate these factors after nerve injury.[18] Several investigators have leveraged this function of Schwann cells in nerve and spinal cord repair by seeding autologous, transgenic or stem cell-derived Schwann cells within implanted conduits and nerve allografts.[25]–[27] These studies have shown that allografts seeded with autologous Schwann cells from degenerated sensory or motor nerves can perform similar to autologous nerve grafts in short (<2 mm) nerve gaps.[28], [29] This strategy still requires donor nerve harvesting and several weeks for autologous cell growth and it has not yet been shown in large nerve defects.

Affinity Based Delivery of Growth Factors

In order to discuss the use of exogenous growth factors for treatment, we must first identify a method for controlled peptide release. Controlled local peptide delivery has been widely investigated as a tool for wound healing and organ regeneration due to the lack of systemic effects, prolonged local effects and protection of peptide-based drugs from degradation over long periods. Several reservoir-based methods of controlled peptide delivery have been investigated for neurotrophic factor delivery within nerve conduits,

including crosslinked hydrogel entrapment, polymeric microsphere encapsulation, electrospun nanofibers and combined systems.[30] In reservoir-based delivery systems, the material properties of the system are chosen to modulate the release of the embedded peptide. However, the material properties required in these systems may not provide the optimal substrate for neurite outgrowth. In affinity-based delivery systems, the release of peptide is determined by non-covalent interactions of the peptide and the material, which is meant to mimic the natural interactions in the extracellular matrix. Two types of affinity-based delivery systems relevant to neurotrophic factor delivery, heparin-based delivery systems and extracellular matrix-based delivery systems, are discussed below.

Heparin-Based Delivery Systems

Edelman and coworkers first introduced heparin-based delivery systems for controlled release of fibroblast growth factor (bFGF) in wounds.[31] This system used the native affinity of bFGF and heparin to release the growth factor from heparin-coated Sepharose beads and prevented its normally rapid degradation. Sakiyama-Elbert and Hubbell evaluated a similar technology in which fibrin matrices containing cross-linked heparin-binding proteins and heparin were used for affinity-based delivery of neurotrophins.[32] Although neurotrophins (β-NGF, NT-3 and BNDF) have only low affinity to heparin, this study showed that heparin-containing fibrin matrices were able to slow their diffusion-based release when a large molar excess of heparin was immobilized relative to growth factor. In the presence of this heparin-based delivery system, there was an initial release of up to 50% of loaded neurotrophin in the first day, but up to 30% of the initial total neurotrophin remained after 15 days.[32] Other studies have used bidomain peptides for modulation of heparin binding and controlled release of NGF and GDNF from fibrin matrices.[14], [24]

Extracellular Matrix-Based Delivery Systems

Affinity-based delivery scaffolds have the additional advantage of extracellular matrix-mimicking properties. Recently, Martino and coworkers investigated whether native extracellular matrix could also be used for sustained growth factor release.[33] By fusing a domain of placenta growth factor-2 (PlGF-2) that was found to bind strongly with several extracellular matrix proteins to other growth factors, the engineered growth factors were strongly retained by native extracellular matrix *in vivo*. Other growth factors that showed strong binding to extracellular matrix proteins included platelet-derived growth factor (PDGF), bone morphogenetic protein-2 (BMP-2) and the neurotrophins. It is well known that extracellular matrix acts as a reservoir for growth factors and cytokines involved in tissue regeneration. However, elimination of exogenous growth factors is rapid in vascular and cellular tissue after local injection. Recently, our group has shown conserved effect of exogenous β-NGF loaded in acellular nerve allografts that contain native nerve extracellular matrix but lack all cells, blood and lymphatic vessels.[34] This finding indicates that acellular nerve allografts may be able to serve as biological affinity based delivery systems for exogenous neurotrophic factors in addition to providing a native nerve extracellular matrix scaffold.

Dissertation Overview

This dissertation is a critical analysis of 1) the effects of Nerve Growth Factor and Glial-Derived Neurotrophic Factor as adjuvant therapies with state-of-the-art acellular nerve allografts for peripheral nerve repair, 2) the feasibility of sustained neurotrophic factor delivery using acellular nerve allografts as affinity-based delivery scaffolds, and 3) the characterization of peripheral nerve transection and repair using high-resolution diffusion tensor imaging.

In the first two chapters, I investigate the effects of Nerve Growth Factor and Glial Derived Neurotrophic Factor as adjuvant treatments in acellular nerve allografts (Chapter II) and I present a method for extracellular matrix-affinity based delivery of Nerve Growth Factor using acellular nerve allografts as a tool for nerve guidance and protein delivery (Chapter III). In the following chapters, high-resolution diffusion tensor imaging is first validated for characterization of peripheral nerve transection (Chapter IV) and then used to perform serial evaluations of neurite outgrowth in Nerve Growth Factor-eluting acellular nerve allografts (Chapter V). Chapter VI concludes the dissertation and discusses future directions. A supplemental chapter is provided on the topic of polyethylene glycol fusion of peripheral nerve axons (Chapter VII).

References

[1] G. M. Bove, "Epi-perineurial anatomy, innervation, and axonal nociceptive mechanisms.," *J. Bodyw. Mov. Ther.*, vol. 12, no. 3, pp. 185–90, Jul. 2008.

[2] J. S. Belkas, M. S. Shoichet, and R. Midha, "Axonal guidance channels in peripheral nerve regeneration," *Oper. Tech. Orthop.*, vol. 14, no. 3, pp. 190–198, Jul. 2004.

[3] J. Noble, C. A. Munro, V. S. Prasad, and R. Midha, "Analysis of upper and lower extremity peripheral nerve injuries in a population of patients with multiple injuries.," *J. Trauma*, vol. 45, no. 1, pp. 116–22, Jul. 1998.

[4] J. B. Jaquet, A. J. Luijsterburg, S. Kalmijn, P. D. Kuypers, A. Hofman, and S. E. Hovius, "Median, ulnar, and combined median-ulnar nerve injuries: functional outcome and return to productivity.," *J. Trauma*, vol. 51, no. 4, pp. 687–92, Oct. 2001.

[5] J. D. Cross, J. R. Ficke, J. R. Hsu, B. D. Masini, and J. C. Wenke, "Battlefield orthopaedic injuries cause the majority of long-term disabilities.," *J. Am. Acad. Orthop. Surg.*, vol. 19 Suppl 1, pp. S1–7, Jan. 2011.

[6] L. G. Stansbury, J. G. Branstetter, and S. J. Lalliss, "Amputation in military trauma surgery.," *J. Trauma*, vol. 63, no. 4, pp. 940–4, Oct. 2007.

[7] S. W. Wolfe, R. N. Hotchkiss, W. C. Pederson, and S. H. Kozin, *Green's Operative Hand Surgery E-Book: Expert Consult: Online and Print, Volume 2*. Elsevier Health Sciences, 2010.

[8] A. Pabari, S. Y. Yang, A. M. Seifalian, and A. Mosahebi, "Modern surgical management of peripheral nerve gap," *J Plast Reconstr Aesthet Surg*, vol. 63, no. 12, pp. 1941–1948, 2010.

[9] G. E. Omer, "Injuries to nerves of the upper extremity.," *J. Bone Joint Surg. Am.*, vol. 56, no. 8, pp. 1615–24, Dec. 1974.

[10] W. Z. Ray and S. E. Mackinnon, "Management of nerve gaps: autografts, allografts, nerve transfers, and end-to-side neurorrhaphy.," *Exp. Neurol.*, vol. 223, no. 1, pp. 77–85, May 2010.

[11] C. E. Henderson, H. S. Phillips, R. A. Pollock, A. M. Davies, C. Lemeulle, M. Armanini, L. Simmons, B. Moffet, R. A. Vandlen, and L. Simpson LC [corrected to Simmons, "GDNF: a potent survival factor for motoneurons present in peripheral nerve and muscle," *Science (80-.).*, vol. 266, no. 5187, pp. 1062–1064, 1994.

[12] E. G. Fine, I. Decosterd, M. Papaloïzos, A. D. Zurn, and P. Aebischer, "GDNF and NGF released by synthetic guidance channels support sciatic nerve regeneration across a long gap," *Eur J Neurosci*, vol. 15, no. 4, pp. 589–601, 2002.

[13] M. D. Wood, M. R. MacEwan, A. R. French, A. M. Moore, D. A. Hunter, S. E. Mackinnon, D. W. Moran, G. H. Borschel, and S. E. Sakiyama-Elbert, "Fibrin matrices with affinity-based delivery systems and neurotrophic factors promote functional nerve regeneration," *Biotechnol Bioeng*, vol. 106, no. 6, pp. 970–979, 2010.

[14] M. D. Wood, A. M. Moore, D. A. Hunter, S. Tuffaha, G. H. Borschel, S. E. Mackinnon, and S. E. Sakiyama-Elbert, "Affinity-based release of glial-derived neurotrophic factor from fibrin matrices enhances sciatic nerve regeneration," *Acta Biomater*, vol. 5, no. 4, pp. 959–968, 2009.

[15] P. Naveilhan, W. M. ElShamy, and P. Ernfors, "Differential regulation of mRNAs for GDNF and its receptors Ret and GDNFR alpha after sciatic nerve lesion in the mouse.," *Eur. J. Neurosci.*, vol. 9, no. 7, pp. 1450–60, Jul. 1997.

[16] S. Bauer, B. J. Kerr, and P. H. Patterson, "The neuropoietic cytokine family in development, plasticity, disease and injury.," *Nat. Rev. Neurosci.*, vol. 8, no. 3, pp. 221–32, Mar. 2007.

[17] Y. Ito, M. Yamamoto, M. Li, N. Mitsuma, F. Tanaka, M. Doyu, A. Suzumura, T. Mitsuma, and G. Sobue, "Temporal Expression of mRNAs for Neuropoietic Cytokines, Interleukin-11 (IL-11), Oncostatin M (OSM), Cardiotrophin-1 (CT-1) and Their Receptors (IL-11Rα and OSMRβ) in Peripheral Nerve Injury," *Neurochem. Res.*, vol. 25, no. 8, pp. 1113–1118.

[18] J. G. Boyd and T. Gordon, "Neurotrophic factors and their receptors in axonal regeneration and functional recovery after peripheral nerve injury," *Mol Neurobiol*, vol. 27, no. 3, pp. 277–324, 2003.

[19] S. W. P. Kemp, P. D. Phua, K. N. Stanoulis, M. D. Wood, E. H. Liu, T. Gordon, and G. H. Borschel, "Functional recovery following peripheral nerve injury in the transgenic Thy1-GFP rat.," *J. Peripher. Nerv. Syst.*, vol. 18, no. 3, pp. 220–31, Sep. 2013.

[20] J. R. Bain, S. E. Mackinnon, and D. A. Hunter, "Functional evaluation of complete sciatic, peroneal, and posterior tibial nerve lesions in the rat," *Plast Reconstr Surg*, vol. 83, no. 1, pp. 129–138, 1989.

[21] M. E. Sebert and E. M. Shooter, "Expression of mRNA for neurotrophic factors and their receptors in the rat dorsal root ganglion and sciatic nerve following nerve injury," *J Neurosci Res*, vol. 36, no. 4, pp. 357–367, 1993.

[22] M. A. Tria, M. Fusco, G. Vantini, and R. Mariot, "Pharmacokinetics of nerve growth factor (NGF) following different routes of administration to adult rats.," *Exp. Neurol.*, vol. 127, no. 2, pp. 178–83, Jun. 1994.

[23] R. LANGER and J. FOLKMAN, "Polymers for the sustained release of proteins and other macromolecules," *Nature*, vol. 263, no. 5580, pp. 797–800, Oct. 1976.

[24] M. D. Wood, D. Hunter, S. E. Mackinnon, and S. E. Sakiyama-Elbert, "Heparin-binding-affinity-based delivery systems releasing nerve growth factor enhance sciatic nerve regeneration," *J Biomater Sci Polym Ed*, vol. 21, no. 6, pp. 771–787, 2010.

[25] F. J. Rodríguez, E. Verdú, D. Ceballos, and X. Navarro, "Nerve guides seeded with autologous schwann cells improve nerve regeneration.," *Exp. Neurol.*, vol. 161, no. 2, pp. 571–84, Feb. 2000.

[26] T. Hadlock, C. Sundback, D. Hunter, M. Cheney, and J. P. Vacanti, "A polymer foam conduit seeded with Schwann cells promotes guided peripheral nerve regeneration," *Tissue Eng*, vol. 6, no. 2, pp. 119–127, 2000.

[27] T. Hadlock, C. Sundback, D. Hunter, M. Cheney, and J. P. Vacanti, "A Polymer Foam Conduit Seeded with Schwann Cells Promotes Guided Peripheral Nerve Regeneration," Jul. 2004.

[28] X.-H. Sun, Y.-Q. Che, X.-J. Tong, L.-X. Zhang, Y. Feng, A.-H. Xu, L. Tong, H. Jia, and X. Zhang, "Improving nerve regeneration of acellular nerve allografts seeded with SCs bridging the sciatic nerve defects of rat.," *Cell. Mol. Neurobiol.*, vol. 29, no. 3, pp. 347–53, May 2009.

[29] N. J. Jesuraj, K. B. Santosa, M. R. Macewan, A. M. Moore, R. Kasukurthi, W. Z. Ray, E. R. Flagg, D. A. Hunter, G. H. Borschel, P. J. Johnson, S. E. Mackinnon, and S. E. Sakiyama-Elbert, "Schwann cells seeded in acellular nerve grafts improve functional recovery.," *Muscle Nerve*, vol. 49, no. 2, pp. 267–76, Feb. 2014.

[30] N. K. Mohtaram, A. Montgomery, and S. M. Willerth, "Biomaterial-based drug delivery systems for the controlled release of neurotrophic factors.," *Biomed. Mater.*, vol. 8, no. 2, p. 022001, Apr. 2013.

[31] E. R. Edelman, E. Mathiowitz, R. Langer, and M. Klagsbrun, "Controlled and modulated release of basic fibroblast growth factor," *Biomaterials*, vol. 12, no. 7, pp. 619–626, Sep. 1991.

[32] S. E. Sakiyama-Elbert and J. A. Hubbell, “Controlled release of nerve growth factor from a heparin-containing fibrin-based cell ingrowth matrix,” *J. Control. Release*, vol. 69, no. 1, pp. 149–158, Oct. 2000.

[33] M. M. Martino, P. S. Briquez, E. Guc, F. Tortelli, W. W. Kilarski, S. Metzger, J. J. Rice, G. A. Kuhn, R. Muller, M. A. Swartz, and J. A. Hubbell, “Growth factors engineered for super-affinity to the extracellular matrix enhance tissue healing,” *Science (80-.).*, vol. 343, no. 6173, pp. 885–888, 2014.

[34] R. B. Boyer, K. W. Sexton, C. L. Rodriguez-Feo, R. Nookala, A. C. Pollins, N. L. Cardwell, K. Y. Tisdale, L. B. Nanney, R. B. Shack, and W. P. Thayer, “Adjuvant neurotrophic factors in peripheral nerve repair with chondroitin sulfate proteoglycan-reduced acellular nerve allografts.,” *J. Surg. Res.*, vol. 193, no. 2, pp. 969–77, Mar. 2015.

CHAPTER II

ADJUVANT EFFECTS OF NEUROTROPHIC FACTORS IN NERVE ALLOGRAFTS

This chapter is adapted from the following publication: R. B. Boyer, K. W. Sexton, C. L. Rodriguez-Feo, R. Nookala, A. C. Pollins, N. L. Cardwell, K. Y. Tisdale, L. B. Nanney, R. B. Shack, and W. P. Thayer, "Adjuvant neurotrophic factors in peripheral nerve repair with chondroitin sulfate proteoglycan-reduced acellular nerve allografts," *J. Surg. Res.*, vol. 193, no. 2, pp. 969–77, Mar. 2015.

Introduction

The peripheral nervous system has an impressive resilience to injury, in part, due to the ability of peripheral neurons to regenerate axons following injury. After transection, proximal segments of injured axons form growth cones that respond to neurotrophic and chemotropic extracellular signals to direct neurite outgrowth. Supportive endoneurial cells, such as Schwann cells and fibroblasts, secrete growth factors that participate in complex signaling pathways with regenerating nerve fibers, and ultimately promote either neuron survival or cell death. Extracellular matrix components also provide growth cues, either stimulatory or inhibitory, in addition to serving as a guiding substrate for nerve regeneration. For example, chondroitin sulfate proteoglycans (CSPGs) are well known inhibitors of neurite elongation and their degradation by the bacterial enzyme chondroitinase ABC has been studied extensively as a potential treatment for spinal cord injury.(1)

Theoretically, all peripheral nerve injuries with intact spinal roots and ganglia have the potential for near-complete functional recovery. However, in high-grade nerve injuries this is rarely the case due to several impeding conditions – aberrant neurite growth and neuroma formation, physical barriers to innervation, anterograde degeneration and insufficient rates of neurite outgrowth. The rate of neurite outgrowth at only 1-2 mm/d is an important determinant of functional outcomes, because proximal injuries have an extended period of target muscle denervation and increased muscle atrophy.(2)

There are numerous reports on the topic of enhanced peripheral nerve regeneration using various experimental therapeutics, nerve grafts and nerve conduits. Experimental pharmacotherapeutics have mainly targeted the neurotrophic signaling pathways, using recombinant human neurotrophic factors, such as NGF, BDNF and GDNF.(3, 4) Additionally, significant progress has been made toward the development of biomimetic nerve scaffolds, using materials such as poly-L-lactic acid, electrospun nanofibers and Schwann cell seeded poly-ε-caprolactone.(5-7) Total regenerating axon counts has been the primary outcome for most of these studies, reflecting changes in the regenerative potential of all neurons in the injured nerve. Less effort has been made to understand the specific characteristics of the nerve fibers that are targeted by these regenerative therapeutics, or the molecular events involved in promoting axon elongation and survival *in vivo*.

Neurotrophic factors, such as nerve growth factor (NGF) and glial cell line-derived neurotrophic factor (GDNF), have well characterized individual signaling pathways *in vitro*. NGF has two primary receptors – the p75 low affinity neurotrophic factor receptor and TrkA high affinity tyrosine kinase receptor. $P75^{NTR}$ binds a wide range of neurotrophins and is known to play a major role in apoptotic signaling through activation of JNK and caspase pathways.(8) While TrkA is the primary NGF pro-survival receptor, $p75^{NTR}$ has also been found to activate the MAPK pathway and the NF-κB transcription factor, resulting in anti-apoptotic effects.(9, 10) In addition to promoting survival of sensory neurons *in vitro*, NGF has been shown to protect injured neurons from apoptosis *in vivo* in transected rat sciatic nerves.(11, 12) In contrast, GDNF binds to GFRα1 and GFRα2, which both interact with the RET

tyrosine kinase receptor to activate multiple pro-survival, intracellular signaling pathways.(13, 14) In addition to promoting sensory and motor neuron survival, GDNF has been found to be protective against injury-induced degeneration of motor neurons *in vivo*.(15-17)

Chondroitin sulfate proteoglycans (CSPG) are commonly discussed in the context of spinal cord injury and CNS plasticity, but they are also highly expressed in the extracellular matrix (ECM) of peripheral nerves and have been found to be up-regulated after peripheral nerve injury.(18) In the PNS, Schwann cells lining the basal lamina of endoneurial compartments produce CSPGs that are believed to interfere with the neurite-promoting activity of ECM-integrin interactions.(19) Chondroitinase ABC, an enzyme that degrades CSPG, has been reported to promote elongation of neurites when injected directly into acellular peripheral nerve grafts in rodent nerve injury models.(20) In fact, CSPG degradation is now a standard practice during the decellularization of cadaveric nerve in commercially available nerve allografts.(21)

Interestingly, neurotrophic factors have been reported to overcome the inhibitory signaling of CSPGs and restore neurite outgrowth.(22) However, this effect is likely reduced *in vivo* as shown in previous reports of CSPG-induced RhoA activation causing down-regulation of NGF-induced neurite outgrowth.(23, 24) Due to this complex regulatory cascade of neurite growth mediated by neurotrophic factors and ECM interactions, it is difficult to estimate the effects of specific neurotrophic factors following CSPG inhibition *in vivo*.

In this study, we attempt to measure the effects of neurotrophic factors, specifically nerve growth factor and glial-cell derived neurotrophic factor, on neurites regenerating into chondroitinase ABC pre-treated substrates. We began by evaluating the effects of each neurotrophic factor independently in the presence of chondroitinase ABC in a dorsal root ganglion (DRG) explant model. DRG neurite outgrowth is well known to be inhibited by CSPG and promoted by NGF and GDNF. This model thereby provided an initial measurement of neurotrophic factor bioactivity at optimal concentrations in the presence of a

CSPG-reduced substrate and absence of uncontrollable *in vivo* factors, such as endogenous growth factors and variable pharmacokinetics. After this initial analysis, we investigated the adjuvant effects of NGF and GDNF in acellular nerve grafts using a rat sciatic gap nerve injury model. Acellular nerve grafts were pre-treated with ChABC to mimic commercially available nerve grafts that have reduced CSPG content.

Materials and Methods

All experimental procedures were approved by and performed in accordance with the standards set forth by the Institutional Animal Care and Use Committee at Vanderbilt University.

Dorsal root ganglia explant cultures

Chicken dorsal root ganglia (DRG) neurons were used in the initial in vitro assessment. There were two primary considerations in the choice of chick DRG neurons – first, chick DRG explants have fewer surrounding non-neuronal cells than rodent DRG that can complicate neurite measurements, and second, DRG substrate preferences have not been found to be species dependent.(25) E12 white leghorn chicken embryos of both sexes without regard to sex were dissected in ice-cold L-15 medium under high-magnification. Dorsal root ganglia were isolated, plated on collagen(Sigma)/CSPG(Millipore)-coated 35mm culture dishes in neuronal culture medium [MEM (Gibco) with 10% fetal bovine serum (Gibco), D-glucose 4g/L (Sigma) and L-glutamine 2mM (Sigma)] and incubated at 37C with 5% CO2 overnight. Adherent DRG explants were treated the following day with Neurobasal medium [Neurobasal A (Mediatech) with 2% B27 supplement (Gibco), D-glucose 4g/L (Gibco) and L-glutamine 2mM (Gibco)]

supplemented with ChABC, ChABC + NGF (50ng/ml; Proteintech), ChABC + GDNF (50ng/ml; Sigma) or control Neurobasal medium. Explants were photographed with a Nikon AZ100M fluorescent microscope and Nikon DS-Ri1 camera after 3 days of incubation. Cell membranes were live-cell stained prior to imaging with the Neurite Outgrowth Staining Kit (Molecular Probes A15001). Images were analyzed for neurite outgrowth area and neurite length using ImageJ (Fiji Distribution, National Institute of Health, Bethesda, MA), as shown in Figure 1.(26, 27)

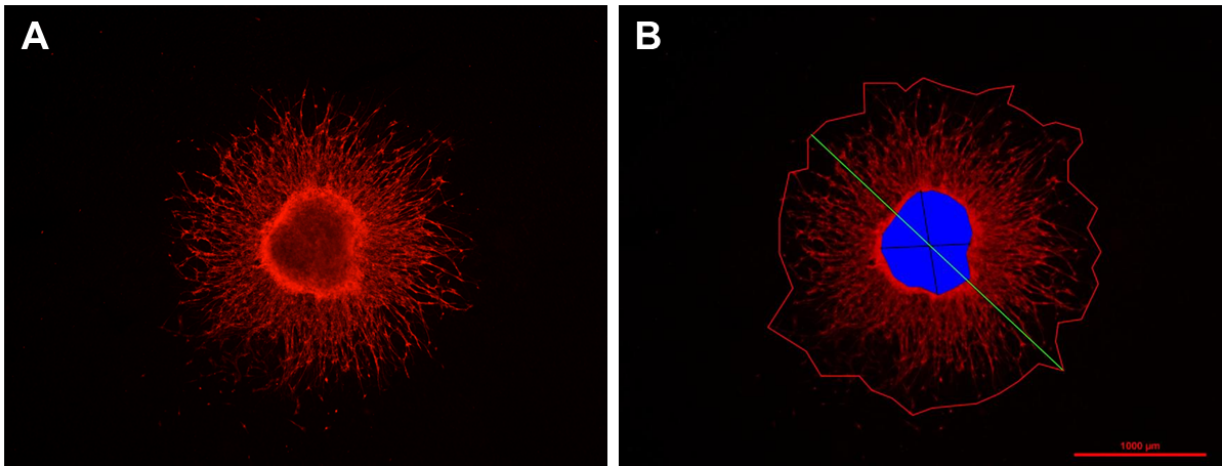

FIG 1. Examples of (A) live-cell stained DRG explant and (B) measurement of a DRG explant using ImageJ. Blue is shaded area is the outlined ganglion. Red outline is the axon border. Black lines are the minimum and maximum Ferret diameters of the ganglion and their intersection represents the ganglion's center of mass. Green line is the longest axonal Ferret diameter passing through the center of mass.

Rat sciatic nerve injury model

In vivo neurotrophic factor supplementation to CSPG-reduced nerve allografts was evaluated in this study using a rat sciatic nerve injury model repaired microsurgically. Twelve donor animals were

sacrificed for nerve graft harvesting. Two experimental groups (n=8) received ChABC pre-treated nerve allografts impregnated with either nerve growth factor or glial cell line-derived neurotrophic factor. The control group (n=8) received a ChABC pre-treated nerve allograft impregnated with sterile water. Subsets of each group (n=4) were sacrificed at 5 days post-injury for acute histologic analysis during the period of neurite outgrowth. The remaining animals were sacrificed at 8 weeks post-injury. One rat in the GDNF group was excluded from analysis due to illness and untimely death.

Animal procurement and housing

Thirty-six (12 donors and 24 recipients) adult female Sprague Dawley rats weighing 250 to 350 g were housed 2-3 per cage and maintained in a 12/12h light-dark cycled room with *ad libitum* access to food and water. Animals used in this study were cared for in accordance with the guidelines of the Institutional Animal Care and Use Committee of Vanderbilt University.

Graft preparation

Sciatic nerves were harvested from donors on the day prior to graft implantation as described in Surgical Procedures. The harvested nerves were trimmed to 20 mm in length and aberrantly bifurcated nerves were discarded. The trimmed ends were collected and frozen for C4S analysis. Immediately following harvest, nerves were placed in a sterile cryogenic vial and decellularized with repeated freeze-thaw cycles in liquid nitrogen and thawing in a 37° C water bath. Decellularized grafts were incubated in chondroitinase ABC for 16 h at 37° C, as described by Neubauer(20). The grafts were then rinsed in

Lactated Ringers solution and incubated in sterile H_20, nerve growth factor solution (10 ug/ml) or glial cell line-derived neurotrophic factor solution (20 ug/ml) for 1 h at room temperature. Processed grafts were washed repeatedly in Lactacted Ringers and stored on ice until implantation.

Donor graft harvest

Donor rats were euthanized at age 20 to 24 weeks by CO2 inhalation with cervical dislocation. Immediately following sacrifice, the hindlimbs were shaved with clippers and prepped aseptically. Sciatic nerves were excised bilaterally from the sciatic notch to the distal trifurcation, with careful attention paid to dissecting perineural tissue and minimizing injury to the nerve. The harvested nerves were immediately rinsed in sterile Lactated Ringers (Hospira; Lake Forest, IL) and placed in sterile cryogenic vials to be processed as previously described.

Interposition graft implantation

Female Sprague-Dawley rats were anesthetized with inhaled isoflourane and the left hindlimb shaved with clippers and prepped aseptically. A 1-cm incision was made parallel, and just caudal, to the femur. Using sharp dissection, the cephalad border of the biceps femoris was freed to allow for caudal retraction and exposure of the left sciatic nerve. The exposed nerve was then dissected free of perineural tissue using sharp dissection and minimal retraction.

A 5 mm segment of sciatic nerve was then excised with iris scissors and the wound was irrigated with Lactated Ringers (Hospira; Lake Forest, IL). Using standard microsurgical techniques, the

processed allograft was trimmed at each end, for a final graft length of 10mm, and was then sutured in place using 9-0 Ethilon (Ethicon, Sommerville, NJ). The trimmed ends of the chondroitinase ABC treated grafts were collected and frozen for C4S analysis. Proximal and distal ends were approximated in an end-to-end fashion using an interrupted suturing technique and microscopic magnification, followed by wound irrigation with sterile Lactated Ringers. All animals were then given a subcutaneous injection of ketoprofen (5 mg/kg) and allowed to emerge from anesthesia.

Recipient nerve harvest

Recipient rats were anesthetized with inhaled isoflurane and sacrificed via intracardiac injection of Fatal-Plus Solution (Vortech, Dearborn, MI) at 5 days or 8 weeks following graft implantation. The left sciatic nerve was harvested immediately after sacrifice with careful attention paid to maintaining nerve integrity with at least 5-mm margin. Excised nerves were stored in 10% neutral buffered formalin for tissue fixation prior to paraffin embedding.

Nerve immunohistochemistry

Immunohistochemical staining was performed using commercial antibodies specifically directed against myelin basic protein (MBP) (Abcam, Cambridge, MA), choline acetyltransferase (ChAc) (Santa Cruz Biotechnology, Santa Cruz, CA), and Chondroitin-4-Sulfate (MP Biomedicals). Isolectin GS-IB4, biotin-XX conjugate (IB4; Invitrogen) was also used to detect GDNF-dependent nociceptive sensory neurons.(28, 29)

For MBP, ChAc, and IB4 staining, formalin-fixed paraffin embedded tissues were sectioned at 5 µm, placed on slides and warmed overnight at 60°C. Slides were deparaffinized and rehydrated with graded alcohols ending in Tris buffered saline (TBS-T Wash Buffer, LabVision, Freemont, CA). For MBP and IB4, heat mediated target retrieval was performed in 1X Target Retrieval Solution (pH 6.0, DAKO, Carpenteria, CA). Endogenous peroxidases and non-specific background were blocked by subsequent incubations in 3% H2O2 (Fisher, Suwanee, GA) in TBS-T and serum-free Protein Block (RTU, DAKO). Primary antibody to MBP was applied at 1:800 dilution for 1 hr, followed by incubation in EnVision+ HRP Labelled Polymer (RTU, DAKO). For IB4 staining, Isolectin IB4, biotin-XX conjugate (10ug/ml) was applied for 1 hr, followed by incubation in SA-HRP (BD Pharmingen).

For ChAc staining, no target retrieval was required. Endogenous peroxidases were blocked as previously described. Non-specific background, secondary, and tertiary labeling of target was accomplished by use of Vector's ABC Elite Goat IgG kit (Vector Laboratories, Burlingame, CA). Primary antibody to ChAc was applied at 1:35 dilution for 1 hour.

For C4S staining, frozen tissues were embedded in OCT and sectioned at 5 µm, and stored in the -80C till ready to stain. Tissues were adhered to the slides by washing in ice-cold acetone, followed by air-drying at room temp. OCT was removed by washing in TBS-T. Endogenous peroxidases and non-specific background were blocked by subsequent incubations in 3% H2O2 (Fisher, Suwanee, GA) in TBS-T and serum-free Protein Block (RTU, DAKO). Primary antibody to C4S was applied at 1:4,000 dilution overnight at +4C, followed the next morning by incubation in horse biotinylated anti-mouse secondary antibody (1:200), and finally incubated in SA-HRP.

For all targets, slides were rinsed with TBS-T between each reagent treatment and all steps were carried out at room temperature unless otherwise noted. Visualization was achieved with DAB+ chromogen (DAKO). Slides were counterstained with Mayer's hematoxylin, dehydrated through a series of alcohols and xylenes, and then coverslipped with Acrytol Mounting Media (Surgipath, Richmond, IL).

Quantification of myelinated axons

Anti-MBP stained sections of nerve distal to the interposition allograft were analyzed for quantification of myelinated axons. Myelinated axon number was determined in four random fields in the distal sciatic nerve at 40x magnification. Axon profiles were counted using semi-automated analysis with NIH *ImageJ* software, which has been previously validated for axon quantification.(30) Post-processing of images was performed with an *ImageJ* Color Deconvolution Plug-in(31) to isolate the DAB color channel followed by conversion to 8-bit grayscale images. A threshold was then applied to the grayscale image to produce a binary representation of axon profiles, with careful attention paid to accuracy of the resultant image. Axon count, area and Feret diameter was measured using the *ImageJ* particle analysis feature with constant selection thresholds.

Statistical analysis

All statistical analyses were performed using GraphPad Prism 5 for Mac OS X (GraphPad Software; San Diego, CA). For comparison of axon counts Student's t-test was used to compare specific groups. All p values were two-tailed and significance was determined at $p < .01$.

Results

Dorsal root ganglion explants were used to test the effects of neurotrophic factor supplementation on neurite outgrowth in CSPG-reduced substrate. Chondroitinase ABC (ChABC) was supplemented to degrade nascent CSPG produced by Schwann cells present in cultured dorsal root ganglia explants.

Neurite outgrowth and axon length was evaluated after 3d incubation in supplemented neuronal growth medium. At 3d, similar maximum axon lengths was observed in control, ChABC and NGF + ChABC supplemented medium. Neurite length was significantly increased in GDNF + ChABC supplemented medium, in addition to increased axonal arbor density. ChABC and NGF + ChABC supplemented media showed a trend towards increased neurite outgrowth, but they did not reach significance. Table 1 lists the neurite outgrowth and maximum axon length for each condition. Representative photomicrographs of live-stained dorsal root ganglia with fiducial markers are shown in Figures 2A-D.

Table 1. Dorsal root ganglion neurite measurements at 3 days post-injury (Mean ± SEM)

	Neurite outgrowth (mm^2)		Neurite Length (μm)		
	Raw	*Corrected*	*Raw*	*Corrected*	***n***
Control	3.94 ± 0.80	4.25 ± 0.74	2780 ± 282	2075 ± 114	8
ChABC	5.70 ± 1.76	5.99 ± 1.68	3122 ± 457	2432 ± 413	8
ChABC + NGF	4.79 ± 0.58	4.79 ± 0.58	2870 ± 153	2286 ± 123	7
ChABC + GDNF	6.93 ± 1.86	6.93 ± 1.86	3745 ± 254*	3011 ± 161**	8

Asterisks indicate conditioned group is significantly different from the control group (**p < 0.01, two-tailed *t* test; *p <0.05, two tailed *t* test). Corrected values exclude areas of axonal arbor with no visible outgrowth by 3 days post-injury, most likely injured during tissue transfer.

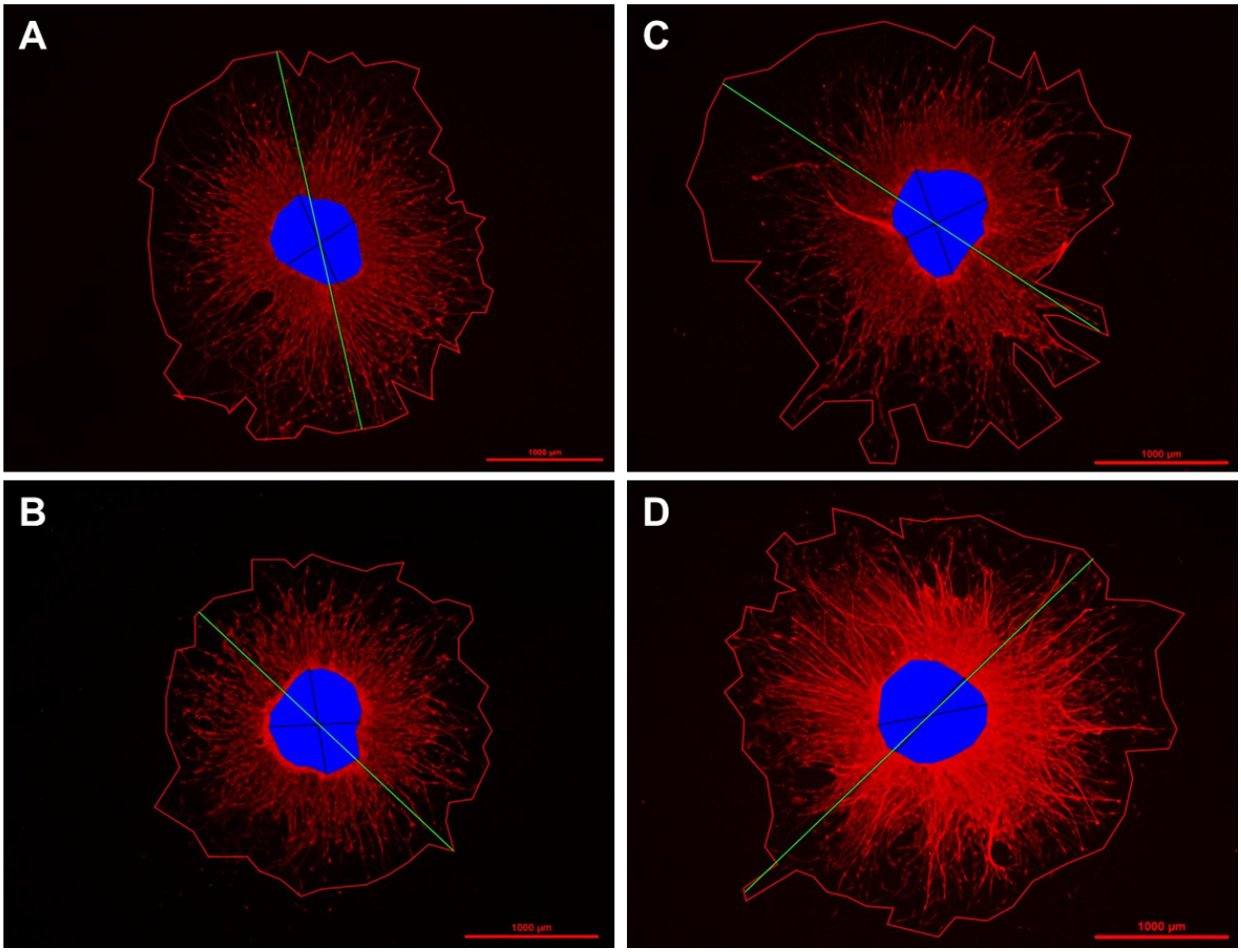

FIG 2. Dorsal root ganglion explants at 3 days of incubation in (A) control medium, (B) ChABC, (C) NGF + ChABC and (D) GDNF + ChABC. Increased axonal arbor density is visible in the GDNF + ChABC conditioned group.

To study the *in vivo* effects of CSPG inhibition and neurotrophic factors on injured peripheral nerves, we treated acellular nerve grafts with H_2O, NGF or GDNF prior to engrafting into a rat sciatic nerve lesion. Acellular nerve allograft was incubated with chondroitinase ABC (ChABC) to cleave native chondroitin sulfate proteoglycans (CSPG), which are well-known extracellular inhibitors of nerve regeneration and plasticity. In Figure 3, anti-chondrointin-4-sulfate (C-4-S) antibody immunohistochemistry is shown as validation of CSPG digestion in the processed nerve allografts. Chondroitin-4-sulfate is the proteoglycan stub that remains after enzymatic digestion of CSPG by

ChABC. Following overnight incubation in ChABC solution, we observed significantly increased anti-C-4-S staining compared to untreated nerve allograft, confirming its proteolytic activity.

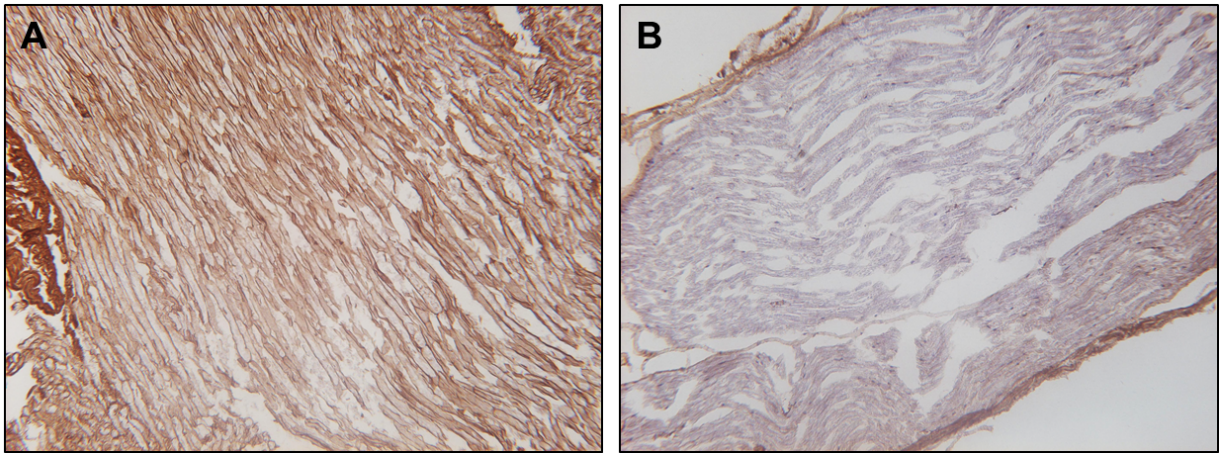

FIG 3. Chondroitin-4-sulfate antibody immunohistochemistry in processed nerve grafts following (A) chondroitinase ABC and (B) vehicle treatment. Increased specific C-4-S antibody staining is visible in the longitudinal nerve fiber tracts in the ChABC-treated nerve grafts, confirming degradation of CSPGs. Epineurial staining is visible in vehicle-treated nerve grafts, possibly due to tissue edge artifact.

To assess total axon regeneration in the processed nerve allografts, we quantified the total number of myelinated axons in distal sections of the lesioned sciatic nerve using anti-myelin basic protein (MBP) immunohistochemistry. Figure 4 shows total myelinated axon counts at 8 weeks post-injury. Myelinated axons were not visible mid-graft at 5 days post-injury, as expected due to immaturity of nascent axons. Total myelinated axon counts were assessed using the semi-automated ImageJ analysis previously described. Nerve growth factor was found to significantly increase total myelinated axon count compared to control ($p<0.001$). No significant difference was found with control and GDNF treated nerve allografts.

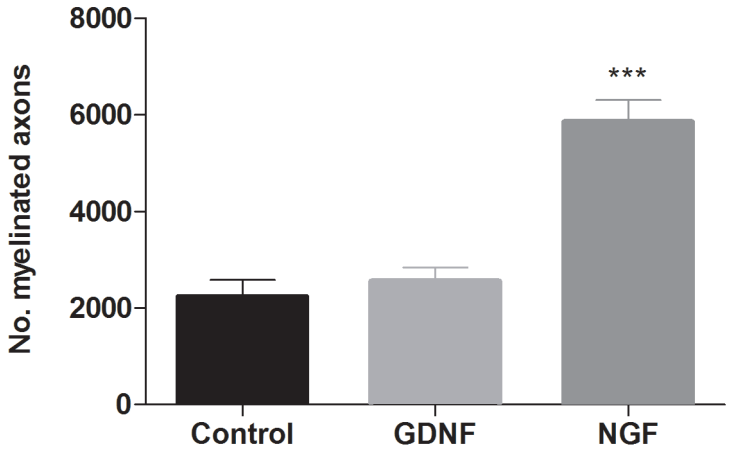

FIG 4. Myelin basic protein antibody immunohistochemistry at 8 weeks post-injury of control, GDNF and NGF treated interposition allografts. Semi-automated counts of myelinated axons located in the sciatic nerve distal to the allograft. Total myelinated axon count is significantly increased in the NGF treated group. Asterisks indicate treatment group is significantly different from the control group (***$p < 0.005$, two-tailed *t* test).

Under strictly controlled *in vitro* conditions nerve growth factor and glial cell line-derived neurotrophic factor affect only specific pools of neuronal cells; however, indirect signaling pathways and extrinsic factors, such as extracellular matrix components, may augment *in vivo* neurotrophic activity. To classify regenerated neurons in our experimental model we performed immunohistochemistry with choline acetyltransferase, predominantly expressed in motor neurons, to identify efferent motor neurons. Figure 5 shows representative sections of choline acetyltransferase stained axons mid-graft at 5 days post-injury. Significantly increased stained axons were found in the NGF treated allografts, representing increased motor axon outgrowth compared to control.

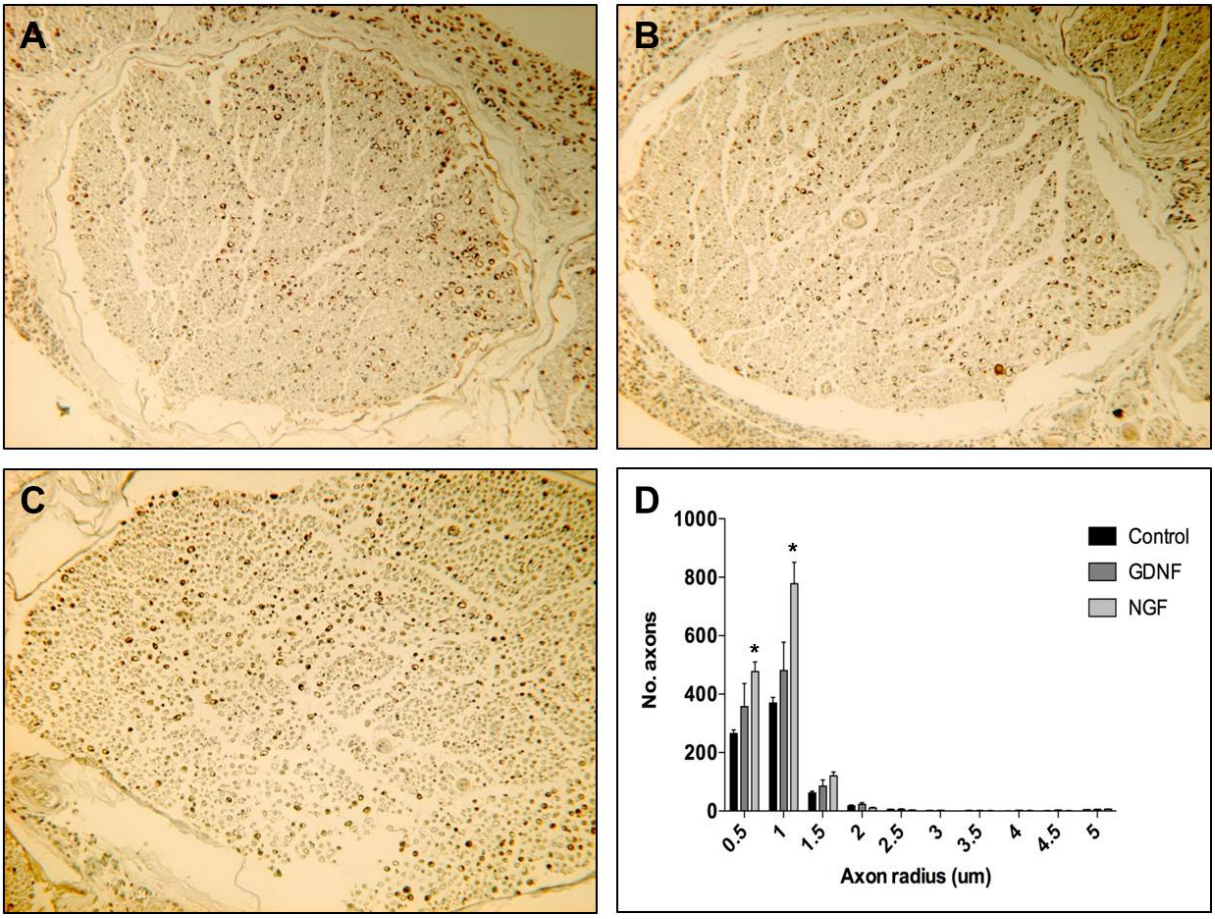

FIG 5. Immunohistochemical analysis of choline acetyltransferase in the mid-graft at 5 days post-injury. Representative sections of (A) Control, (B) GDNF and (C) NGF treated nerve allografts. (D) Quantification of positively stained axons, representing predominantly regenerating motor neurons. Asterisks indicate treatment group is significantly different from the control group (*$p < 0.01$, two-tailed *t* test).

Additionally, isolectin B4 was used to classify GDNF-dependent (*IB4+, TrkA-*) nociceptors and NGF-dependent (*IB4-, TrkA+*) nociceptors. In GDNF seeded grafts, increased regenerating motor axons were found mid-graft at 5 days post-injury compared to control. *IB4+* neurons represent sensory afferents lacking the TrkA receptor and are dependent on GDNF for survival. Therefore, immunohistochemical analysis with isolectin B4 provides a measurement of NGF versus GDNF driven survival following

injury. Figure 6 shows representative sections of mid-graft at 5 days post-injury stained for IB4. NGF allografts significantly decreased IB4-positive axon outgrowth compared to control and GDNF allografts, representing decreased outgrowth or increased apoptosis of GDNF-dependent (IB4+, TrkA-) nociceptors following injury.

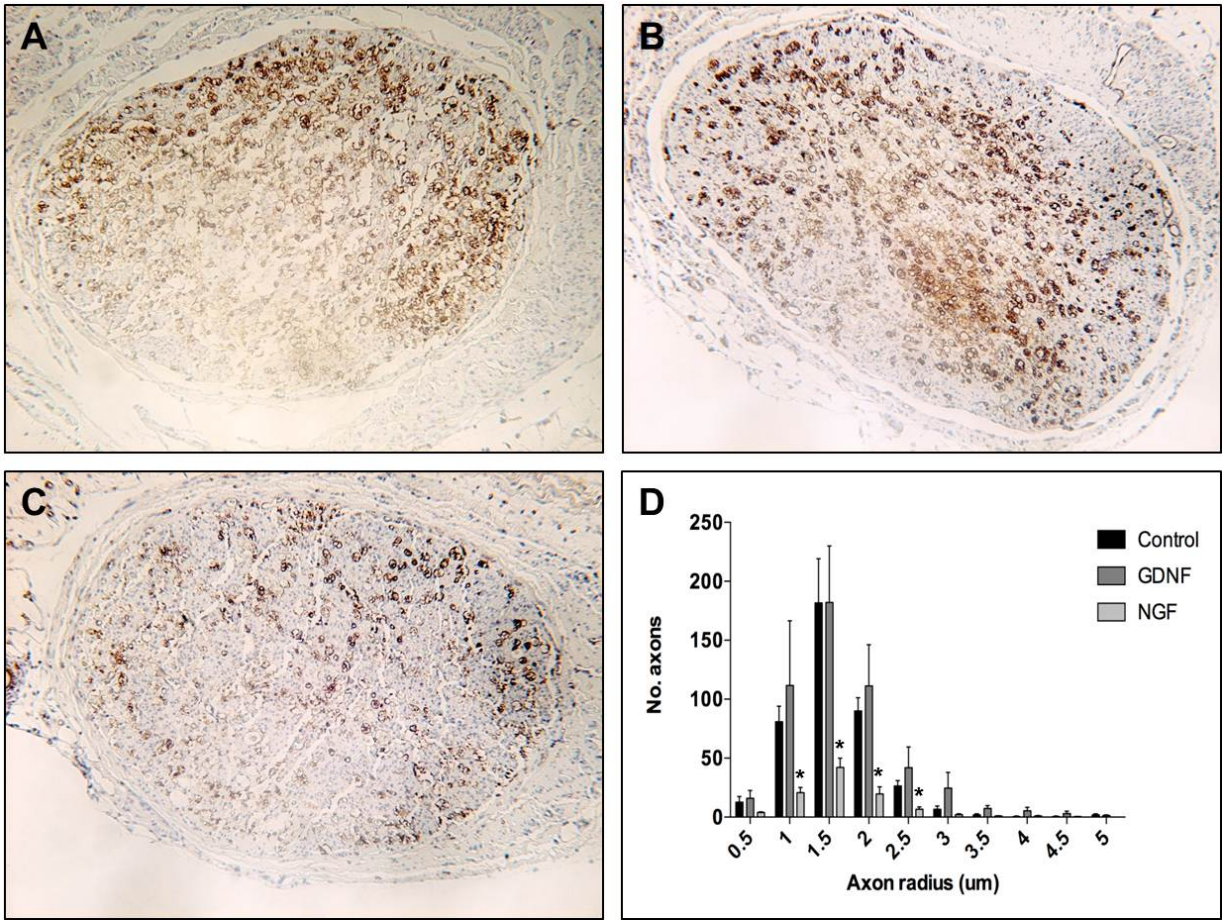

FIG 6. Immunohistochemical analysis of IB4-positive neurons in the mid-graft at 5 days post-injury. Representative sections of (A) Control, (B) GDNF and (C) NGF treated nerve allografts. (D) Quantification of IB4-positive axons, representing GDNF-dependent nociceptive neurons. Significant decreased IB4-positive neuron survival was found in NGF supplemented nerve grafts. Asterisks indicate treatment group is significantly different from the control group (*$p < 0.01$, two-tailed *t* test).

To measure the functional recovery of subjects after surgery, animals were evaluated at 2, 4, 6 and 8 weeks post-injury in their ability to walk across a raised beam (sciatic functional index). Sciatic functional index results are shown in Figure 7. All groups showed progressive improvements in function throughout the study, and there was significant improvement in performance in the NGF treatment group at 6 weeks. Autophagy of one or more digits was observed in animals of each group, possibly contributing to decreases in performance at later time points. Limited functional differences between treatment groups might also be attributed to the resilience of this rodent model to short gap injuries of the sciatic nerve. Larger animals and more severe injury models may be required to observe incremental improvements in gait and motor function.

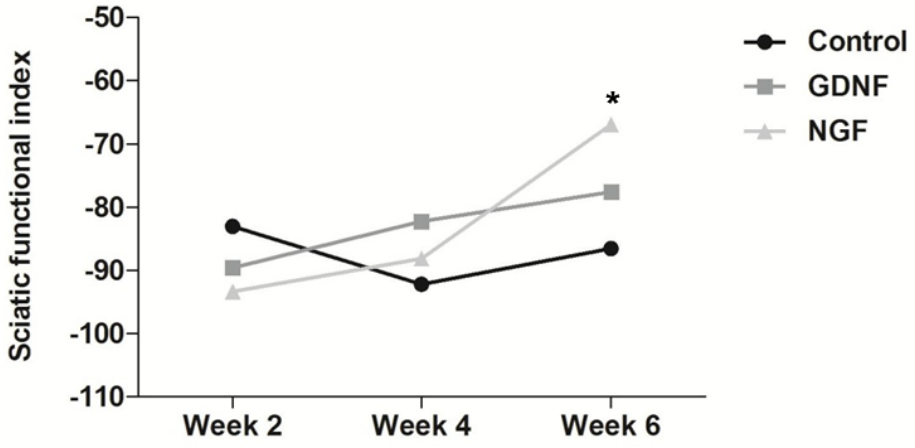

FIG 7. Sciatic functional index at 2 to 6 weeks post-injury. Scores are not shown for week 8 due to significant autophagy of hind limbs. Asterisks indicate treatment group is significantly different from the control group (*$p < 0.01$, two-tailed *t* test).

Discussion

Nerve growth factor is a well-characterized neurotrophin that plays a critical role in sensory neuron development and regeneration. Typically, in the presence of NGF, primary cultures of dorsal root ganglion neurons show increased neurite elongation and reduced apoptosis following injury. However, this was not observed in this study, in which NGF was applied to dorsal root ganglion explants in the presence of chondroitinase ABC. Instead, we found that NGF produced no significant difference in sensory neuron outgrowth compared to control conditions. The effects of NGF on injured neurons involve an elaborate cytosolic signaling cascade initiated by its two membrane-bound receptors – TrkA and p75. TrkA is a tyrosine receptor kinase with high-affinity for nerve growth factor, whose upregulation after injury has been shown to be protective against apoptosis. The p75 neurotrophin receptor binds with low-affinity to all neurotrophins, including NGF, BDNF and NT-3, and is known to play a significant role in apoptotic signaling in addition to having pro-survival effects via the NF-κB pathway. While chondroitinase ABC would be expected to further enhance NGF-induced neurite growth, these effects may not be additive, as both pathways intersect at common secondary messengers and regulatory proteins, such as RhoA.

In addition to the neurotrophin family of proteins, glial cell line-derived neurotrophic factor is a highly conserved ligand that is important to neuronal regeneration and survival after injury, particularly in motor neurons and the IB4-positive, TrkA-negative subpopulation of nociceptors. In this study, dorsal root ganglion neuron outgrowth was found to significantly increase in the presence of GDNF and chondroitinase ABC. The GNDF/RET signaling pathway is completely independent of known pathways of CSPG inhibition and therefore may have additive effects with chondroitinase ABC in inducting neurite outgrowth.

Interestingly, the *in vivo* model found that early NGF supplementation of CSPG-reduced nerve allografts resulted in improved motor neuron survival and increased myelinated axon outgrowth. NGF is

well known to enhance sensory neuron growth and survival, but is not expected to have these effects on motor neurons because they lack the pro-survival TrkA receptor. However, the low-affinity p75 neurotrophin receptor is present in motor neurons and also has the capacity to promote neuron survival and growth. These data support a possible role for chondroitinase ABC in disinhibiting the p75-NFκB pro-survival pathway. This relationship has been discussed in prior *in vitro* studies of CSPG-induced activation of RhoA, which is thought to inhibit NGF-induced nerve outgrowth, but to our knowledge has not been shown with an *in vivo* model.

NGF also appears to promote apoptosis (or inhibit regeneration) of IB4-positive sensory neurons, causing a significant reduction of surviving nociceptive neurons in CSPG-reduced nerve allografts. While this could be explained by decreased outgrowth of all sensory neurons, our *in vitro* model shows no significant difference in total sensory neuron outgrowth between NGF and control conditions. This effect may be prevented with combined NGF/GDNF adjuvant therapy, but this was beyond the scope of the current study.

Additional limitations of this study include minor variation in microsurgical technique between surgeons and a single method of nerve graft processing. Since this was a study of adjuvant neurotrophic factor therapy in CSPG-reduced nerve allografts, all nerve grafts were pre-treated with Chondroitinase ABC. We did not include a group without Chondroitinase ABC pre-treatment, because all commercially available nerve grafts at time of publication have been similarly processed to reduce CSPG content. The benefits of CSPG-reduced nerve allografts are supported by several in vitro and in vivo studies, and are currently being evaluated in the AxoGen Ranger® multicenter clinical study. The goal of this study was to evaluate the benefits of adjuvant neurotrophic factor therapy and not to reassess the current standards in nerve allograft processing.

Conclusions

Pre-treatment with chondroitinase ABC is now standard practice in commercially available nerve allografts. The effects of ECM and integrin modifications in these conduits may not only provide a fertile substrate for nascent neurite elongation, but they may also produce significant alterations in the molecular effects of neurotrophic factors, such as NGF and GDNF. It is important for the surgical community to understand these overlapping molecular pathways, which may provide answers to the variable effects observed with chondroitinase ABC treatment in the peripheral nervous system, as well as in the spinal cord.

This study provides initial evidence that the pro-survival effects of NGF *in vivo* may be disinhibited in CSPG-reduced substrates (such as ChABC pre-treated nerve grafts), promoting motor axon outgrowth and reducing the outgrowth of a specific subpopulation of nociceptive neurons. Future studies of CSPG-reduced nerve allografts with adjuvant growth factor therapy in rodent and large animal models should be pursued to answer these questions.

References

1. Bradbury EJ, Moon LD, Popat RJ, King VR, Bennett GS, Patel PN, Fawcett JW, McMahon SB. Chondroitinase ABC promotes functional recovery after spinal cord injury. Nature. 2002;416(6881):636-40. doi: 10.1038/416636a. PubMed PMID: 11948352.

2. Schmidt CE, Leach JB. Neural tissue engineering: strategies for repair and regeneration. Annu Rev Biomed Eng. 2003;5:293-347. doi: 10.1146/annurev.bioeng.5.011303.120731. PubMed PMID: 14527315.

3. Boyd JG, Gordon T. Neurotrophic factors and their receptors in axonal regeneration and functional recovery after peripheral nerve injury. Mol Neurobiol. 2003;27(3):277-324. doi: 10.1385/MN:27:3:277. PubMed PMID: 12845152.

4. Gordon T, Sulaiman O, Boyd JG. Experimental strategies to promote functional recovery after peripheral nerve injuries. J Peripher Nerv Syst. 2003;8(4):236-50. PubMed PMID: 14641648.

5. Schnell E, Klinkhammer K, Balzer S, Brook G, Klee D, Dalton P, Mey J. Guidance of glial cell migration and axonal growth on electrospun nanofibers of poly-epsilon-caprolactone and a collagen/poly-epsilon-caprolactone blend. Biomaterials. 2007;28(19):3012-25. doi: 10.1016/j.biomaterials.2007.03.009. PubMed PMID: 17408736.

6. Wang HB, Mullins ME, Cregg JM, Hurtado A, Oudega M, Trombley MT, Gilbert RJ. Creation of highly aligned electrospun poly-L-lactic acid fibers for nerve regeneration applications. J Neural Eng. 2009;6(1):016001. doi: 10.1088/1741-2560/6/1/016001. PubMed PMID: 19104139.

7. Hadlock T, Sundback C, Hunter D, Cheney M, Vacanti JP. A polymer foam conduit seeded with Schwann cells promotes guided peripheral nerve regeneration. Tissue Eng. 2000;6(2):119-27. doi: 10.1089/107632700320748. PubMed PMID: 10941207.

8. Gentry JJ, Barker PA, Carter BD. The p75 neurotrophin receptor: multiple interactors and numerous functions. Prog Brain Res. 2004;146:25-39. doi: 10.1016/S0079-6123(03)46002-0. PubMed PMID: 14699954.

9. Carter BD, Kaltschmidt C, Kaltschmidt B, Offenhäuser N, Böhm-Matthaei R, Baeuerle PA, Barde YA. Selective activation of NF-kappa B by nerve growth factor through the neurotrophin receptor p75. Science. 1996;272(5261):542-5. PubMed PMID: 8614802.

10. Yoon SO, Casaccia-Bonnefil P, Carter B, Chao MV. Competitive signaling between TrkA and p75 nerve growth factor receptors determines cell survival. J Neurosci. 1998;18(9):3273-81. PubMed PMID: 9547236.

11. Lee AC, Yu VM, Lowe JB, Brenner MJ, Hunter DA, Mackinnon SE, Sakiyama-Elbert SE. Controlled release of nerve growth factor enhances sciatic nerve regeneration. Exp Neurol. 2003;184(1):295-303. PubMed PMID: 14637100.

12. Otto D, Unsicker K, Grothe C. Pharmacological effects of nerve growth factor and fibroblast growth factor applied to the transectioned sciatic nerve on neuron death in adult rat dorsal root ganglia. Neurosci Lett. 1987;83(1-2):156-60. PubMed PMID: 3441295.

13. Takahashi M. The GDNF/RET signaling pathway and human diseases. Cytokine Growth Factor Rev. 2001;12(4):361-73. PubMed PMID: 11544105.

14. Treanor JJ, Goodman L, de Sauvage F, Stone DM, Poulsen KT, Beck CD, Gray C, Armanini MP, Pollock RA, Hefti F, Phillips HS, Goddard A, Moore MW, Buj-Bello A, Davies AM, Asai N, Takahashi M, Vandlen R, Henderson CE, Rosenthal A. Characterization of a multicomponent receptor for GDNF. Nature. 1996;382(6586):80-3. doi: 10.1038/382080a0. PubMed PMID: 8657309.

15. Chen ZY, Chai YF, Cao L, Lu CL, He C. Glial cell line-derived neurotrophic factor enhances axonal regeneration following sciatic nerve transection in adult rats. Brain Res. 2001;902(2):272-6. PubMed PMID: 11384621.

16. Fine EG, Decosterd I, Papaloïzos M, Zurn AD, Aebischer P. GDNF and NGF released by synthetic guidance channels support sciatic nerve regeneration across a long gap. Eur J Neurosci. 2002;15(4):589-601. PubMed PMID: 11886440.

17. Henderson CE, Phillips HS, Pollock RA, Davies AM, Lemeulle C, Armanini M, Simmons L, Moffet B, Vandlen RA, Simpson LC [corrected to Simmons L. GDNF: a potent survival

factor for motoneurons present in peripheral nerve and muscle. Science. 1994;266(5187):1062-4. PubMed PMID: 7973664.

18. Zuo J, Hernandez YJ, Muir D. Chondroitin sulfate proteoglycan with neurite-inhibiting activity is up-regulated following peripheral nerve injury. J Neurobiol. 1998;34(1):41-54. PubMed PMID: 9469617.

19. Zuo J, Neubauer D, Graham J, Krekoski CA, Ferguson TA, Muir D. Regeneration of axons after nerve transection repair is enhanced by degradation of chondroitin sulfate proteoglycan. Exp Neurol. 2002;176(1):221-8. PubMed PMID: 12093099.

20. Neubauer D, Graham JB, Muir D. Chondroitinase treatment increases the effective length of acellular nerve grafts. Exp Neurol. 2007;207(1):163-70. doi: 10.1016/j.expneurol.2007.06.006. PubMed PMID: 17669401; PubMed Central PMCID: PMCPMC2956445.

21. Moore AM, MacEwan M, Santosa KB, Chenard KE, Ray WZ, Hunter DA, Mackinnon SE, Johnson PJ. Acellular nerve allografts in peripheral nerve regeneration: a comparative study. Muscle Nerve. 2011;44(2):221-34. doi: 10.1002/mus.22033. PubMed PMID: 21660979; PubMed Central PMCID: PMCPMC3136642.

22. Zhou FQ, Walzer M, Wu YH, Zhou J, Dedhar S, Snider WD. Neurotrophins support regenerative axon assembly over CSPGs by an ECM-integrin-independent mechanism. J Cell Sci. 2006;119(Pt 13):2787-96. doi: 10.1242/jcs.03016. PubMed PMID: 16772333.

23. Walker BA, Ji SJ, Jaffrey SR. Intra-axonal translation of RhoA promotes axon growth inhibition by CSPG. J Neurosci. 2012;32(41):14442-7. doi: 10.1523/JNEUROSCI.0176-12.2012. PubMed PMID: 23055514; PubMed Central PMCID: PMCPMC3509224.

24. Yamaguchi Y, Katoh H, Yasui H, Mori K, Negishi M. RhoA inhibits the nerve growth factor-induced Rac1 activation through Rho-associated kinase-dependent pathway. J Biol Chem. 2001;276(22):18977-83. doi: 10.1074/jbc.M100254200. PubMed PMID: 11279039.

25. Tuttle R, Matthew WD. Neurotrophins affect the pattern of DRG neurite growth in a bioassay that presents a choice of CNS and PNS substrates. Development. 1995;121(5):1301-9. PubMed PMID: 7789262.

26. Cregg JM, Wiseman SL, Pietrzak-Goetze NM, Smith MR, Jaroch DB, Clupper DC, Gilbert RJ. A rapid, quantitative method for assessing axonal extension on biomaterial platforms. Tissue Eng Part C Methods. 2010;16(2):167-72. doi: 10.1089/ten.TEC.2009.0108. PubMed PMID: 19409034; PubMed Central PMCID: PMCPMC2946908.

27. Schindelin J, Arganda-Carreras I, Frise E, Kaynig V, Longair M, Pietzsch T, Preibisch S, Rueden C, Saalfeld S, Schmid B, Tinevez JY, White DJ, Hartenstein V, Eliceiri K, Tomancak P, Cardona A. Fiji: an open-source platform for biological-image analysis. Nat Methods. 2012;9(7):676-82. doi: 10.1038/nmeth.2019. PubMed PMID: 22743772; PubMed Central PMCID: PMCPMC3855844.

28. Molliver DC, Wright DE, Leitner ML, Parsadanian AS, Doster K, Wen D, Yan Q, Snider WD. IB4-binding DRG neurons switch from NGF to GDNF dependence in early postnatal life. Neuron. 1997;19(4):849-61. PubMed PMID: 9354331.

29. Stucky CL, Lewin GR. Isolectin B(4)-positive and -negative nociceptors are functionally distinct. J Neurosci. 1999;19(15):6497-505. PubMed PMID: 10414978.

30. Marina N, Bull ND, Martin KR. A semiautomated targeted sampling method to assess optic nerve axonal loss in a rat model of glaucoma. Nat Protoc. 2010;5(10):1642-51. doi: 10.1038/nprot.2010.128. PubMed PMID: 20885376.

31. Ruifrok AC, Johnston DA. Quantification of histochemical staining by color deconvolution. Anal Quant Cytol Histol. 2001;23(4):291-9. PubMed PMID: 11531144.

32. Bain JR, Mackinnon SE, Hunter DA. Functional evaluation of complete sciatic, peroneal, and posterior tibial nerve lesions in the rat. Plast Reconstr Surg. 1989;83(1):129-38. PubMed PMID: 2909054.

CHAPTER III

DEVELOPMENT OF NEUROTROPHIC FACTOR ELUTING NERVE ALLOGRAFTS

Introduction

The gold standard therapy for a nerve gap repair is autologous nerve grafting. [1] In addition to significant donor site morbidity, this surgery requires increased operative time and post-operative rehabilitation. Transplants of fresh cadaveric nerve allografts are precluded by the need for cytotoxic immunosuppressive drugs, such as tacrolimus and cyclosporine. [2] However, nerve allografts that have been decellularized lack human leukocyte antigen (HLA) and therefore do not require immunosuppression. Similar to other decellularized organs, acellular nerve allografts are processed with specific detergents, enzymes and physical alterations, e.g., freeze-thaw cycling, to lyse and remove the membranous and cytoplasmic components of the neuronal and non-neuronal cells. [3] Meanwhile, nerve processing is optimized to preserve extracellular matrix (ECM) proteins and microstructure of the basal lamina and endoneurium.

Gap length is the primary factor for selecting the modality of nerve repair. In gaps over 3 cm in length, artificial and biological conduits have been shown to be ineffective in producing regeneration. [4], [5] Acellular nerve allografts have been shown to be superior to artificial conduits in short nerve gaps, but they remain less effective than autografts in large nerve defects. The failure of acellular nerve grafts in large gap injuries is thought to be associated with loss of Schwann cells and their products. Schwann cells

synthesize neurotrophic factors, extracellular matrix proteins and myelin, which is essential to nerve regeneration. Immediately following implantation, host Schwann cells migrate from the proximal and distal nerve stumps into the acellular nerve allograft and proliferate. [6], [7] In larger gap injuries, this process is slower and may place greater stress on proliferating Schwann cells, possibly leading to cell senescence. [8] Absence or senescence of Schwann cells in acellular nerve allografts may lead to an altered microenvironment without the neurotrophic support necessary for robust axonal regeneration, such as nerve growth factor.

The neurotrophins are a family of growth factors important to neural development and regeneration, which include nerve growth factor (NGF), brain-derived neurotrophic factor (BDNF) and neurotrophin-3 (NT-3). NGF is the prototypical neurotrophin that supports survival and regeneration of neuronal cells after injury. In general, NGF mediates cell survival and apoptosis through its two receptors, the high-affinity TrkA receptor and the low-affinity p75 receptor, respectively. [9], [10] However, p75 has also been shown to have pro-survival effects by activation of NF-κB transcription factor. [11] Although the TrkA receptor is not expressed in motor neurons, we showed that NGF had a positive regenerative effect in choline acetyltransferase-positive motor neurons in the previous chapter.

Although the beneficial effects of NGF in regenerating neurons has been known for several decades and demonstrated with in-vitro models, its use clinically is complicated by our inability to provide sustained delivery of growth factor. Oral and injected NGF has been shown to be ineffective due to rapid proteolysis and elimination. The elimination half-life of NGF in a rat model was found to be 2.3 hours following intravenous injection and 4.5 hours following subcutaneous injection. [12] However, the absorbance of NGF in subcutaneous depot sites have been shown to have much slower kinetics with an elimination half-life of up to 150 hours. [12] Since nerve regeneration occurs over a period of weeks to months, there have been numerous attempts to develop a long-term NGF delivery mechanism. The earliest attempts at controlled delivery used osmotic pumps to continuously delivery NGF locally in the wound. Although this may be a viable solution for short-term research, the large amount of growth factor

required and risk of infection make this an impractical approach for clinical use. The use of nerve conduits as both a method of surgical repair and a delivery device for growth factors has also been widely investigated. [13]–[17] Studies of implantable silastic chambers prefilled with NGF have produced mixed results with worse outcomes found in tubes that lack pores for cellular motility and diffusion. [18] Synthetic biomaterials capable of controlled release of peptide have shown the most promise for sustained NGF delivery. [14], [19] Biomimetic polymers such as poly-ε-capro lactone (PCL) or poly-lactic-co-glycolic acid (PLGA) are capable of immobilizing peptides that are released during degradation.

More recently, affinity-based delivery systems using extracellular matrix proteins containing growth-factor binding domains have been investigated for growth factor delivery. Wood et al demonstrated NGF and GDNF delivery using fibrin matrices cross-linked with heparin binding proteins. [20]–[22] In a recent study by Martino et al, a domain of placenta-growth factor-2 (PlGF-$2_{123-144}$) was found to bind with high affinity to several extracellular matrix (ECM) proteins, including collagen I, fibronectin and fibrinogen. [23] Insertion of this domain into other growth factors, including vascular endothelial growth factor-A (VEGF-A) and platelet-derived growth factor (PDGF) produced similar super-affinity to ECM while maintaining their biological activity. Interestingly, in the initial screening for growth factor domains with ECM super-affinity, the neurotrophin family was found to have significant affinity to ECM proteins, approaching that of PlGF-$2_{123-144}$ (Fig. 1). [23]

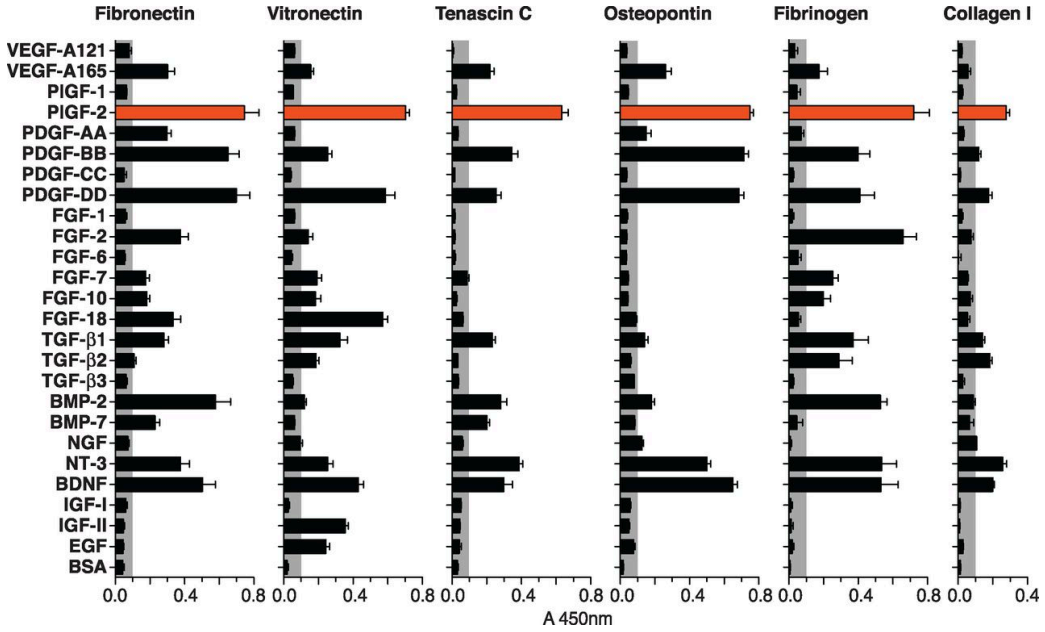

Figure 1. Growth factor binding to extracellular matrix proteins, measured by ELISA (reused with permission from Martino 2014 [23]). Signals over the gray box indicate significant binding.

Leveraging innate neurotrophic factor affinity to ECM proteins, acellular nerve allografts may be capable of retaining these growth factors for sustained effect. Mathematical models of simple affinity-based delivery systems have shown that the protein release profile is affected by the binding affinity (K_D), concentration of binding ligand, rate of dissociation (k_{off}), matrix thickness and geometry.[24] Retention of neurotrophins in acellular nerve allografts is likely dependent on the method of tissue decellularization, as this will effect both the preservation of ECM proteins and the permeability of the tissue. We have previously shown that NGF is retained after incubation with freeze-thaw cycled nerve allografts and produces early improvement of neurite outgrowth in rat sciatic gap nerve injury. In this study, we first investigate NGF loading in acellular nerve allografts processed with three existing methods of nerve decellularization and we then characterize nerve graft retention of NGF in-vitro over 3 weeks. The best performing acellular nerve allograft is then evaluated in vivo with a rat sciatic nerve gap injury model.

We expect the total loading and release kinetics of NGF in acellular nerve allografts to be dependent on the method of nerve processing. While freeze-thaw decellularization is expected to provide optimal ECM ultrastructure, it is likely to leave cellular debris that may impede growth factor binding and neurite outgrowth. Although detergent decellularization may increase ECM protein loss and disorganization, reduced cellular debris and increased tissue permeability may increase diffusion and binding of growth factor to the residual ECM and produce a superior environment for axonal regeneration.

Materials and Methods

All experimental procedures were approved by and performed in accordance with the standards set forth by the Institutional Animal Care and Use Committee at Vanderbilt University.

Growth factor and reagents

NGF-β (>98% pure as determined by RP-HPLC and SDS-PAGE) was purchased from ProSpec in its mature form, carrier free and lyophilized.

Donor nerve harvesting

Sprague Dawley rats were 12 weeks old and weighed 250 to 300g at the start of the experiment. The hind legs were shaved and longitudinal incisions of the skin and underlying biceps femori were made bilaterally. Using blunt dissection, the sciatic nerves were dissected from surrounding tissue and excised with iris scissors. Directly after excision, sciatic nerves were placed on a glass slide, cleaned of all excess connective tissue and trimmed to 2-cm using an ophthalmic scalpel (Micro Feather No. 715, Feather Safety Razor Company) while hydrating with phosphate buffered saline. After 3 washes with PBS, cleaned nerve segments were stored in RPMI 1640 medium (Life Technologies) at 4 °C until processing.

Nerve graft processing

Nerve segments were decellularized with the Sondell technique [25], Hudson optimized acellular technique [26], or freeze-thaw cycling [27]. Table 1 lists the protocols for Sondell and Hudson nerve decellularization performed prior to nerve decellularization. Freeze-thaw cycling was performed with liquid nitrogen submersion for two minutes and subsequent thawing at 37 °C for two minutes, repeated in triplicate. After 3 washes with PBS, processed nerves grafts were stored in PBS solution at 4 °C.

Table 1. Nerve decellularization protocols adapted from existing literature.

	Sondell Protocol [25]		**Hudson Protocol** [26]	
Step	**Solution**	**Time (h)**	**Solution**	**Time (h)**
1	46mM (3%) Triton X-100	15	125mM SB-10, 10mM phosphate, 50 mM sodium	15
2	96mM (4%) sodium	24	0.14% Triton X-200, 0.6mM SB-16, 10mM	24

	deoxycholate		phosphate, 50mM sodium	
3	DI H2O	1 x 7	50mM phosphate, 100mM sodium	0.5 x 3
4	46mM (3%) Triton X-100	15	125mM SB-10, 10mM phosphate, 50 mM sodium	7
5	96mM (4%) sodium deoxycholate	24	0.14% Triton X-200, 0.6mM SB-16, 10mM phosphate, 50mM sodium	15
6	PBS (pH 7.2) at 4 C	Until use	10mM phosphate, 50mM sodium	Until use

Growth factor loading of decellularized nerves

NGF-β was reconstituted to 100 μg/ml in sterile 18MΩ-cm H2O and filtered through a 0.22 μm filter. Processed nerve grafts were incubated in NGF-β solution for 16 h at RT under agitation. Concentration of incubation solution was initially evaluated in a dilution series with freeze-thaw processed nerve grafts and sandwich ELISA (ChemiKine NGF Sandwich ELISA, Millipore) of tissue lysates. Optimal incubation concentration of 10 μg/ml was chosen at the saturation point of NGF loading of tissue samples.

Growth factor release assay

Following incubation in NGF solution, loading and release of growth factor was evaluated under infinite sink conditions in vitro at 37 °C. NGF release was measured for 21 days following initial treatment. Allografts were washed three times in the first 24 hours and once every 24 hours subsequently with 1ml of Tris-buffered saline per wash. The washes were be collected and stored in silanized Eppendorf tubes at -20 °C. After 21 days, the nerves were homogenized. Concentrations of NGF in nerve lysates and

collected washes were then quantified in triplicate using an NGF sandwich ELISA (ChemiKine NGF Sandwich ELISA, Millipore).

Growth factor bioactivity assay

Primary embryonic dorsal root ganglion neurons were purified from E16 Sprague Dawley rat embryos as previously described. [28] Dissociated neurons were plated at a density of 10,000 cells/well in 12-well collagen-coated plates containing minimum essential medium (MEM, Gibco) supplemented with 10% fetal bovine serum (FBS, Gibco), 4 g/L D-glucose (Sigma) and 2 mM L-glutamine (Gibco) and incubated at 37 °C with 5% CO_2 overnight. Allograft washes collected from the seventh day of the growth factor release assay were approximately 20x concentrated using 10K MWCO PES membrane protein concentrators (Pierce Concentrators, Thermo Scientific). Recovered NGF was equivalently diluted in culture medium. Positive control culture medium was prepared with lyophilized NGF reconstituted to 50 ng/ml with culture medium. Negative control culture medium was prepared with the culture medium alone. At 1 d in culture, the media was replaced with Sondell allograft-NGF supplemented media (n=4), Hudson allograft-NGF supplemented media (n=4), Freeze-thaw allograft-NGF supplemented media (n=4), positive control culture media (n=4) or negative control culture media (n=4). At 7 d in culture, neurons were stained using a neurite outgrowth and cell viability fluorescent dye (Neurite Outgrowth Staining Kit, Life Technologies) and Hoechst 33342 nuclear counterstain (NucBlue Live ReadyProbes Reagent, Life Technologies), then photographed with an inverted fluorescent microscope (EVOS FL Cell Imaging System, Life Technologies). ImageJ was used to measure neurite outgrowth in neurons showing positive membrane and viability staining.

Quantification of GAGs and Collagen

Glycosaminoglycan (GAG) content was quantified with the dimethyl methylene blue (DMMB) assay (1,9 dimethyl-methylene blue, Sigma). Collagen content in acellular nerve samples was measured with hydroxyproline level as determined by the colorimetric reaction of oxidized hydroxyproline with 4-(dimethylamino)benzaldehyde (Hydroxyproline Assay Kit, Sigma).

Electron microscopy

Axial cross-sections of acellular nerve samples were fixed with 2% paraformaldehyde and 2.5% glutaraldehyde in 0.1 M cacodylate buffer (pH 7.4). The specimens were post-fixed with 1% OsO_4 solution in 0.1 M cacodylate buffer (pH 7.4) for 2 h, dehydrated through a graded ethanol series in PBS, and sputter coated with 3.5 μm of gold. Quanta 250 ESEM (FEI, Hillsboro, OR) was used to capture surface images at 300× to 3000×.

In vivo rat nerve injury

Eight adult Sprague Dawley rats weighing 250 to 300g had a 1-cm NGF-loaded (n=4) or saline-loaded (n=4), Sondell-processed acellular nerve allograft engrafted in sciatic nerve in the left hind limb. The graft was epineurially sutured to the proximal and distal sciatic nerve stumps following an acute transection injury. After 21 days, the animal was euthanized with intracardiac injection of pentobarbital

(Euthasol). The sciatic nerve was dissected and immersion fixed in 4% paraformaldehyde/0.5% glutaraldehyde in PBS.

Histology and immunohistochemistry

Immediately following decellularization, twelve acellular nerve allografts were fixed in 10% neutral buffered formalin for histological analysis with toluidine blue, Gomori's trichrome and phalloidin immunohistochemistry. Alexa Fluor 488® phalloidin (Life Technologies, Grand Island, NY) was used to selectively label F-actin filaments. Standard immunohistochemical protocols were used. In brief, formalin-fixed paraffin embedded tissues were sectioned at 5 μm, placed on slides and warmed overnight at 60°C. Slides were deparaffinized and rehydrated with graded alcohols ending in Tris buffered saline (TBS-T Wash Buffer, LabVision, Freemont, CA). Heat mediated target retrieval was performed in 1X Target Retrieval Buffer (DAKO, Carpenteria, CA). Non-specific background was blocked by serum-free Protein Block (RTU, DAKO). Alexa Fluor 488® phalloidin was used at 1:41 for 30 min, followed by several washes in D.H_2O. Slides were rinsed with TBS-T between each reagent treatment and all steps were carried out at room temperature. Slides were counterstained and coverslipped with ProLong® Gold Antifade Mountant with DAPI (Life Technologies), and stored at +4°C until viewed under the microscope.

Paraformaldehyde-fixed in vivo nerve grafts were paraffin embedded and sectioned at 5 um, placed on slides and warmed overnight in 60°C.

Statistical analysis

All statistical analyses were performed using GraphPad Prism 5 for Mac OS X (GraphPad Software; San Diego, CA). For comparison of axon counts Student's t-test was used to compare specific groups. All p values were two-tailed and significance was determined at $p < .01$.

Results

Extracellular matrix of properties of acellular nerve allografts

Twelve decellularized nerves were evaluated for their extracellular matrix composition, including myelin, collagen, glycosaminoglycan and actin content. The presence of connective tissue, cellular debris and myelin was first evaluated with semi-quantitative histology of Gomori's trichrome-stained cross-sections. The presence of myelin was greatest in unprocessed nerve and freeze-thaw decellularized nerve, with a myelin:collagen ratio of 2.44 ± 0.49 and 1.61 ± 0.24 respectively.

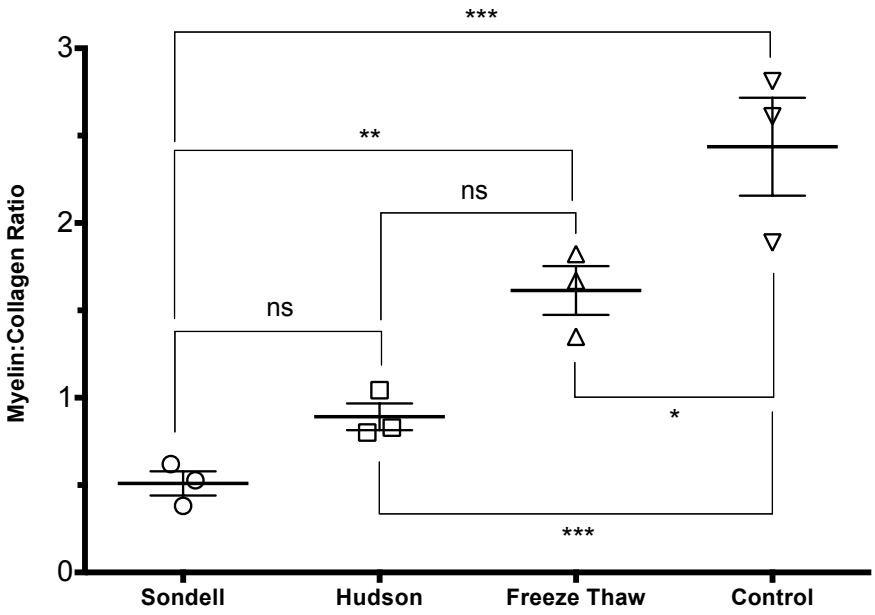

Figure 2. Myelin-connective tissue ratio in Gomori's trichrome stained cross-sections of acellular nerve allografts.

Glycosaminoglycan (GAG) content is known to inhibit the performance of acellular nerve allografts. Particularly, the cleavage of GAG side chains of chondroitin sulphate proteoglycans (CSPGs) is known to attenuate inhibitory activity and promote axon regeneration. Chondroitinase ABC (ChABC) is an enzyme used to cleave GAG side chains from CSPGs and has shown promise as a treatment for central and peripheral nerve lesions. In the previous chapter, we found that freeze-thaw decellularized nerve allografts pre-treated with ChABC had improved axon regeneration after loading with NGF. Prior to enzymatic treatment of allografts, total GAG content is highest in unprocessed nerve (0.423 ± 0.068 ug/mg) and freeze-thaw decellularized nerve (0.457 ± 0.073 ug/mg) and significantly reduced in Sondell-processed nerve (0.167 ± 0.036 ug/mg, $p = 0.029$) (Fig. 3).

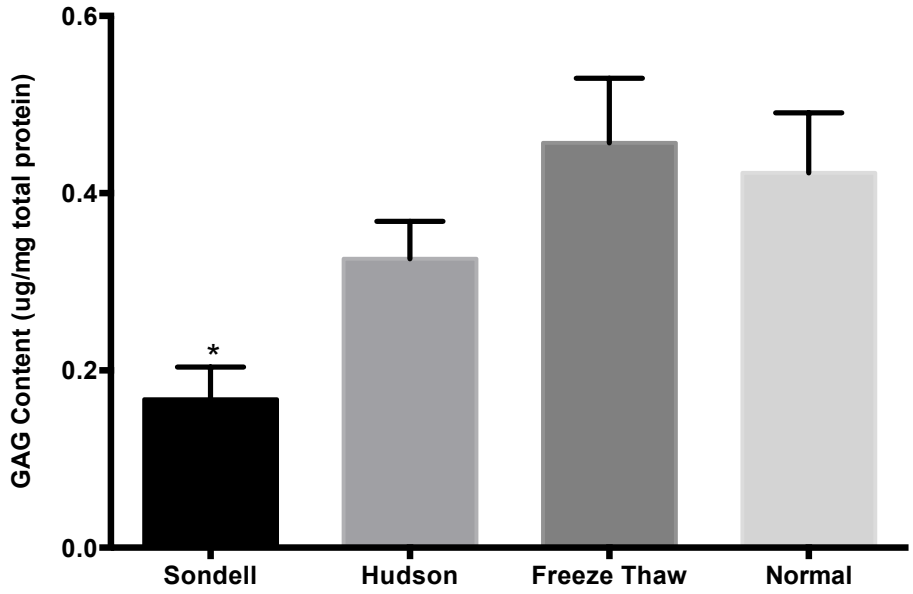

Figure 3. Glycosaminoglycan content in acellular nerve allografts quantified with DMMB assay.

Clearance of intracellular debris from nerve allografts was assessed by visual inspection of F-actin with a fluorescent-tagged Phalloidin probe. F-actin is known to co-localize with myelin-associated glycoprotein, and to be present in the periaxonal membrane, outer and inner mesaxon, paranodal myelin loops and Schmidt-Lanterman incisures of myelinating Schwann cells.[29] Minimal F-actin was observed within the epineurium of Sondell-processed nerve allografts and no nuclear staining was observed (Fig. 4a-c). Pinpoint F-actin staining and nuclear staining was observed within the epineurium of Hudson-processed nerve allografts (Fig. 4d-f). Freeze-thaw allografts showed high F-actin density throughout the cross-section with preserved tubular distribution (Fig. 4g-i). F-actin was observed in the connective tissue of the epineurium in all nerve allografts.

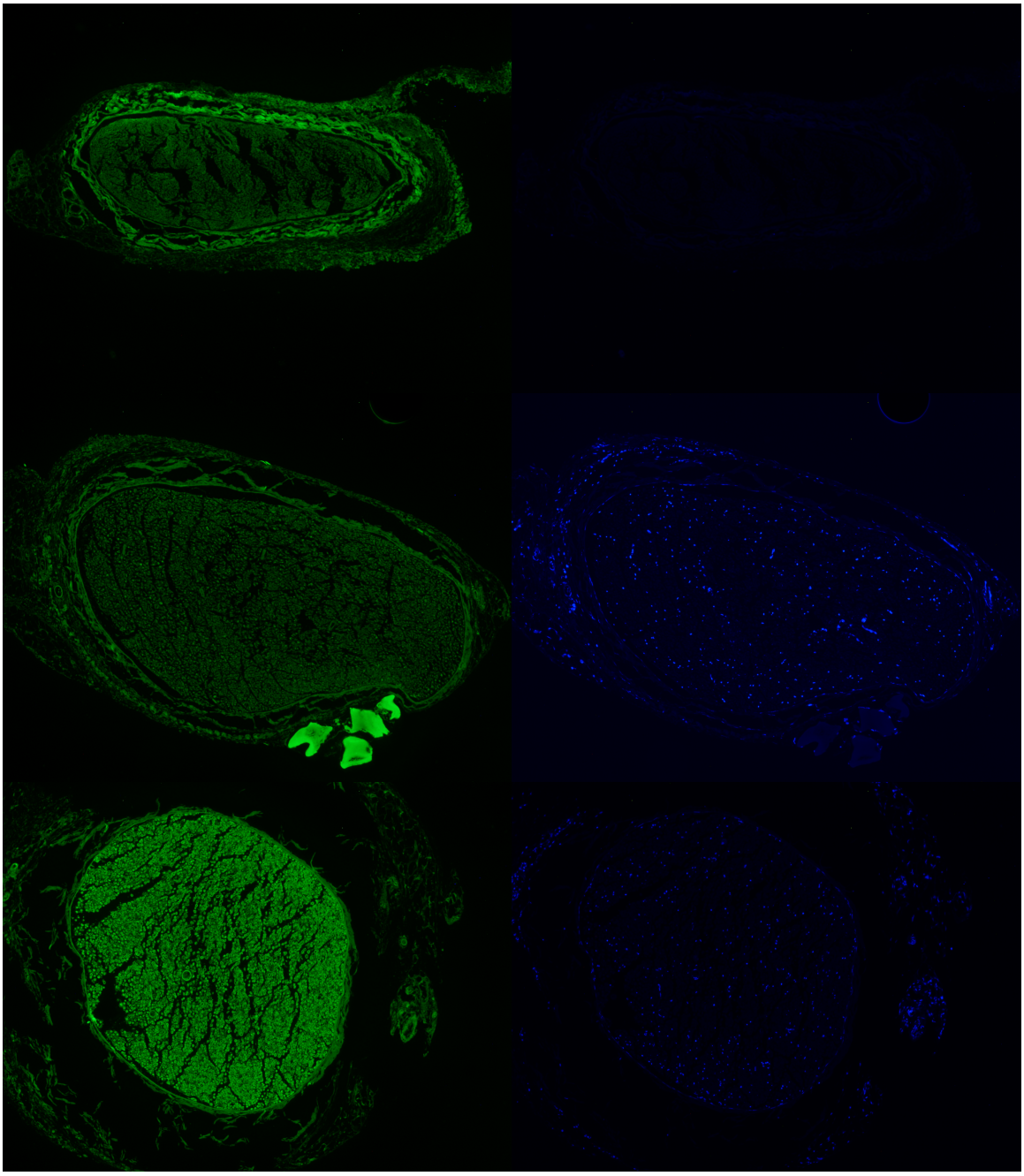

Figure 4. F-actin and DAPI staining of Sondell (top), Hudson (middle) and freeze-thaw (bottom) processed allografts. Minimal F-actin is observed within the epineurium of Sondell processed allografts. Nuclear staining with DAPI follows similar trend. Freeze-thaw cycling shows the lowest clearance of cytoplasmic and nuclear content.

Organization and porosity of nerve allografts was evaluated with scanning electron microscopy. Sondell-processed allografts demonstrated the best preservation of tubular endoneurium and collagen fibril organization (Fig. 5a-d). Empty endoneurial sheaths are visible with diameters up to 10-um with intact surrounding basal lamina (Fig. 5c-d).

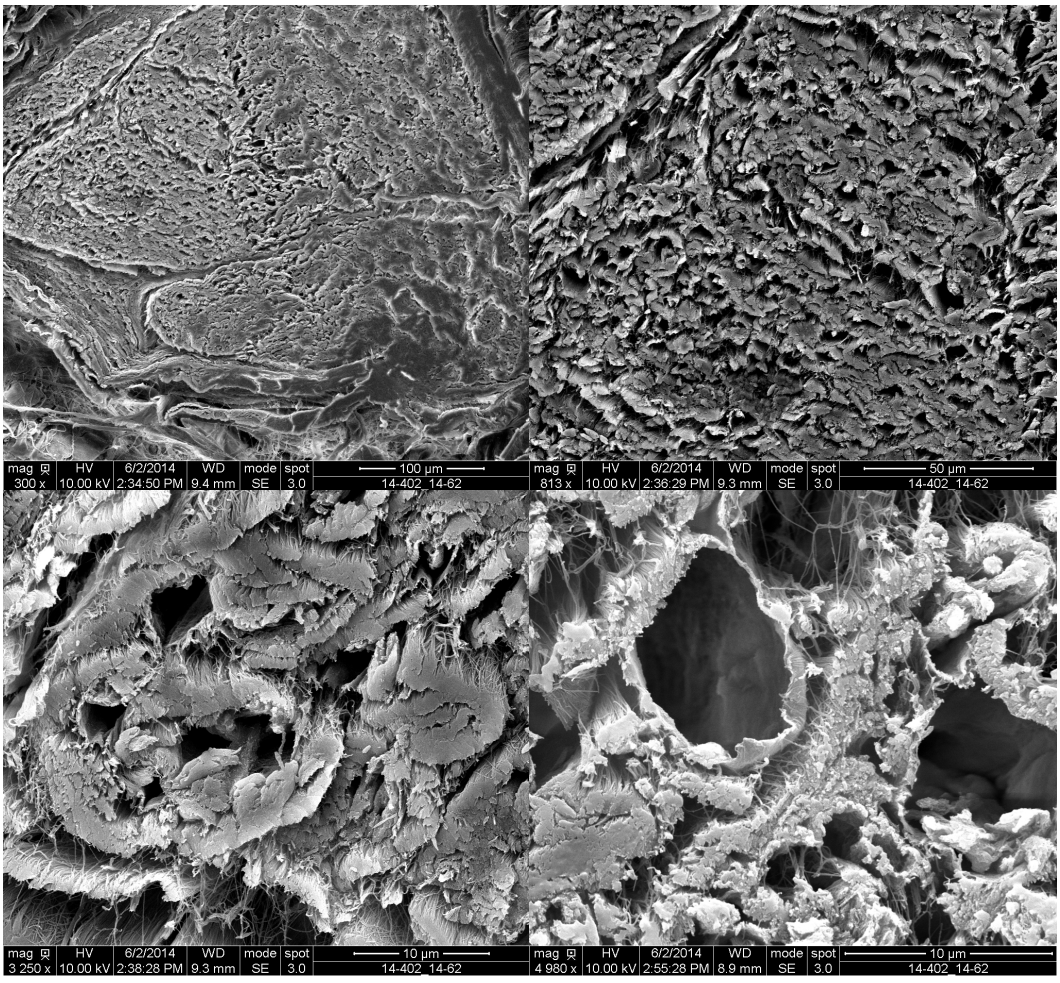

Figure 5. Scanning electron microscopy of Sondell-processed acellular nerve allograft at a) 300x, b) 813x, c) 3250x and d) 4960x magnification.

Hudson-processed nerve allografts showed high disorganization of collagen fibrils and protrusion of axon bundles from the perineurium (Fig. 6a-d). There were no intact endoneurial tubes or basal lamina, and all pores were below 1-um in diameter.

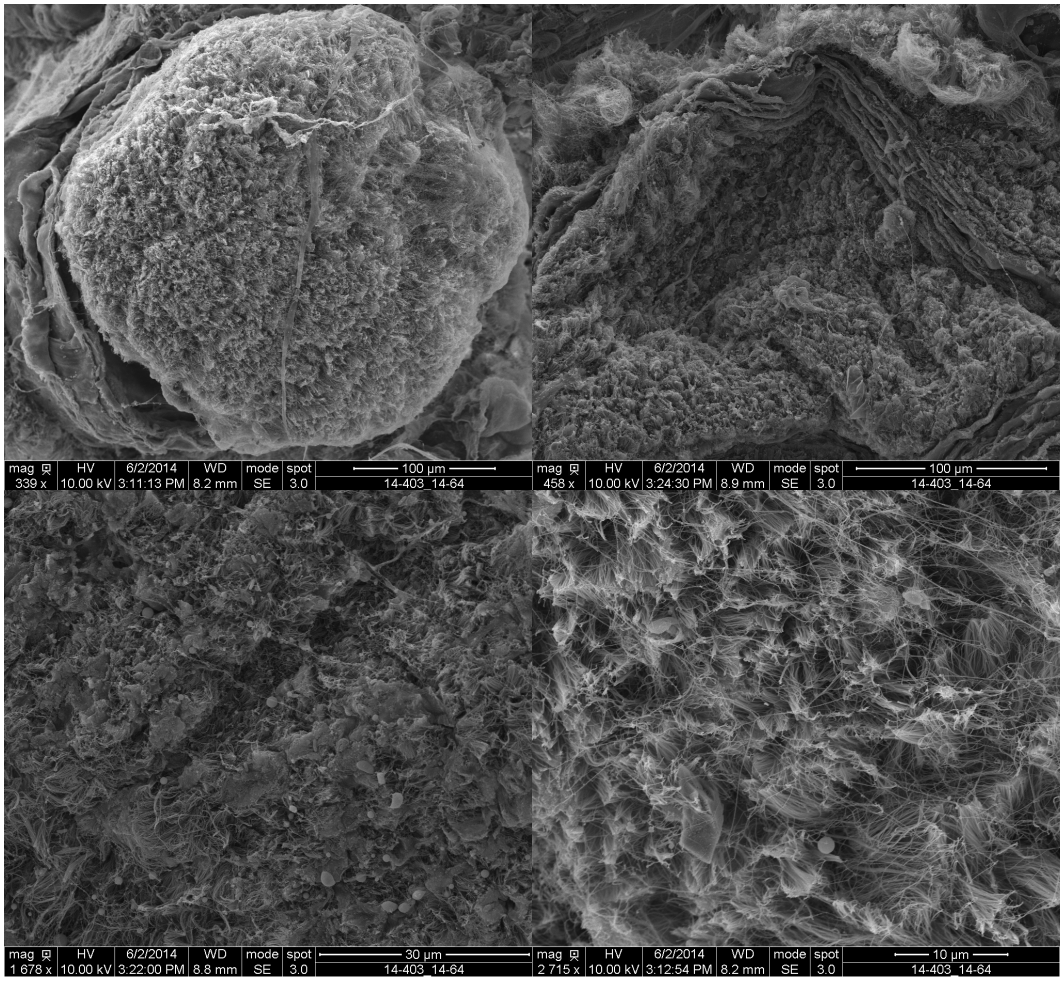

Figure 6. Scanning electron microscopy of Hudson-processed acellular nerve allograft at a) 339x, b) 458x, c) 1678x and d) 2715x magnification.

Freeze-thaw cycled nerve allografts were well organized with intact myelin sheaths and basal lamina tubes (Fig. 7a-d). However, cellular debris also appeared to remain within the endoneurium (Fig. 7d), in agreement with our F-actin results. The debris appears to reduce the effective porosity of the allograft and potentially obstructs neurite outgrowth.

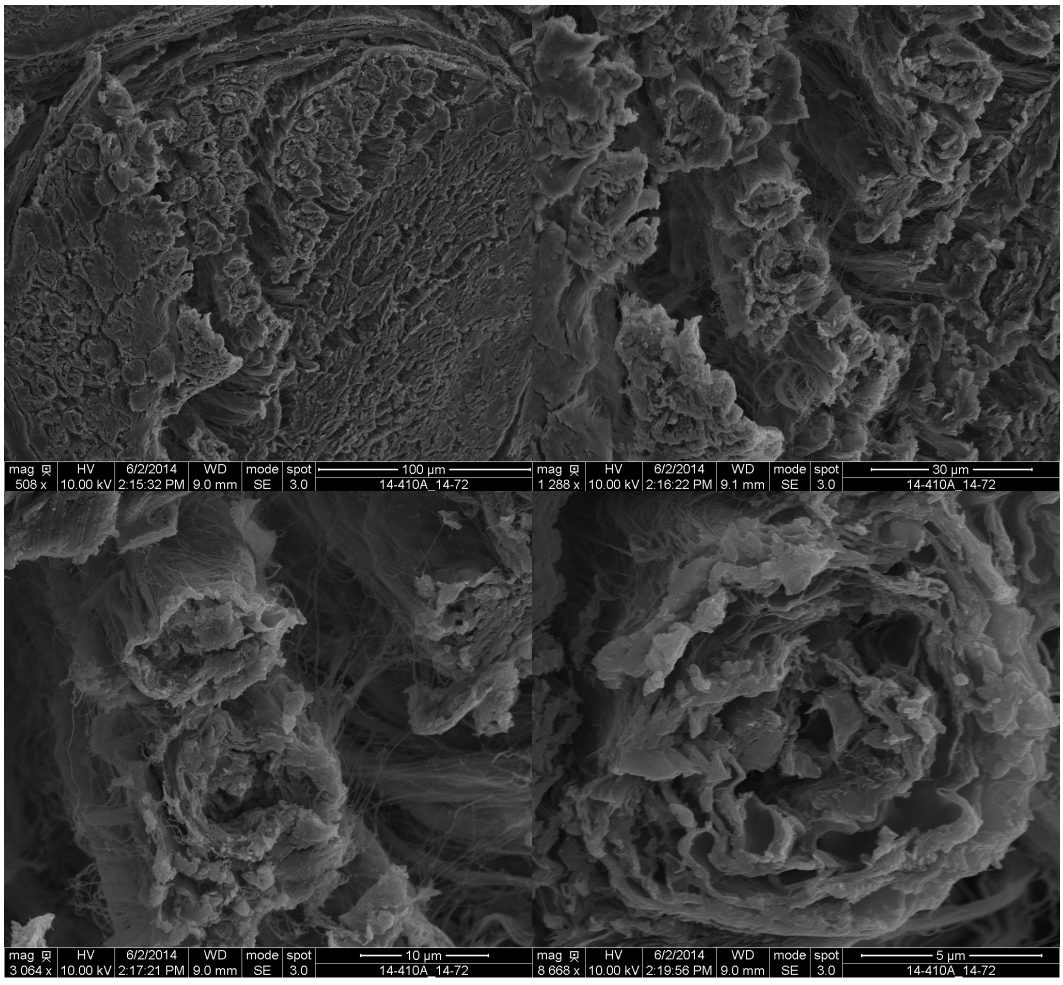

Figure 7. Scanning electron microscopy of Freeze-Thaw cycled acellular nerve allograft at a) 508x, b) 1288x, c) 3064x and d) 8668x magnification.

Nerve growth factor retention in acellular nerve allografts

Twelve acellular nerve allografts processed by Sondell, Hudson or Freeze-Thaw methods were evaluated for nerve growth factor retention in vitro over a period of 21 days under infinite sink conditions (Fig. 8a). Sondell-processed allografts were found to have far superior NGF loading (9.25 ± 1.09 ng/mg) after incubation for 1 hour in storage solution at 37 °C. Freeze-Thaw and Hudson processed allografts showed low initial NGF loading after 1 hour in storage solution, 1.81 ± 0.60 ng/mg and 1.30 ± 0.36 ng/mg respectively. In Sondell-processed allografts, approximately half of the loaded NGF is released in 1 d, but the remainder is released slowly over following 3 weeks (0.939 ug/mg/wk, $r^2 = 0.962$, $p<0.0001$). After 21 d of incubation, Sondell allografts have significantly greater retained NGF (1.55 ± 0.25 ng/mg) compared to Hudson (0.60 ± 0.17 ng/mg, p=0.013) and Freeze-Thaw (0.35 ± 0.16 ng/mg, p=0.003) nerve allografts and compared to unprocessed nerve immediately after NGF incubation (0.18 ± 0.01 ng/mg, p=0.002) (Fig. 8b).

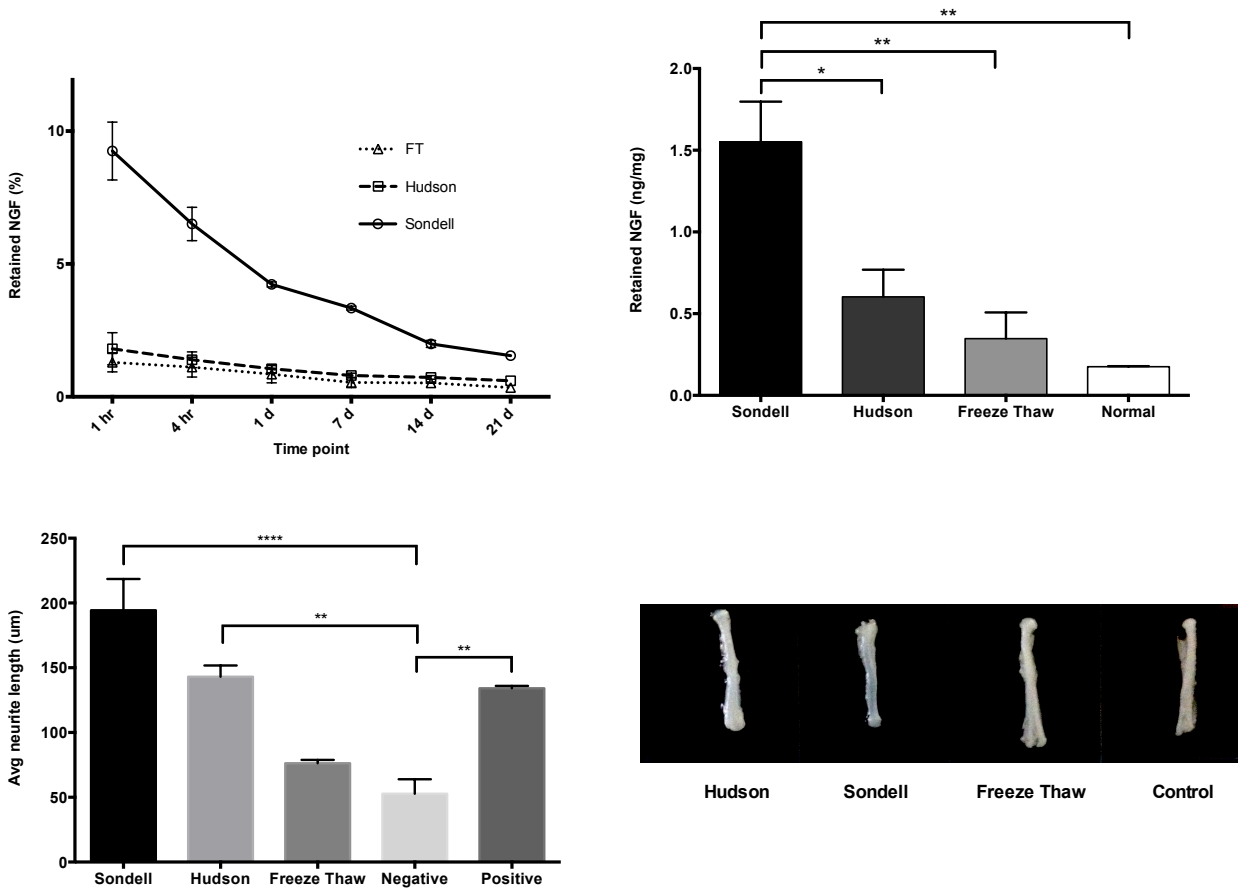

Figure 8. In vitro release (top) and bioactivity assay (bottom) of nerve growth factor in Sondell, Hudson and freeze-thaw processed nerve allografts.

NGF released from day 7 of allograft incubation was used to evaluate bioactivity of the retained growth factor in primary embryonic dorsal root ganglion neuron cultures (Fig. 8c and 9). After 7 d of DRG neuron incubation, NGF released from Sondell and Hudson allografts produced neurite outgrowth greater than or equal to the positive control media (50 ng/ml NGF supplemented). However, NGF released from freeze-thaw allograft was not significantly different from negative control media (NGF absent). Although the concentrations of Hudson and Freeze-Thaw allograft NGF were nearly equivalent, significantly greater bioactivity was found for Hudson-derived NGF. This may indicate that NGF bound to freeze-thaw

processed nerves is modified by other unknown graft constituents (e.g. plasma components) or environmental conditions (e.g. pH), which could diminish its bioactivity.[30]

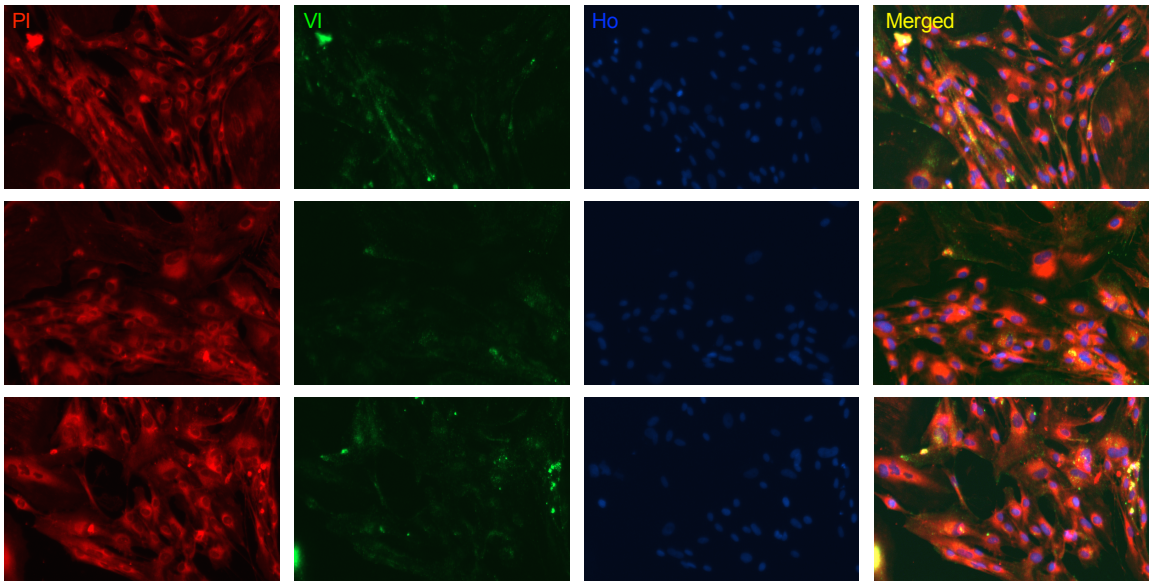

Figure 9. Bioactivity assay of nerve growth factor released from Sondell (*top*), Hudson (*middle*) and freeze-thaw (*bottom*) processed nerve allografts. PI = plasma membrane indicator, VI = viability indicator, Ho = Hoechst 33342. Neurite outgrowth was measured in neurons positively stained with the membrane and viability indicators.

In vivo assessment of NGF eluting acellular nerve allografts

Eight adult Sprague-Dawley rats were implanted with 1-cm interposition allografts in a sciatic nerve injury using NGF-loaded (n=4) or control (n=4) Sondell-processed nerve allografts. Neurite outgrowth was assessed mid-graft with GAP-43 immunohistochemistry. Robust neurite outgrowth was visible in all NGF-loaded nerve allografts and was largely organized in regenerative clusters within the perineurium. Control nerve allografts showed few regenerating neurites and most were found scattered in the epineurial connective tissue.

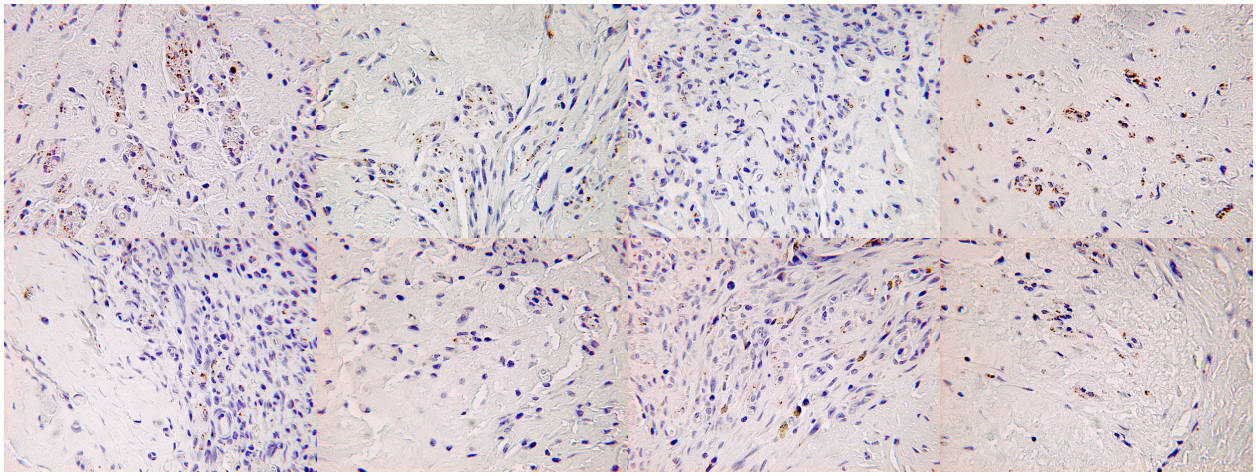

Figure 10. GAP-43 immunohistochemistry of mid-graft sections of NGF-loaded (*top*) and control (*bottom*) Sondell-processed acellular nerve allografts.

Discussion

This study has several important findings that could be impactful in the practice of peripheral nerve repair. In our characterization of different methods of decellularization using scanning electron microscopy and immunohistochemistry, we found that Sondell allografts had the best preservation of extracellular matrix architecture and clearance of cellular debris. This is different from the initial findings by Hudson and coworkers, and may have important implications in the manufacturing of current commercially available acellular nerve allografts. Specifically, disorganized collagen fibers and loss of basal lamina tubes in Hudson allografts may hinder outgrowth and diffusion, and may indicate loss of important growth factor-binding ECM proteins. Similar to previous affinity-based delivery systems, the release of NGF from loaded nerve allografts was found to have an initial burst in the first 24 hours followed by a slow release over 21 days. Sondell allografts retained much higher molar ratios of NGF than Hudson and freeze-thaw allografts, and retained greater than 35% of the initial NGF load at 7 days and greater than 15% at 21 days. The cellular debris and ECM disruption observed in Hudson and freeze-thaw allografts may contribute to lower NGF diffusion and available binding sites during loading.

One major limitation of this study is the use of a rodent model of sciatic nerve injury, which cannot accurately reproduce large (>2 cm) nerve gap injuries. Rat sciatic nerve injury is a well-established research model for peripheral nerve repair, but large animal studies would be required prior to translating these findings. Another major limitation of this study is the lack of a complete proteomic characterization of the acellular nerve allografts. Future studies are recommended to determine the proteomic composition and molecular-level binding of NGF in acellular nerve allografts.

Conclusion

In this study we established the feasibility of affinity-based delivery of neurotrophins within acellular nerve allografts. We found that the extracellular matrix characteristics of Sondell-processed nerve allografts showed the greatest NGF binding affinity and release profile. Initial rodent studies provide evidence of improved early neurite regeneration in NGF-eluting acellular nerve allografts. Additionally, we found that Sondell-processed nerve allografts showed the greatest clearance of cellular debris and preservation of nerve architecture.

References

[1] S. W. Wolfe, R. N. Hotchkiss, W. C. Pederson, and S. H. Kozin, *Green's Operative Hand Surgery E-Book: Expert Consult: Online and Print, Volume 2*. Elsevier Health Sciences, 2010.

[2] W. Z. Ray and S. E. Mackinnon, "Management of nerve gaps: autografts, allografts, nerve transfers, and end-to-side neurorrhaphy," *Exp Neurol*, vol. 223, no. 1, pp. 77–85, 2010.

[3] P. M. Crapo, T. W. Gilbert, and S. F. Badylak, "An overview of tissue and whole organ decellularization processes.," *Biomaterials*, vol. 32, no. 12, pp. 3233–43, Apr. 2011.

[4] G. Lundborg, L. B. Dahlin, N. Danielsen, R. H. Gelberman, F. M. Longo, H. C. Powell, and S. Varon, "Nerve regeneration in silicone chambers: influence of gap length and of distal stump components.," *Exp. Neurol.*, vol. 76, no. 2, pp. 361–75, May 1982.

[5] M. F. Meek and J. H. Coert, "Clinical use of nerve conduits in peripheral-nerve repair: review of the literature.," *J. Reconstr. Microsurg.*, vol. 18, no. 2, pp. 97–109, Feb. 2002.

[6] E. L. Whitlock, T. M. Myckatyn, A. Y. Tong, A. Yee, Y. Yan, C. K. Magill, P. J. Johnson, and S. E. Mackinnon, "Dynamic quantification of host Schwann cell migration into peripheral nerve allografts," *Exp Neurol*, vol. 225, no. 2, pp. 310–319, 2010.

[7] A. Hayashi, J. W. Koob, D. Z. Liu, A. Y. Tong, D. A. Hunter, A. Parsadanian, S. E. Mackinnon, and T. M. Myckatyn, "A double-transgenic mouse used to track migrating Schwann cells and regenerating axons following engraftment of injured nerves," *Exp Neurol*, vol. 207, no. 1, pp. 128–138, 2007.

[8] M. Saheb-Al-Zamani, Y. Yan, S. J. Farber, D. A. Hunter, P. Newton, M. D. Wood, S. A. Stewart, P. J. Johnson, and S. E. Mackinnon, "Limited regeneration in long acellular nerve allografts is associated with increased Schwann cell senescence.," *Exp. Neurol.*, vol. 247, pp. 165–77, Sep. 2013.

[9] J. J. Gentry, P. A. Barker, and B. D. Carter, "The p75 neurotrophin receptor: multiple interactors and numerous functions," *Prog Brain Res*, vol. 146, pp. 25–39, 2004.

[10] S. O. Yoon, P. Casaccia-Bonnefil, B. Carter, and M. V Chao, "Competitive signaling between TrkA and p75 nerve growth factor receptors determines cell survival," *J Neurosci*, vol. 18, no. 9, pp. 3273–3281, 1998.

[11] B. D. Carter, C. Kaltschmidt, B. Kaltschmidt, N. Offenhäuser, R. Böhm-Matthaei, P. A. Baeuerle, and Y. A. Barde, "Selective activation of NF-kappa B by nerve growth factor through the neurotrophin receptor p75," *Science (80-.).*, vol. 272, no. 5261, pp. 542–545, 1996.

[12] M. A. Tria, M. Fusco, G. Vantini, and R. Mariot, "Pharmacokinetics of nerve growth factor (NGF) following different routes of administration to adult rats.," *Exp. Neurol.*, vol. 127, no. 2, pp. 178–83, Jun. 1994.

[13] S. Madduri, K. Feldman, T. Tervoort, M. Papaloïzos, and B. Gander, "Collagen nerve conduits releasing the neurotrophic factors GDNF and NGF," *J Control Release*, vol. 143, no. 2, pp. 168–174, 2010.

[14] S. Madduri, P. di Summa, M. Papaloïzos, D. Kalbermatten, and B. Gander, "Effect of controlled co-delivery of synergistic neurotrophic factors on early nerve regeneration in rats," *Biomaterials*, vol. 31, no. 32, pp. 8402–8409, 2010.

[15] J. G. Spector, P. Lee, A. Derby, G. E. Frierdich, G. Neises, and D. G. Roufa, "Rabbit facial nerve regeneration in NGF-containing silastic tubes.," *Laryngoscope*, vol. 103, no. 5, pp. 548–58, May 1993.

[16] Y. Chen, “Facial nerve regeneration in the silicone chamber: The influence of nerve growth factor,” *Exp. Neurol.*, vol. 103, no. 1, pp. 52–60, Jan. 1989.

[17] J. G. Spector, A. Derby, P. Lee, and D. G. Roufa, “Comparison of Rabbit Facial Nerve Regeneration in Nerve Growth Factor-Containing Silicone Tubes to that in Autologous Neural Grafts,” *Ann. Otol. Rhinol. Laryngol.*, vol. 104, no. 11, pp. 875–885, Nov. 1995.

[18] C. B. Jenq, L. L. Jenq, and R. E. Coggeshall, “Nerve regeneration changes with filters of different pore size.,” *Exp. Neurol.*, vol. 97, no. 3, pp. 662–71, Sep. 1987.

[19] H. B. Wang, M. E. Mullins, J. M. Cregg, A. Hurtado, M. Oudega, M. T. Trombley, and R. J. Gilbert, “Creation of highly aligned electrospun poly-L-lactic acid fibers for nerve regeneration applications,” *J Neural Eng*, vol. 6, no. 1, p. 16001, 2009.

[20] M. D. Wood, D. Hunter, S. E. Mackinnon, and S. E. Sakiyama-Elbert, “Heparin-binding-affinity-based delivery systems releasing nerve growth factor enhance sciatic nerve regeneration,” *J Biomater Sci Polym Ed*, vol. 21, no. 6, pp. 771–787, 2010.

[21] M. D. Wood, A. M. Moore, D. A. Hunter, S. Tuffaha, G. H. Borschel, S. E. Mackinnon, and S. E. Sakiyama-Elbert, “Affinity-based release of glial-derived neurotrophic factor from fibrin matrices enhances sciatic nerve regeneration,” *Acta Biomater*, vol. 5, no. 4, pp. 959–968, 2009.

[22] M. D. Wood, M. R. MacEwan, A. R. French, A. M. Moore, D. A. Hunter, S. E. Mackinnon, D. W. Moran, G. H. Borschel, and S. E. Sakiyama-Elbert, “Fibrin matrices with affinity-based delivery systems and neurotrophic factors promote functional nerve regeneration,” *Biotechnol Bioeng*, vol. 106, no. 6, pp. 970–979, 2010.

[23] M. M. Martino, P. S. Briquez, E. Güç, F. Tortelli, W. W. Kilarski, S. Metzger, J. J. Rice, G. a Kuhn, R. Müller, M. a Swartz, and J. a Hubbell, “Growth factors engineered for super-affinity to the extracellular matrix enhance tissue healing.,” *Science*, vol. 343, no. 6173, pp. 885–8, Feb. 2014.

[24] K. Vulic, M. M. Pakulska, R. Sonthalia, A. Ramachandran, and M. S. Shoichet, “Mathematical model accurately predicts protein release from an affinity-based delivery system.,” *J. Control. Release*, vol. 197, pp. 69–77, Jan. 2015.

[25] M. Sondell, G. Lundborg, and M. Kanje, “Regeneration of the rat sciatic nerve into allografts made acellular through chemical extraction.,” *Brain Res.*, vol. 795, no. 1–2, pp. 44–54, Jun. 1998.

[26] T. W. Hudson, S. Zawko, C. Deister, S. Lundy, C. Y. Hu, K. Lee, and C. E. Schmidt, “Optimized acellular nerve graft is immunologically tolerated and supports regeneration.,” *Tissue Eng.*, vol. 10, no. 11–12, pp. 1641–51, Jan. .

[27] C. A. Krekoski, D. Neubauer, J. Zuo, and D. Muir, “Axonal regeneration into acellular nerve grafts is enhanced by degradation of chondroitin sulfate proteoglycan.,” *J. Neurosci.*, vol. 21, no. 16, pp. 6206–13, Aug. 2001.

[28] M. I. Johnson, R. P. Bunge, and P. M. Wood, *Protocols for Neural Cell Culture*. Springer Science & Business Media, 2001, pp. 95–100.

[29] B. D. Trapp, S. B. Andrews, A. Wong, M. O'Connell, and J. W. Griffin, "Co-localization of the myelin-associated glycoprotein and the microfilament components, F-actin and spectrin, in Schwann cells of myelinated nerve fibres.," *J. Neurocytol.*, vol. 18, no. 1, pp. 47–60, Feb. 1989.

[30] C. B. Nguyen, E. Szonyi, M. D. Sadick, T. E. Hotaling, J.-L. Mendoza-Ramirez, and E. Escandon, "Stability and Interactions of Recombinant Human Nerve Growth Factor in Different Biological Matrices: In Vitro and In Vivo Studies," *Drug Metab. Dispos.*, vol. 28, no. 5, pp. 590–597, May 2000.

CHAPTER IV

CHARACTERIZATION OF PERIPHERAL NERVE INJURY USING DIFFUSION TENSOR IMAGING

Introduction

Neurotmesis or peripheral nerve transection is a common, but difficult to distinguish, diagnosis following traumatic injury. Electrodiagnostic studies and clinical examination are standard practice for peripheral nerve assessment, but neither can perfectly discriminate a severe nerve laceration from a self-resolving axonotmetic or neurapraxic injury in the acute setting [1]. Additionally, Wallerian degeneration may take up to four weeks before these injuries can be accurately diagnosed in the absence of exploratory surgery [2]. This is also true for peripheral nerve repair where it may take up to a year, depending on the site and severity of injury, before targets are reinnervated and surgical outcome is known. Although a "watch and wait" approach might appear to be the optimal conservative management, the time following a severe Sunderland fourth or fifth degree peripheral nerve lesion is critical to recovery [3]. Failure to microsurgically repair a nerve in a timely manner may result in irreversible muscle atrophy, weakness, paralysis or formation of painful traumatic neuromas [3].

Peripheral nerve injury is one of the few acute neurologic disorders in which imaging is not standard-of-care. Magnetic resonance neurography (MRN) leverages the microstructural features of axonal bundles to produce enhancement of peripheral nerves in magnetic resonance imaging (MRI) [4]–[8]. Nerves

normally exhibit a moderate signal on T2-weighted sequences, but they become hyperintense following injury due to prolongation of the T2-relaxation time [9]. While this can be sensitive marker of peripheral nerve pathology, conventional T2-weighted MRI lacks specificity for type and severity of nerve injury, [10], [11]. In the most severe cases of nerve injury involving gaps, MRN is capable of detecting nerve discontinuity [12]. However, over half of all high-grade nerve transections have no gap or minimal gap present.

Diffusion tensor imaging (DTI) is an MRI sequence that leverages the anisotropic diffusion of water molecules through axons to visualize neural tracts and assess microstructural features. DTI parameters, such as fractional anisotropy (FA), mean diffusivity (MD) and individual eigenvalues (λ_1, λ_2, λ_3) are able to quantify microstructural characteristics of nerves, such as axon density and myelin thickness [13]. In the CNS, DTI has been particularly useful in detecting axonal pathology in traumatic brain injury and spinal cord injury [14], [15]. Multiple investigators have evaluated DTI for detecting peripheral nerve crush and traction nerve injuries, which show significant changes in FA following injury [16]–[19]. However, limited data exist on high-grade nerve lacerations and there are no prior animal studies of DTI following microsurgical coaptation.

The ability to non-invasively assess axonal integrity could have vast implications in the management on peripheral nerve disorders. In the case of traumatic nerve injury, an accurate non-invasive measurement of axonal continuity could assist in surgical planning and post-operative management [4]. Iatrogenic peripheral nerve injury may also occur during certain medical procedures, such as nerve blocks, leading to an expensive and time-consuming neurologic and musculoskeletal workup [20]. DTI may be able to quickly diagnose these conditions and expedite therapy. Lastly, there has recently been growing interest in neuromodulatory therapy, which leverages the peripheral nerve tracts as targets for electrophysiological interventions. As peripheral nerve interventions are developed, it will be important to have non-invasive tools for diagnosis and management of adverse events, e.g. needle injuries. The specificity of DTI for axonal tracts makes it an ideal candidate for guiding these cases.

Peripheral nerve research may also benefit from DTI. Nerve regeneration models are highly dependent on behavioral testing and histology, which require large animal trials with multiple endpoints and error-prone assessments, such as sciatic functional index [21], [22]. High-resolution DTI may not only provide real-time, non-invasive measurements of axon viability, but also allow for several intermediate measurements of nerve recovery in survival studies. This could reduce the large number of animals required in nerve regeneration studies in addition to providing greater understanding of the regeneration timeline.

As DTI can accurately detect acute peripheral nerve crush and traction injuries, we hypothesized that high-resolution diffusion tensor imaging could accurately distinguish acute peripheral nerve transection lesions from intact nerve in the absence of macroscopic discontinuity. We tested this hypothesis using a complete and partial rat sciatic nerve injury model and high-resolution DTI at 4.7 T. Immediately following injury, sciatic nerves were microsurgically repaired to maintain close approximation of the epineurium, mimicking a lesion that would be difficult to detect with conventional MR imaging. In addition to determining the diagnostic capabilities of DTI in high-grade nerve lesions, this study provides a baseline for post-operative evaluation of peripheral nerve repairs using DTI.

Materials and Methods

Experimental design

The objective of this study was to evaluate the accuracy of DTI parameters, including fractional anisotropy (FA), mean diffusivity (MD), radial diffusivity ($\lambda_\perp$) and individual eigenvalues (λ_1, λ_2, λ_3) in detecting acute peripheral nerve transection. This study was performed using a rat sciatic nerve injury

model with sham, partial and complete transection injuries. Diffusion tensor imaging was performed on preparations of excised sciatic nerve and amputated hind limbs following fixation.

Animal use

Adult female Sprague Dawley rats aged 10-12 wk (200-250g; Charles River Lab) were used in the experiments. Rats were housed in central animal care facility and provided food and water *ad libitum*. All study procedures involving animals were approved by our institutional animal care and use committee.

Sciatic nerve injury

In each rat, the left hindquarter was shaved and the lateral thigh was incised from the sciatic notch to the popliteal fossa. The biceps femoris was reflected to expose the sciatic nerve. Surrounding fascia was sharply dissected and the sciatic nerve mobilized. The injury was created by completely or partially transecting the sciatic nerve with extra fine Vannas microsurgical scissors (RS-5640, Roboz Surgical Instrument, Gaithersburg, MD, USA). In partial transections, approximately 25% or 50% of the nerve diameter was advanced onto the cutting edge of the scissor under high magnification. Sham nerves were mobilized and not transected. Microsurgical suturing of the epineurium was performed on injured nerves to control for variable nerve gaps and to stabilize injury sites. The muscle was repaired and skin incision closed in a subgroup of rats for *in situ* imaging. All rats were sacrificed at 1h post-injury with perfusion fixation using 4% PFA in PBS. The sciatic nerve was excised, straightened on a wood dowel and incubated in 4% glutaraldehyde/0.5% PFA in PBS at 4 °C. Hindquarter amputation was performed on the

subgroup of rats with closed wounds and the amputated leg was incubated in 4% glutaraldehyde/0.5% PFA in PBS at 4 °C.

Tissue sample preparation

After 24h of post-fixation, excised nerves were placed in PBS + 2 mM Gd-DTPA (Magnevist, Bayer HealthCare, Wayne, NJ, USA) at 4 °C for at least 24h before imaging. For imaging, excised nerves were trimmed to ≈ 1 cm in length (with the injury site centered) and placed in 2-mm outer diameter glass capillary tubes filled with a perfluropolyether liquid (Fomblin, Solvay Solexis, Thorofare, NJ, USA) for susceptibility matching, preventing tissue dehydration, and a signal-free background. For higher throughput, six excised sciatic nerves in a hexagonal arrangement were imaged simultaneously. Hind limb samples were post-fixed for a period of 1 week, followed by at least 1 week of washing in PBS + 2 mM Gd-DTPA before imaging. For imaging, hind limbs were placed in MR-compatible tubes filled with perfluoropolyether liquid.

Diffusion tensor magnetic resonance imaging

MR imaging was performed on a 4.7T 31-cm horizontal bore Agilent DirectDrive scanner (Agilent Technologies, Santa Clara, CA) using a 38-mm Litz quadrature coil (Doty Scientific, Columbia, SC) for RF transmission and reception. For excised nerve imaging, FOV = 9.6 x 9.6 x 12 mm^3 and matrix size = 96 x 96 x 32 for a nominal resolution of 100 x 100 x 375 μm^3 (375 μm along the nerve). For hind limb imaging, FOV = 48.0 x 25.6 x 28.8 mm^3 and matrix size = 192 x 128 x 144 for a nominal resolution of

250 x 200 x 200 μm^3 (250 μm along the nerve). Diffusion tensor imaging data were acquired using a 3D diffusion-weighted spin-echo sequence with TR/TE = 170/23.0 ms and 12 signal averages for excised nerves, and TR/TE = 170/22.1 ms and 2 signal averages for hind limbs. Diffusion-weighting was achieved with δ/Δ = 4/12 ms, prescribed b-value = 2000 s/mm^2, and 6 directions. One b=0 image was acquired for a total of 7 images in a scan time of ≈ 12h.

DTI post-processing and analysis

Image data reconstruction and diffusion tensor calculations were performed using in-house written code in MATLAB (Mathworks, Natick, MA, USA). 3D image volumes were zero-padded x2 in each direction during reconstruction from k-space data. Diffusion tensors were estimated voxel-wise using a linear least-squares approach. From the diffusion tensor, DTI metrics including fractional anisotropy (FA) and mean, axial and radial diffusivity (MD, AD, and RD, respectively) were computed on a voxel-wise basis. DTI tractography was performed using the ExploreDTI toolbox [30].

Histology

After completion of imaging, the distal end of the nerve was trimmed to provide a fresh stump and chloromethylbenzamido-DiI membrane-labeling paste (NeuroTrace® CM-DiI Tissue Labeling Paste, Life Technologies, Carlsbad, CA), a carbocyanine dye derivative, was applied to the nerve ending using a 27-gauge needle. The dyed nerve ending was embedded in petroleum jelly to prevent leakage of the tracer

and placed in PBS-sodium azide (0.02%). The nerve was stored at 37 °C in the dark for 2 weeks to allow for tracing in the proximodistal direction through the injury site.

Segments of proximal and distal nerve were post-fixed in 10% neutral buffered formalin for 24 hours and paraffin embedded. Formalin-fixed paraffin embedded tissues were sectioned at 5 μm, placed on slides and warmed overnight at 60°C. Slides were deparaffinized with xylene and rehydrated with graded alcohols ending in distilled water. Slides were coverslipped with Prolong Gold antifade reagent with DAPI (Life Technologies, Carlsbad, CA), allowed to dry, and stored at 4°C until ready to view.

Digital images of slides were acquired with a Nikon AZ100M widefield fluorescence microscope. CM-DiI fluorescence was observed using a Cy-3 fluorescence filter with 548 nm/561 nm excitation/emission wavelengths. All sections were viewed with a 5X Zeiss Plan fluorescence objective without coverslips.

Statistical analysis

Prism 6 (GraphPad Software, La Jolla, CA) was used for plots and statistical calculations. Quantitative ROI statistics were performed with Student's *t* tests corrected for multiple comparisons using the Holm-Sidak method, with significance determined as $\alpha=0.05$.

Results

Injury validation

Various degrees of high-grade peripheral nerve injury were evaluated in this study using complete and partial transections of rat sciatic nerves followed by ex-vivo diffusion tensor imaging. The severity of nerve injury was predicted at time of surgery with careful microsurgical nerve dissection and verified with histology. CM-DiI membrane label was observed in all sham and transected nerves and therefore could not be used as a direct marker of injury severity, most likely due to tracer leakage or membrane approximation. However, during evaluation of the proximal nerve sections, we observed that injured nerves had greater axon caliber compared to sham nerves. Completely transected nerves were found to have significantly larger mean axon caliber compared to sham nerves ($p<0.01$; Fig. 1c). As observed in diffuse axonal injury (DAI) in brain white matter, cytotoxic edema occurs rapidly after damage to the axolemmal membrane causing axonal swelling [23]. In this study, we observed that mean axon caliber also scaled with the predicted severity of nerve injury (Fig. 1d), with moderate correlation of predicted percentage of injured axons and mean axon caliber ($r^2=0.60$, $p=0.002$). There was wide variability in axon caliber in nerves predicted to be 75% transected, which we suspect to be due to surgical error. Removing the 75% transected nerves from the statistical analysis improved the correlation of predicted injury severity and mean axon caliber ($r^2=0.82$, $p=0.0001$).

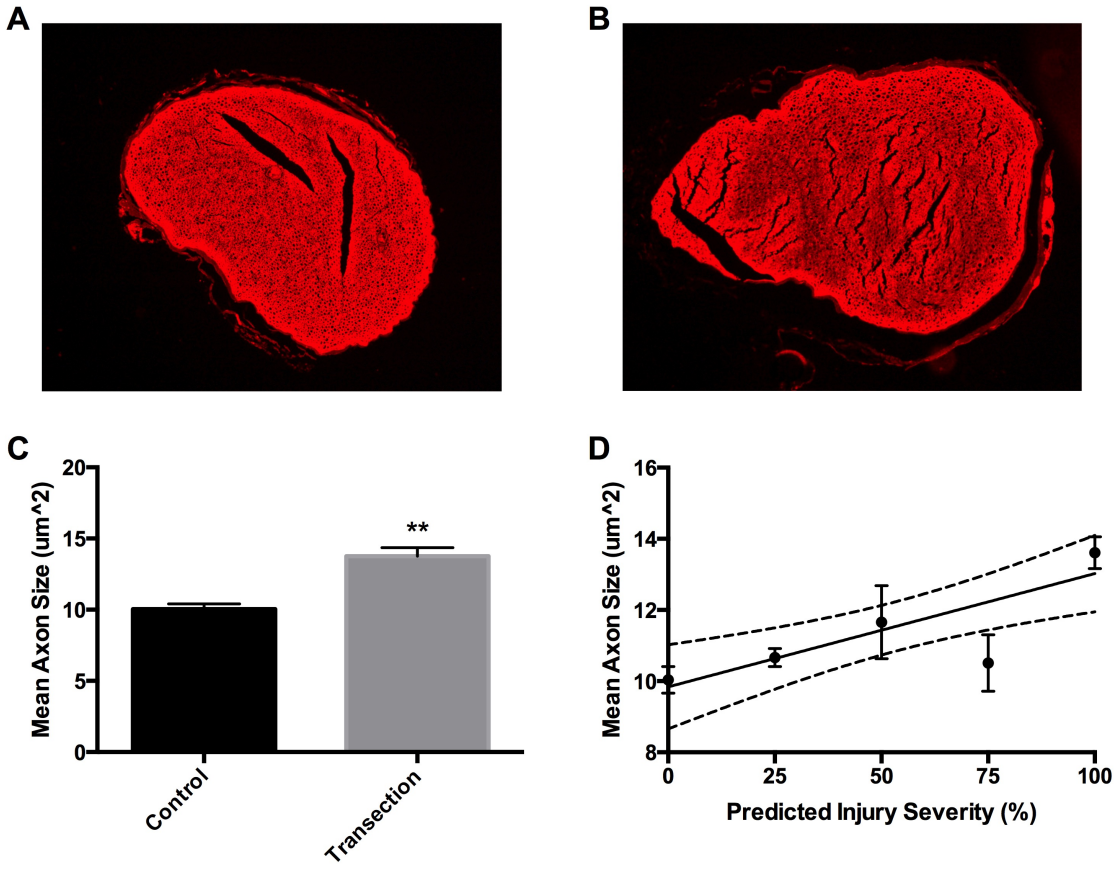

Figure 1. Predicted nerve injury severity correlated with proximal axon caliber. Representative fluorescent microscopy images of CM-DiI membrane label in (**A**) sham and (**B**) completely transected sciatic nerves. Axoplasm is visible as holes in the center of red membrane rings. (**C**) Axon caliber was measured 3 mm proximal to the injury site for all axons visible in the axial cross-sections of sham and completely transected nerves (mean ± SEM; $N = 6$, $^{**}P$-value $< 10^{-2}$, unpaired t test with Welch's correction). (**D**) Mean axon caliber correlated moderately with the predicted injury severity ($r^2 = 0.59$; $N = 15$, P-value $< 10^{-2}$). However, correlation strongly improved after removing the 75% predicted-injury nerves ($r^2 = 0.82$; $N = 12$, P-value $< 10^{-3}$). Dashed lines indicate the 95% confidence interval.

DTI of completely transected nerves

Diffusion tensor images of excised sciatic nerves were evaluated at three regions-of-interest (ROI) – injury site, 3-mm proximal and 3-mm distal. To prevent partial volume effects, a margin of 100-μm was excluded from the ROI. This also prevented the inclusion of suture material in ROI calculations, since knots are limited to the outermost epineurium. Fractional anisotropy (FA), mean diffusivity (MD) and eigenvalues (λ_1, λ_2, λ_3) were measured for each ROI (Fig. 2a-c). As expected, the fractional anisotropy was significantly decreased at the injury sites of transected compared to sham rats ($p<0.01$). Although not as strong as at the injury site, the proximal ROI of transected nerves also had lower FA compared to sham rats ($p<0.01$). While the drop in FA at the injury site indicates axonal loss, the proximal ROI changes are most likely due to edema following nerve injury causing an increase in extracellular fluid compartment as well as an increase in axonal edema, which would be expected to decrease FA while simultaneously increasing MD and eigenvalues. Although MD was significantly lower at the injury site ($p<0.01$) and unchanged in the proximal and distal ROIs, the minor eigenvectors showed an increasing trend at all ROIs in transected nerves compared to sham rats (Fig. 2c). Additionally, radial diffusivity ($\lambda_\perp$), calculated as $(\lambda_2 + \lambda_3)/2$, was significantly increased in the injury site ($p<0.05$) and proximal ROI ($p<0.05$) of transected nerves compared to sham rats. We observed larger variance in distal ROI quantitative measurements, which may be due to variation in fascicular branching at this level in the sciatic nerve. Receiver-operator characteristic (ROC) curves were evaluated for injury-site DTI measurements (Fig. 2d). Injury-site FA produces a near-perfect ROC curve (AUC = 1.000, $p<0.001$), but a larger sample size would be required to prevent type II error. Table 1 shows the calculated sensitivities and specificities of different FA thresholds for diagnosing complete nerve transection.

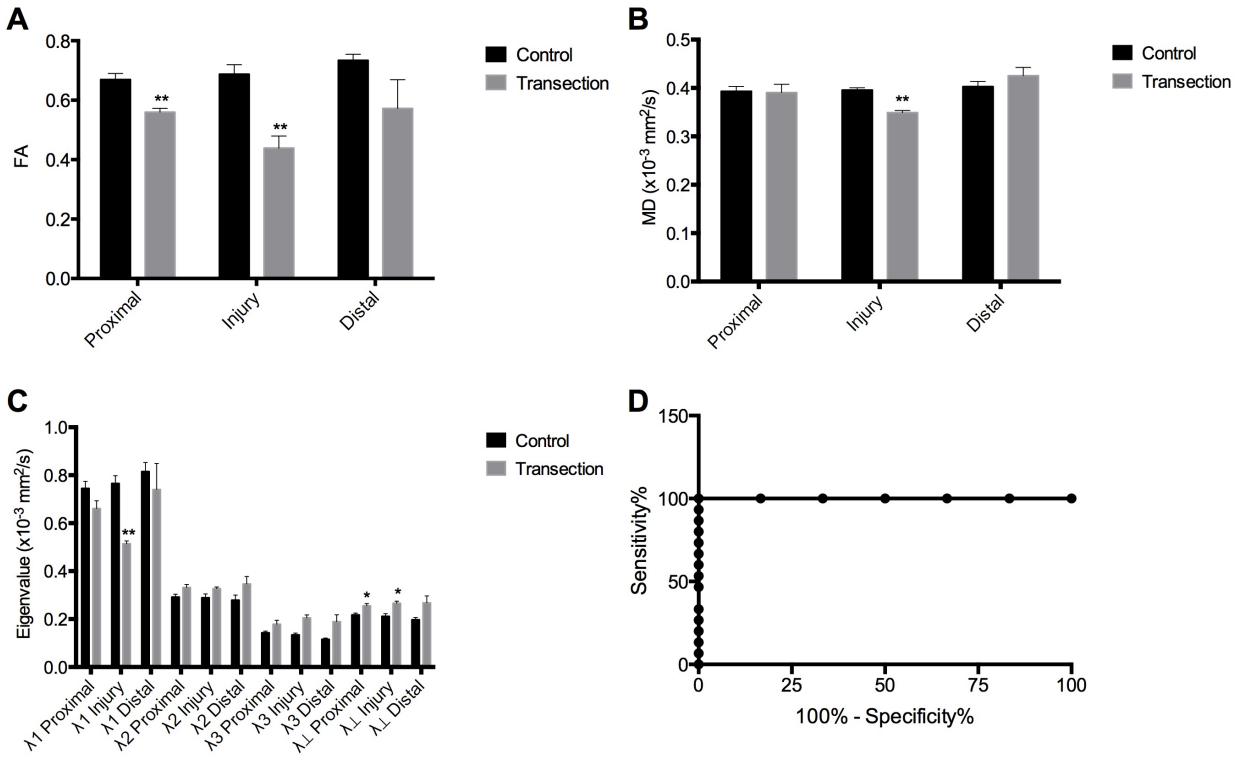

Fig. 2. FA detected complete nerve transection with high sensitivity and specificity. (**A**) FA was reduced at and proximal to injury sites (mean ± SEM; $N = 6$, $^{**}P$-value < 10^{-2}, unpaired t tests corrected for multiple comparisons using the Holm-Sidak method). (**B**) MD was reduced only within injury sites (mean ± SEM; $N = 6$, $^{**}P$-value < 10^{-2}, unpaired t tests corrected for multiple comparisons using the Holm-Sidak method). (**C**) Independent eigenvalues (λ_1, λ_2, λ_3) and radial diffusivity ($\lambda_\perp$) were measured at proximal, injury and distal regions. Axial diffusivity (λ_1) was reduced within injury sites and radial diffusivity was increased at and proximal to injury sites (mean ± SEM; $N = 6$, $^{*}P$-value < 0.05, $^{**}P$-value < 10^{-2}, unpaired t tests corrected for multiple comparisons using the Holm-Sidak method). (**D**) Receiver operative characteristic (ROC) curve analysis of FA shows high sensitivity and specificity for detection of any nerve injury (AUC = 1.00; $N = 21$, P-value < 10^{-3})

Continuous fiber tractography was performed with a maximum 45° angle and threshold FA of 0.49, corresponding to one standard deviation above the mean FA of all injury sites. Continuous tracts were observed throughout the body of each sham nerve (Fig. 3a), while there were multiple discontinuities present in transected nerves (Fig. 3b), particularly at the injury site. Fewer tracts were visible in the proximal segments of injured nerves, most likely due to reduced FA from tissue edema. Additionally, the number of continuous tracts seeded proximally and passing through the injury site and distal ROI were significantly lower in transected nerves compared to sham rats ($p<0.01$), (Fig. 3c). Principal diffusion vectors at injury sites were also observed to be more heterogeneous than sham nerves with greater variability in diffusion direction (Fig. 4).

Table. 1. ROC sensitivity and specificity of FA for all nerve injuries. FA thresholds for detection of any partial or complete nerve injury are shown with 95% confidence intervals (CI) and likelihood ratios.

FA threshold	Sensitivity%	95% CI	Specificity%	95% CI	Likelihood ratio
< 0.5630	100.0	78.20% to 100.0%	100.0	54.07% to 100.0%	
< 0.6197	100.0	78.20% to 100.0%	83.33	35.88% to 99.58%	6.000
< 0.6406	100.0	78.20% to 100.0%	66.67	22.28% to 95.67%	3.000
< 0.6838	100.0	78.20% to 100.0%	50.00	11.81% to 88.19%	2.000
< 0.7127	100.0	78.20% to 100.0%	33.33	4.327% to 77.72%	1.500
< 0.7219	100.0	78.20% to 100.0%	16.67	0.4211% to 64.12%	1.200

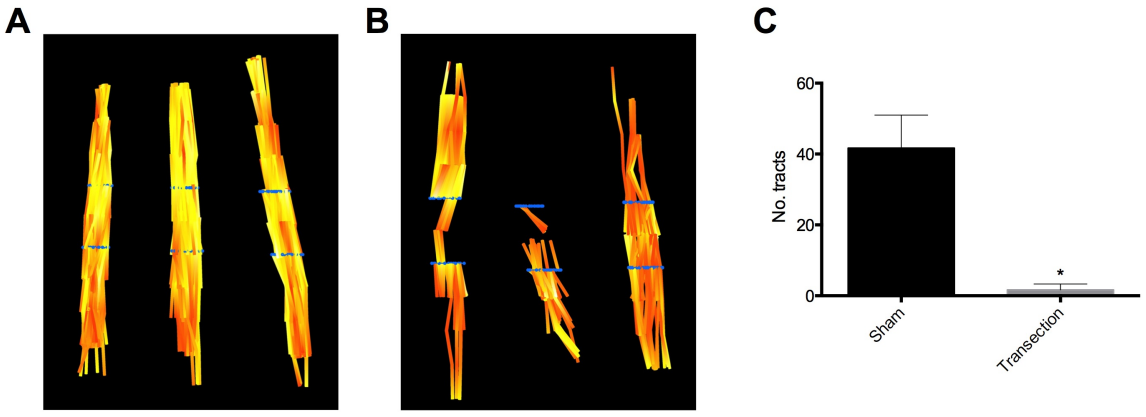

Fig. 3. Tract continuity diminished in completely transected nerves. Diffusion tensor tractography in sham (**A**) and completely transected (**B**) sciatic nerves. Blue lines indicate seed points for tractography located at 3-mm proximal and distal to the injury sites. (**C**) Continuous tract counts through the injury region were significantly reduced in completely transected nerves (mean ± SEM; $N = 6$, *P-value < 0.05, unpaired t test with Welch's correction).

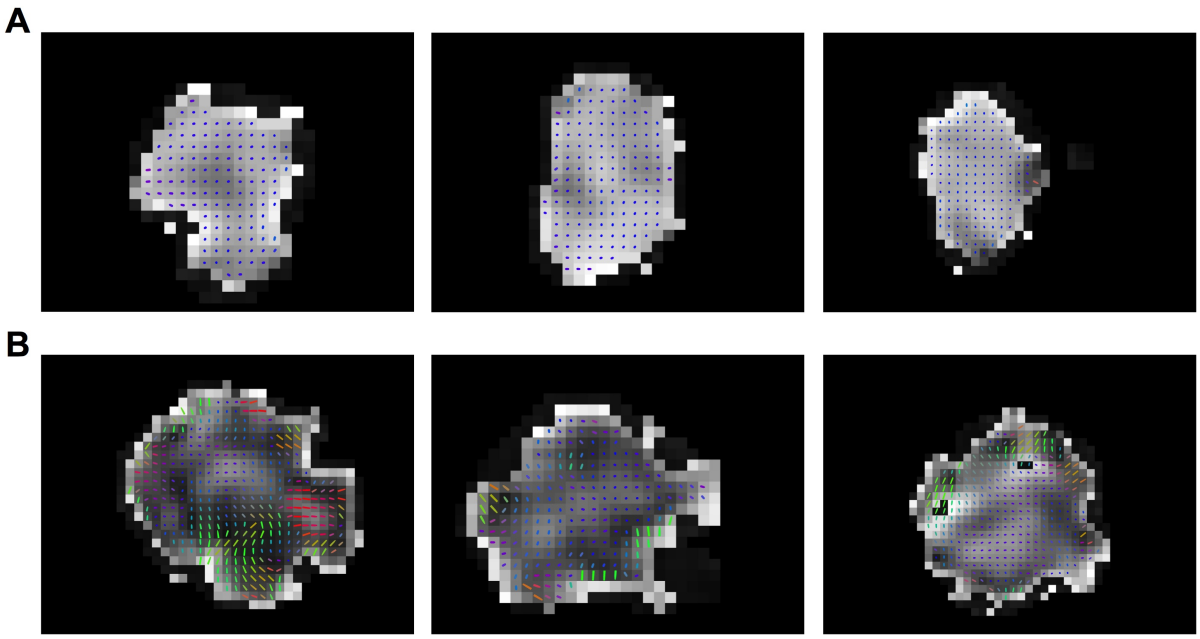

Fig. 4. Principal diffusion vectors are heterogeneous at transection sites. Principal diffusion vector glyphs overlaying the axial FA map of the injury region in sham (**A**) and completely transected (**B**) nerves. Colors indicate vector direction. Lighter regions of the map indicate higher FA.

DTI of partially transected nerves

For determining the degree to which partial severance of the sciatic nerve could be distinguished with DTI, we imaged partially transected nerves that were graded at the time of surgery as 25%, 50% or 75% nerve severance and validated histologically as described above. DTI parameters were evaluated at the injury ROI for each injured nerve and at the center of each sham nerve. Mean FA was significantly reduced in all injured nerves compared to sham nerves (Fig. 5a). However, there were no significant differences between the levels of injury. Mean FA of sham nerves was strongly correlated with the nerve axon count, but this relationship was not present in injured nerves (Fig. 5b). Interestingly, no significant differences were found in MD (Fig. 5c) or axial diffusivity ($\lambda_{\parallel}$) (Fig. 5e), as has been observed in prior studies of pre-degenerated contusive nerve injuries [18]. Following Wallerian degeneration, sciatic nerves have been shown to have normal MD, but markedly decreased axial diffusivity and increased radial diffusivity [24]. In this study, minor eigenvalues (λ_2, λ_3) and radial diffusivity ($\lambda_{\perp}$) were profoundly increased at all injury sites immediately following injury (Fig. 5e). This substantial difference could be the result of immediate membrane and myelin disruption present in severance but not contusive nerve injuries.

Although there was no significant correlation between eigenvalues and predicted degree of injury, there was a weak negative correlation between λ_2 and $\lambda_{\perp}$ to proximal axon caliber (Fig. 5g). If proximal axon caliber is a true reflection of axonal swelling following nerve injury, then this could indicate that λ_2 and $\lambda_{\perp}$ are inversely proportional to the degree of nerve severance following injury. Although this is counter-intuitive since both parameters were significantly increased following injury, it is likely that there are multiple microstructural factors contributing to these changes. One possible explanation is that severance largely increases λ_2 and $\lambda_{\perp}$ due to membrane and myelin disruption, while simultaneously and to a lesser extent decreasing due to immediate axonal swelling. Neither parameter was correlated to nerve axon count in sham or injured nerves.

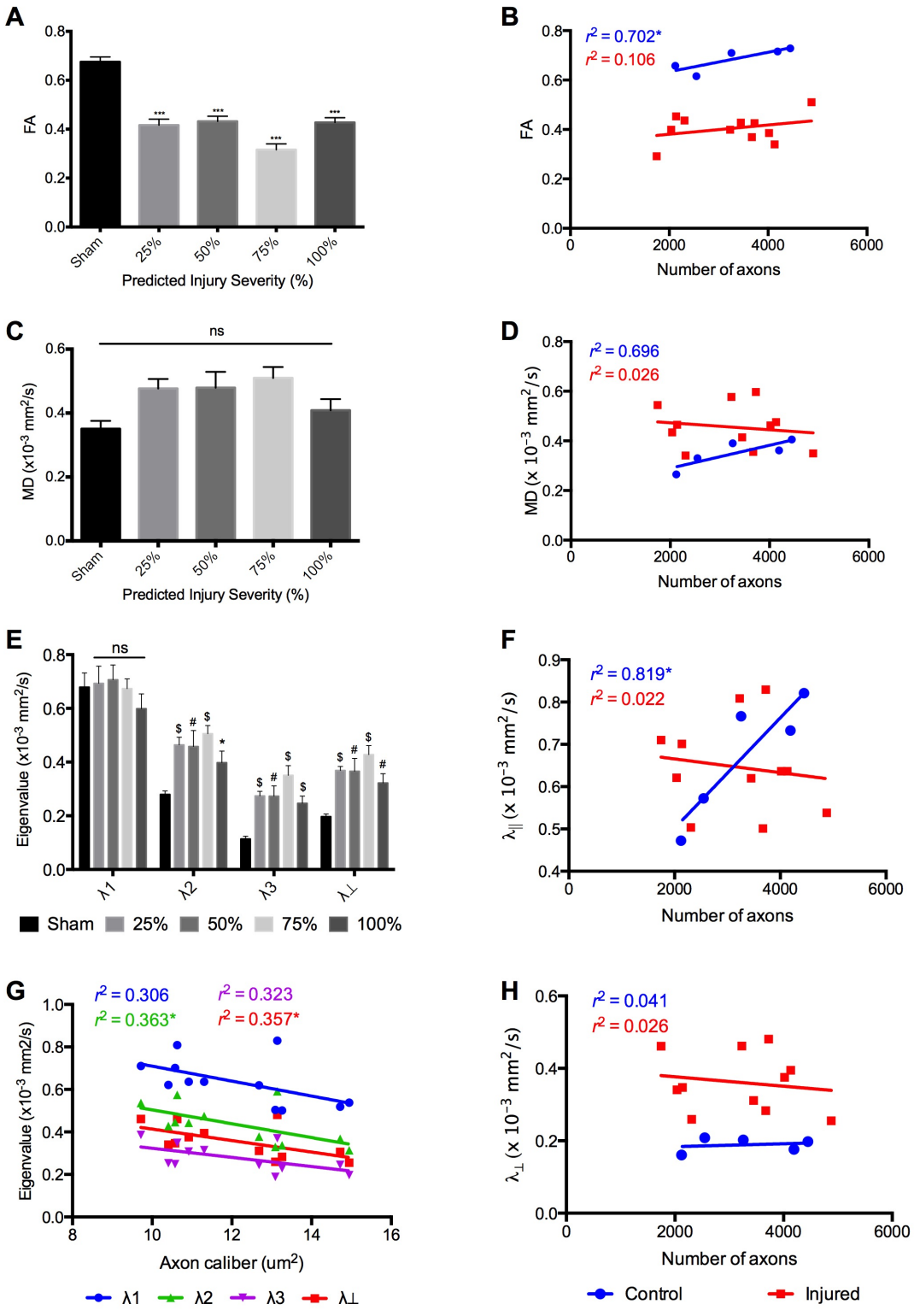

Fig. 5. FA and RD detected all partial injuries and RD correlated with injury severity. Quantitative analysis of DTI parameters in sham, partial and complete sciatic nerve transection injuries. (**A**) Fractional

anisotropy was similarly reduced in the injury region of all complete and partial nerve injuries (mean ± SEM; $N = 21$, ***P-value < 10^{-4}, ordinary one-way ANOVA corrected for multiple comparisons with Tukey's test). (**C**) Mean diffusivity showed a non-significant increase in all injury groups. (**E**) Minor eigenvalues and radial diffusivity were significantly increased in the injury region in all injury groups (mean ± SEM; $N = 21$, *P-value < 0.05, $^{\#}P$-value < 10^{-2}, $^{\$}P$-value < 10^{-3}, ordinary one-way ANOVA corrected for multiple comparisons with Tukey's test). There was no correlation of fractional anisotropy (**B**), mean diffusivity (**D**), axial diffusivity (**F**) or radial diffusivity (**H**) measured at injury sites with the number of axons in injured nerves. (**G**) Radial diffusivity was negatively correlated to axon caliber in injured nerves and indirectly to injury severity ($r^2 = 0.357$; *P-value < 0.05).

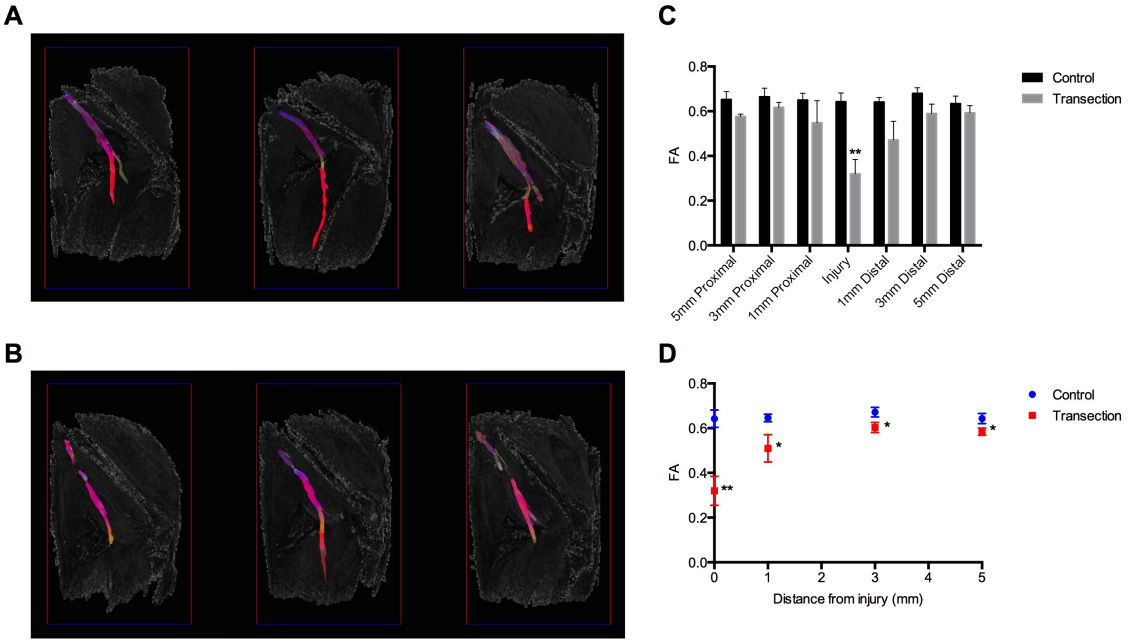

Fig. 6. FA remained sensitive to nerve transection in ex vivo hind limbs. Ex vivo diffusion tensor tractography of rat hind limbs with sham (**A**) and completely transected (**B**) sciatic nerves. (**C**) Fractional anisotropy measured at each proximal, injury and distal region (mean ± SEM; $N = 8$, **P-value < 10^{-2}, unpaired t tests corrected for multiple comparisons using the Holm-Sidak method). (**D**) Fractional anisotropy approached sham values with increasing distance from the injury site, but remained

significantly lower at all points (mean ± SEM; $N = 8$, *P-value < 0.05, **P-value < 10^{-2}, unpaired t tests corrected for multiple comparisons using the Holm-Sidak method).

DTI of hind limbs

As proof-of-concept, ex vivo imaging was performed on amputated rat hind limbs with sham or complete transection injuries. Tractography was performed with multiple seed points spaced 1-mm apart along the axial length of the sciatic nerve. We found that seeding from a single axial slice as was done in all excised nerves resulted in short tracts, even at low FA thresholds. By seeding from multiple axial slices along the nerve, we were able to capture the length of the nerve while continuing to observe discontinuities at all injury sites (Fig. 6 a-f). Quantitative DTI measurements were calculated at multiple ROIs – injury site, proximal (1-mm, 3-mm and 5-mm) and distal (1-mm, 3-mm and 5-mm). The additional proximal and distal ROIs were included in this analysis to compare effects of surrounding tissue inflammation and edema. Similar to excised nerves, FA was significantly reduced at the injury site of transected nerves (p<0.01) and to a lesser extent in the proximal and distal ROIs (Fig. 6g). We hypothesized that external tissue effects should be similar within the entire surgical site, while sciatic nerve injury effects should diminish with increasing distance from the injury site. This was confirmed by our measurements of FA at multiple distances from each injury site (Fig. 6h), in which the FA appears to reach an asymptote at 3-mm, but remains significantly lower than sham animals (p<0.05).

Discussion

Here we present findings that high-resolution DTI is capable of detecting acute peripheral nerve severance injuries in the absence of macroscopic nerve discontinuity. We also provide a baseline measurement of DTI parameters following microsurgical neurorrhaphy, which builds a foundation for the use of DTI in post-operative management. Importantly, intralesional fractional anisotropy was a highly sensitive and specific marker of nerve injury even with partial nerve lacerations, and unlike nerve crush injuries, there was a concurrent increase in radial diffusivity. Radial diffusivity following injury was also correlated to the degree of nerve severance. These findings are supported by prior studies of DTI following sciatic nerve transection or traction injuries [16], [17], and suggest that high resolution DTI may be capable of both diagnosis and grading of traumatic peripheral nerve injuries.

Prior studies evaluating DTI of peripheral nerve injuries have focused on the effects of crush or contusion with blunt force trauma [17]–[19]. Although nerve crush is a significant cause of morbidity typically occurring as a surgical complication, traumatic nerve injuries often involve partial or complete neurotmesis that can result in lifelong disability if not promptly diagnosed and microsurgically repaired [3]. Providing a new method of detecting nerve transection could prevent delays in surgical repair that lead to irreversible weakness, loss of function and other undesirable sequelae. Additionally, DTI could be highly valuable as a tool for assessing nerve repairs and determining when a revision surgery is necessary.

There are multiple limitations in this study. Most importantly, the majority of this study was conducted on excised sciatic nerves that had been cleaned and cross-linked in fixative prior to imaging. Fixation is known to reduce isotropic diffusion, but should have minimal effect on relative tissue anisotropy [25]. As observed in our hind limb imaging, surrounding tissue and edema confounds the in vivo nerve DTI signal. Although fractional anisotropy remained an accurate marker of traumatic nerve injury, tractography capabilities were limited and required a different approach for tract seeding. Use of a multi-compartment

diffusion MRI model such as diffusion basis spectrum imaging (DBSI) could isolate the confounding effects of edema and inflammation and improve nerve assessment [26], [27].

A second limitation of this study was the time required for high-resolution image acquisition, requiring up to twelve hours for one set of six nerves. For translating this technology, it will be critical to find the resolution and FOV that minimizes scan time while maintaining SNR and diagnostic accuracy. New high resolution DTI methods such as outer-volume suppression (OVS) and elliptically refocused zonally oblique multislice (eZOOM) have been developed which leverage reduced FOV imaging to significantly decrease dataset sizes and scan times up to eight-fold [28], [29]. SENSE and other parallel imaging techniques can be used in combination with reduced-FOV techniques to further reduce dataset sizes, but their use is limited by SNR reduction.

The benefits of DTI for non-invasive assessment of axonal pathology have been well established in the central and peripheral nervous systems. This study provides confirmation that high-resolution DTI is capable of acute diagnosis and grading of traumatic peripheral nerve injuries in a rat model. We have also provided an immediate baseline of DTI parameters following microsurgical coaptation of the sciatic nerve. Additional survival studies of traumatic peripheral nerve injury are needed to evaluate DTI as a tool for post-operative monitoring of nerve regeneration.

References

[1] G. A. Grant, R. Goodkin, and M. Kliot, “Evaluation and surgical management of peripheral nerve problems.,” *Neurosurgery*, vol. 44, no. 4, pp. 825–39; discussion 839–40, Apr. 1999.

[2] A. D. Gaudet, P. G. Popovich, and M. S. Ramer, “Wallerian degeneration: gaining perspective on inflammatory events after peripheral nerve injury.,” *J. Neuroinflammation*, vol. 8, no. 1, p. 110, Jan. 2011.

[3] W. W. Campbell, “Evaluation and management of peripheral nerve injury.,” *Clin. Neurophysiol.*, vol. 119, no. 9, pp. 1951–65, Sep. 2008.

[4] G. a Grant, G. W. Britz, R. Goodkin, J. G. Jarvik, K. Maravilla, and M. Kliot, “The utility of magnetic resonance imaging in evaluating peripheral nerve disorders.,” *Muscle Nerve*, vol. 25, no. 3, pp. 314–31, Mar. 2002.

[5] M. Pham, C. Wessig, J. Brinkhoff, K. Reiners, G. Stoll, and M. Bendszus, “MR neurography of sciatic nerve injection injury.,” *J. Neurol.*, vol. 258, no. 6, pp. 1120–5, Jun. 2011.

[6] M. Bendszus and G. Stoll, “Technology insight: visualizing peripheral nerve injury using MRI.,” *Nat. Clin. Pract. Neurol.*, vol. 1, no. 1, pp. 45–53, Nov. 2005.

[7] F. A. Howe, A. G. Filler, B. A. Bell, and J. R. Griffiths, “Magnetic resonance neurography.,” *Magn. Reson. Med.*, vol. 28, no. 2, pp. 328–38, Dec. 1992.

[8] A. G. Filler, F. A. Howe, C. E. Hayes, M. Kliot, H. R. Winn, B. A. Bell, J. R. Griffiths, and J. S. Tsuruda, “Magnetic resonance neurography.,” *Lancet*, vol. 341, no. 8846, pp. 659–61, Mar. 1993.

[9] B. D. Aagaard, D. a. Lazar, L. Lankerovich, K. Andrus, C. E. Hayes, K. Maravilla, and M. Kliot, “High-resolution Magnetic Resonance Imaging Is a Noninvasive Method of Observing Injury and Recovery in the Peripheral Nervous System,” *Neurosurgery*, vol. 53, no. 1, pp. 199–204, Jul. 2003.

[10] M. Bendszus, C. Wessig, L. Solymosi, K. Reiners, and M. Koltzenburg, “MRI of peripheral nerve degeneration and regeneration: correlation with electrophysiology and histology,” *Exp Neurol*, vol. 188, no. 1, pp. 171–177, 2004.

[11] B. Behr, R. Schnabel, U. Mirastschijski, B. Ibrahim, F. Angenstein, and W. Schneider, “Magnetic resonance imaging monitoring of peripheral nerve regeneration following neurotmesis at 4.7 Tesla.,” *Plast. Reconstr. Surg.*, vol. 123, no. 6, pp. 1778–88, Jun. 2009.

[12] A. Chhabra, G. Andreisek, T. Soldatos, K. C. Wang, A. J. Flammang, A. J. Belzberg, and J. a Carrino, “MR neurography: past, present, and future.,” *AJR. Am. J. Roentgenol.*, vol. 197, no. 3, pp. 583–91, Sep. 2011.

[13] Y. Zhou, M. Kumaravel, V. S. Patel, K. a Sheikh, and P. a Narayana, “Diffusion tensor imaging of forearm nerves in humans.,” *J. Magn. Reson. Imaging*, vol. 36, no. 4, pp. 920–7, Oct. 2012.

[14] R. E. Bennett, C. L. Mac Donald, and D. L. Brody, “Diffusion tensor imaging detects axonal injury in a mouse model of repetitive closed-skull traumatic brain injury.,” *Neurosci. Lett.*, vol. 513, no. 2, pp. 160–5, Apr. 2012.

[15] F. Agosta, M. Absinta, M. P. Sormani, a Ghezzi, a Bertolotto, E. Montanari, G. Comi, and M. Filippi, “In vivo assessment of cervical cord damage in MS patients: a longitudinal diffusion tensor MRI study.,” *Brain*, vol. 130, no. Pt 8, pp. 2211–9, Aug. 2007.

[16] H. C. Lehmann, J. Zhang, S. Mori, and K. A. Sheikh, “Diffusion tensor imaging to assess axonal regeneration in peripheral nerves,” *Exp Neurol*, vol. 223, no. 1, pp. 238–244, 2010.

[17] X. Li, J. Chen, G. Hong, C. Sun, X. Wu, M. J. Peng, and G. Zeng, “In vivo DTI longitudinal measurements of acute sciatic nerve traction injury and the association with pathological and functional changes.,” *Eur. J. Radiol.*, vol. 82, no. 11, pp. e707–14, Nov. 2013.

[18] T. Takagi, M. Nakamura, M. Yamada, K. Hikishima, S. Momoshima, K. Fujiyoshi, S. Shibata, H. J. Okano, Y. Toyama, and H. Okano, “Visualization of peripheral nerve degeneration and regeneration: monitoring with diffusion tensor tractography.,” *Neuroimage*, vol. 44, no. 3, pp. 884–92, Feb. 2009.

[19] S. Morisaki, Y. Kawai, M. Umeda, M. Nishi, R. Oda, H. Fujiwara, K. Yamada, T. Higuchi, C. Tanaka, M. Kawata, and T. Kubo, "In vivo assessment of peripheral nerve regeneration by diffusion tensor imaging.," *J. Magn. Reson. Imaging*, vol. 33, no. 3, pp. 535–42, Mar. 2011.

[20] T. Kretschmer, C. W. Heinen, G. Antoniadis, H.-P. Richter, and R. W. König, "Iatrogenic nerve injuries.," *Neurosurg. Clin. N. Am.*, vol. 20, no. 1, pp. 73–90, vii, Jan. 2009.

[21] J. Y. Lee, G. Giusti, H. Wang, P. F. Friedrich, A. T. Bishop, and A. Y. Shin, "Functional evaluation in the rat sciatic nerve defect model: a comparison of the sciatic functional index, ankle angles, and isometric tetanic force," *Plast Reconstr Surg*, vol. 132, no. 5, pp. 1173–1180, 2013.

[22] J. R. Bain, S. E. Mackinnon, and D. A. Hunter, "Functional evaluation of complete sciatic, peroneal, and posterior tibial nerve lesions in the rat," *Plast Reconstr Surg*, vol. 83, no. 1, pp. 129–138, 1989.

[23] D. Liang, S. Bhatta, V. Gerzanich, and J. M. Simard, "Cytotoxic edema: mechanisms of pathological cell swelling.," *Neurosurg. Focus*, vol. 22, no. 5, p. E2, Jan. 2007.

[24] C. Beaulieu, M. D. Does, R. E. Snyder, and P. S. Allen, "Changes in water diffusion due to Wallerian degeneration in peripheral nerve," *Magn. Reson. Med.*, vol. 36, no. 4, pp. 627–631, Oct. 1996.

[25] S.-W. Sun, J. J. Neil, H.-F. Liang, Y. Y. He, R. E. Schmidt, C. Y. Hsu, and S.-K. Song, "Formalin fixation alters water diffusion coefficient magnitude but not anisotropy in infarcted brain.," *Magn. Reson. Med.*, vol. 53, no. 6, pp. 1447–51, Jun. 2005.

[26] Y. Wang, Q. Wang, J. P. Haldar, F.-C. Yeh, M. Xie, P. Sun, T.-W. Tu, K. Trinkaus, R. S. Klein, A. H. Cross, and S.-K. Song, "Quantification of increased cellularity during inflammatory demyelination.," *Brain*, vol. 134, no. Pt 12, pp. 3590–601, Dec. 2011.

[27] X. Wang, M. F. Cusick, Y. Wang, P. Sun, J. E. Libbey, K. Trinkaus, R. S. Fujinami, and S.-K. Song, "Diffusion basis spectrum imaging detects and distinguishes coexisting subclinical inflammation, demyelination and axonal injury in experimental autoimmune encephalomyelitis mice.," *NMR Biomed.*, vol. 27, no. 7, pp. 843–52, Jul. 2014.

[28] W. Gaggl, A. Jesmanowicz, and R. W. Prost, "High-resolution reduced field of view diffusion tensor imaging using spatially selective RF pulses.," *Magn. Reson. Med.*, vol. 1679, pp. 1668–1679, Jan. 2014.

[29] C. J. Wargo and J. C. Gore, "Localized high-resolution DTI of the human midbrain using single-shot EPI, parallel imaging, and outer-volume suppression at 7T.," *Magn. Reson. Imaging*, vol. 31, no. 6, pp. 810–9, Jul. 2013.

[30] A. Leemans, B. Jeurissen, J. Sijbers, and D. Jones, "ExploreDTI: a graphical toolbox for processing, analyzing, and visualizing diffusion MR data.," in *17th Annual Meeting of Intl Soc Mag Reson Med*, 2009, p. 3537.

CHAPTER V

CHARACTERIZATION OF ACELLULAR NERVE ALLOGRAFT REPAIR USING DIFFUSION TENSOR IMAGING

Introduction

In the previous chapter, acute nerve transection was characterized using diffusion tensor imaging (DTI) and the degree of injury was found to correlate with fractional anisotropy and radial diffusivity. The primary goal of acute imaging for peripheral nerve injury is to establish a baseline that can be compared with serial examinations following nerve repair to assess nerve regeneration. Acellular nerve allografts provide an optimal research model for DTI studies of nerve regeneration, because there is no confounding signal from Wallerian degeneration occurring within the allograft.[1]

Axonal membranes and myelin are known to be the key determinants of the degree of anisotropy of nerve fibers.[2] As shown in Chapter IV, proper acellular nerve allografts lack axonal processes and myelin debris and therefore should have unhindered, isotropic water diffusion prior to axonal regeneration and cellular infiltration. Non-neuronal cells, such as Schwann cells, are required to first migrate into a nerve allograft prior to axonal elongation.[3], [4] The 'isotropically' shaped water compartment of Schwann cells may appear as an initial decrease in anisotropy, similar to the signal observed in nerve ischemia.[2] As regenerating axons enter the allograft, we expect an increase in axial diffusivity and fractional anisotropy proceeding distally from the proximal stump.[5], [6]

The goal of this study was to characterize nerve regeneration in NGF-eluting and control acellular nerve allografts that were presented in Chapter IV. We performed ex vivo 4.7T DTI at 1 week and 3 weeks post-repair of sciatic nerve gap injuries. The data were collected ex vivo to reduce the partial-volume effects that were observed in hind limb imaging of the previous chapter. Growth associated protein-43 (GAP-43) immunohistochemistry of graft sections was used for validation of neurite outgrowth.

Materials and Methods

All experimental procedures were approved by and performed in accordance with the standards set forth by the Institutional Animal Care and Use Committee at Vanderbilt University.

Growth factor and reagents

NGF-β (>98% pure as determined by RP-HPLC and SDS-PAGE) was purchased from ProSpec in its mature form, carrier free and lyophilized.

Donor nerve harvesting

Sprague Dawley rats were 12 weeks old and weighed 250 to 300g at the start of the experiment. The hind legs were shaved and longitudinal incisions of the skin and underlying biceps femori were made bilaterally. Using blunt dissection, the sciatic nerves were dissected from surrounding tissue and excised

with iris scissors. Directly after excision, sciatic nerves were placed on a glass slide, cleaned of all excess connective tissue and trimmed to 2-cm using an ophthalmic scalpel (Micro Feather No. 715, Feather Safety Razor Company) while hydrating with phosphate buffered saline. After 3 washes with PBS, cleaned nerve segments were stored in RPMI 1640 medium (Life Technologies) at 4 °C until processing.

Nerve graft processing

Nerve segments were decellularized with the Sondell technique.[4] Table 1 lists the protocols for Sondell nerve decellularization performed prior to nerve decellularization. After 3 washes with PBS, processed nerves grafts were stored in PBS solution at 4 °C.

Table 1. Sondell nerve decellularization protocol adapted from existing literature.

Step	Solution	Time (h)
1	46mM (3%) Triton X-100	15
2	96mM (4%) sodium deoxycholate	24
3	DI H2O	1 x 7
4	46mM (3%) Triton X-100	15
5	96mM (4%) sodium deoxycholate	24
6	PBS (pH 7.2) at 4 C	Until use

Growth factor loading of decellularized nerves

NGF-β was reconstituted to 100 μg/ml in sterile 18MΩ-cm H2O and filtered through a 0.22 μm filter. Processed nerve grafts were incubated in NGF-β solution (10 μg/ml) for 16 h at RT under agitation.

In vivo rat nerve injury

Sixteen adult Sprague Dawley rats weighing 250 to 300g had a 1-cm NGF-loaded (n=8) or saline-loaded (n=8), Sondell-processed acellular nerve allograft engrafted in sciatic nerve in the left hind limb. The graft was epineurially sutured to the proximal and distal sciatic nerve stumps following an acute transection injury. At 7 d or 21 d post-surgery, the animal was euthanized with intracardiac injection of pentobarbital (Euthasol). The sciatic nerve graft and contralateral sciatic nerve was dissected and immersion fixed in 4% paraformaldehyde/0.5% glutaraldehyde in PBS.

Tissue sample preparation

After 24h of fixation, excised nerve grafts and contralateral sciatic nerves were placed in PBS + 2 mM Gd-DTPA (Magnevist, Bayer HealthCare, Wayne, NJ, USA) at 4 °C for at least 24h before imaging. For imaging, excised nerve grafts were trimmed to ≈ 1 cm in length (with the injury site centered) and placed in 2-mm outer diameter glass capillary tubes filled with a perfluropolyether liquid (Fomblin, Solvay Solexis, Thorofare, NJ, USA) for susceptibility matching, preventing tissue dehydration, and a signal-free background. For higher throughput, four excised nerve grafts and two normal sciatic nerves in a hexagonal arrangement were imaged simultaneously.

Diffusion tensor magnetic resonance imaging

MR imaging was performed on a 4.7T 31-cm horizontal bore Agilent DirectDrive scanner (Agilent Technologies, Santa Clara, CA) using a 38-mm Litz quadrature coil (Doty Scientific, Columbia, SC) for RF transmission and reception. For excised nerve imaging, FOV = 9.8 x 9.8 x 12 mm^3 and matrix size = 196 x 196 x 64 for a nominal resolution of 100 x 100 x 375 μm^3 (375 μm along the nerve). Diffusion tensor imaging data were acquired using a 3D diffusion-weighted spin-echo sequence with TR/TE = 170/23.0 ms and 12 signal averages. Diffusion-weighting was achieved with δ/Δ = 4/12 ms, prescribed b-value = 2000 s/mm^2, and 6 directions. One b=0 image was acquired for a total of 7 images in a scan time of ≈ 12h.

DTI post-processing and analysis

Image data reconstruction and diffusion tensor calculations were performed using in-house written code in MATLAB (Mathworks, Natick, MA, USA). 3D image volumes were zero-padded x2 in each direction during reconstruction from k-space data. Diffusion tensors were estimated voxel-wise using a linear least-squares approach. From the diffusion tensor, DTI metrics including fractional anisotropy (FA) and mean, axial and radial diffusivity (MD, AD, and RD, respectively) were computed on a voxel-wise basis. DTI tractography was performed using the ExploreDTI toolbox.[7]

Statistical analysis

All statistical analyses were performed using GraphPad Prism 5 for Mac OS X (GraphPad Software; San Diego, CA). For comparison of axon counts Student's t-test was used to compare specific groups. All p values were two-tailed and significance was determined at $p < .01$.

Results

Diffusion Tensor Imaging

Region-of-interest (ROI) analysis was performed mid-graft for calculation of DTI measurements, including fractional anisotropy (FA), mean diffusivity (MD) and tract quantification. In 1-week samples, there was minimal difference in FA and MD between NGF-eluting and control nerve allografts (Fig. 1a-b). However, FA was significantly reduced in both allografts compared to normal sciatic nerve and MD was significantly increased in control nerve allografts. As expected, mid-graft tract counts and average tract length were lower in both allograft groups at 1 week compared to normal sciatic nerve (Fig. 1c-d).

At 3 weeks post-repair, control allografts continued to have significantly lower FA than normal sciatic nerve, and FA was slightly increased in NGF-eluting allografts (Fig. 2a). Mean MD was greatly increased in control allografts at 3 weeks, while NGF-eluting allografts remained near normal nerve level (Fig. 2b). The greatest difference at 3 weeks was observed in mid-graft tract counts. The mean tract count of control allografts was lower at 3 weeks than was observed at 1 week, and six-fold less than the mean tract count in NGF-eluting grafts and normal nerve (Fig. 2c).

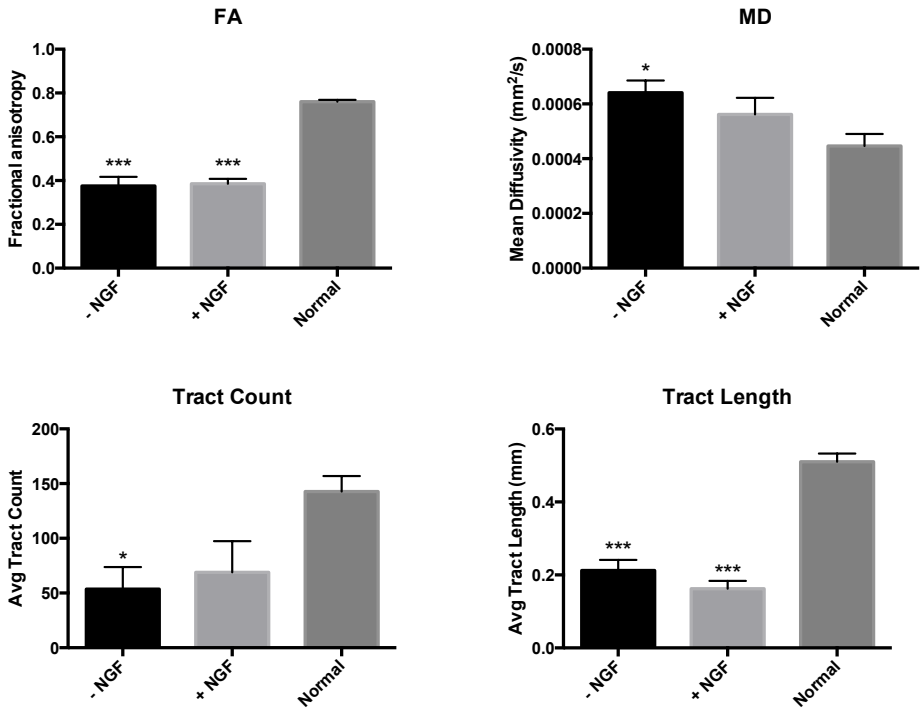

Figure 1. DTI measurements of mid-graft cross-sections at 1 week post-repair. Significance tested with two-tailed Student's t-test and indicated by * $p < 0.05$, *** $p<0.001$.

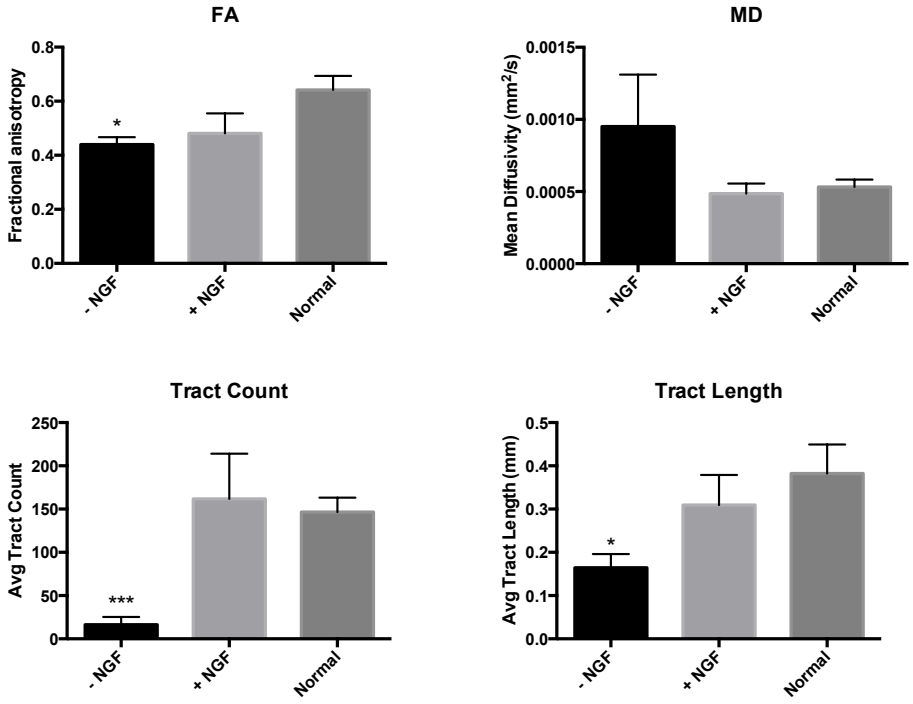

Figure 2. DTI measurements of mid-graft cross-sections at 3 weeks post-repair. Significance tested with two-tailed Student's t-test and indicated by * $p < 0.05$, *** $p<0.001$.

Parallel and radial diffusivity were also measured in mid-graft regions-of-interest (Fig. 3). No significant difference was found in parallel diffusivity at 1 week or at 3 weeks post-repair. Radial diffusivity was significantly increased over normal nerve in both allografts at 1 week. However, only NGF-eluting nerve allografts had normalized at 3 weeks.

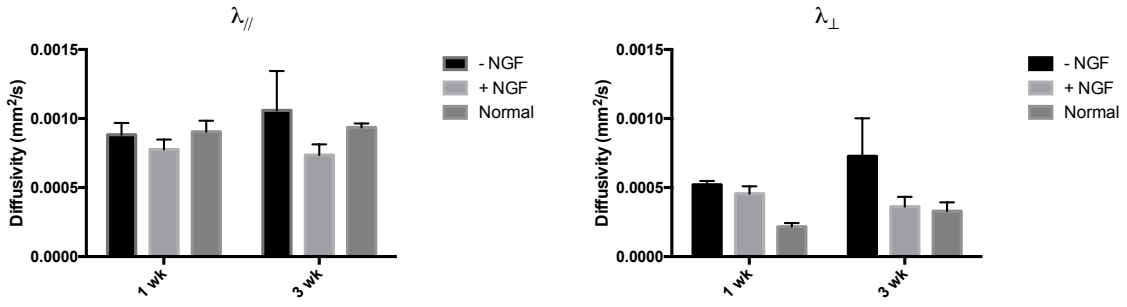

Figure 3. Parallel and radial diffusivity of mid-graft cross-sections.

Diffusion Tensor Tractography

Proximodistal tractography was performed on all 1-week and 3-week nerve graft samples with FA threshold of 0.25 and maximum fiber angle of 45° (Fig. 4). As expected, all normal nerves (indicated by asterisks) showed robust nerve fiber tracts throughout the length of the sample. However, large differences in tract length (Fig. 1d and 2d) and orientation were observed between NGF-eluting and control nerve allografts and between time points. The greatest number of tracts of at least 0.2-mm in length was observed in NGF-eluting nerve allografts at 3 weeks post-repair. Minimal axially oriented tracts were observed at 3 weeks in control nerve allografts and extension of tracts to mid-graft was only found in a single sample.

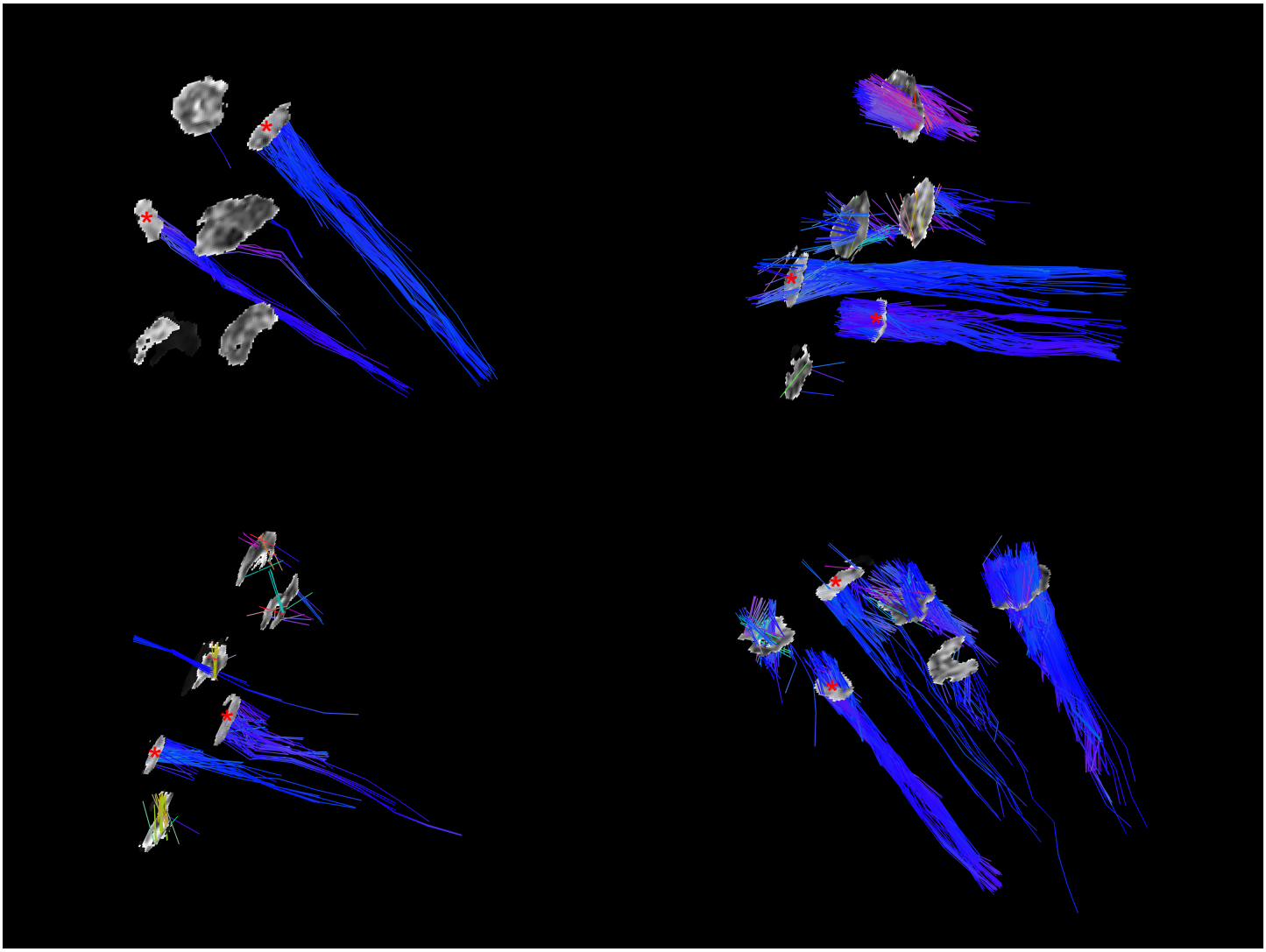

Figure 4. Diffusion tensor tractography of control (left) and NGF-eluting (right) nerve allografts at 1 week (top) and 3 weeks (bottom) post-repair. Red asterisks indicate normal sciatic nerve controls.

Histology

Gap-43 immunohistochemistry was performed on mid-graft sections of 3-week nerve allografts (Fig. 5). Regenerative neurite clusters are visible within the epineurium of all NGF-eluting nerve allografts, but no clusters are visible in the control nerve allografts. Non-neuronal cells also appear to be more confined to the epineurium in control allografts and more confluent in NGF-eluting nerve allografts.

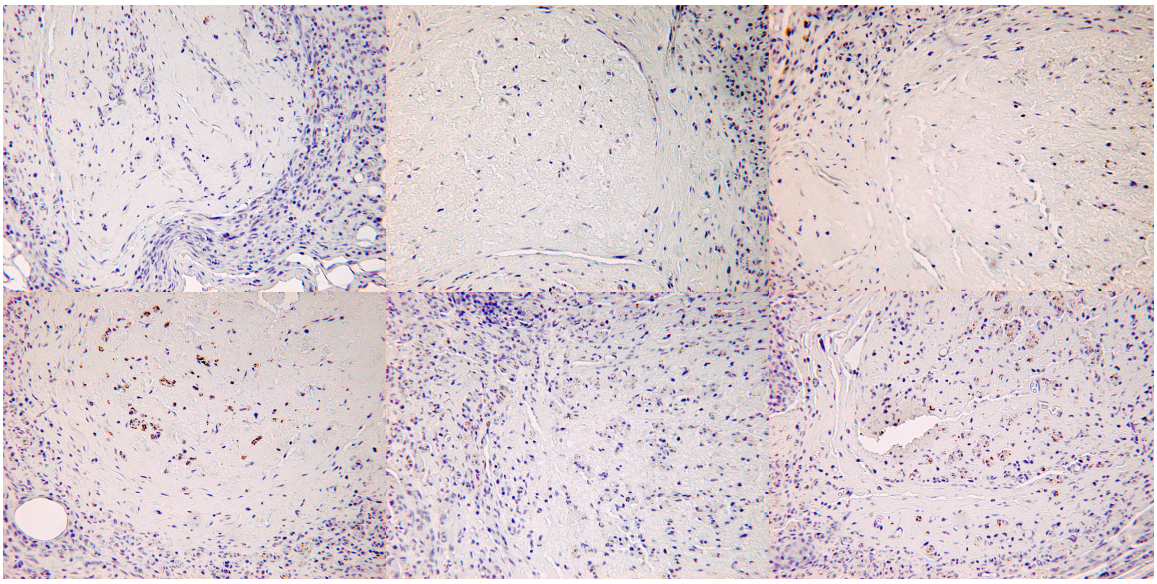

Figure 5. Gap-43 immunohistochemistry of mid-graft sections of control (top) and NGF-eluting (bottom) nerve allografts at 3 weeks post-repair. Regenerative neurites (DAB stain) are visible in NGF-eluting allograft sections.

Toluidine blue sections of distal nerve stump segments were also performed (Fig. 6). Although degenerating axons and myelin bulbs are still present distal to both NGF-eluting and control allografts, thinly myelinated nerve fibers appear slightly larger and more mature in the NGF-treated group. Quantitative histology of the distal nerve would be difficult to perform this early in the regenerative process, but the presence of immature nerve fibers distal to all grafts verifies successful nerve repair and suggests appropriate timing for mid-graft histology.

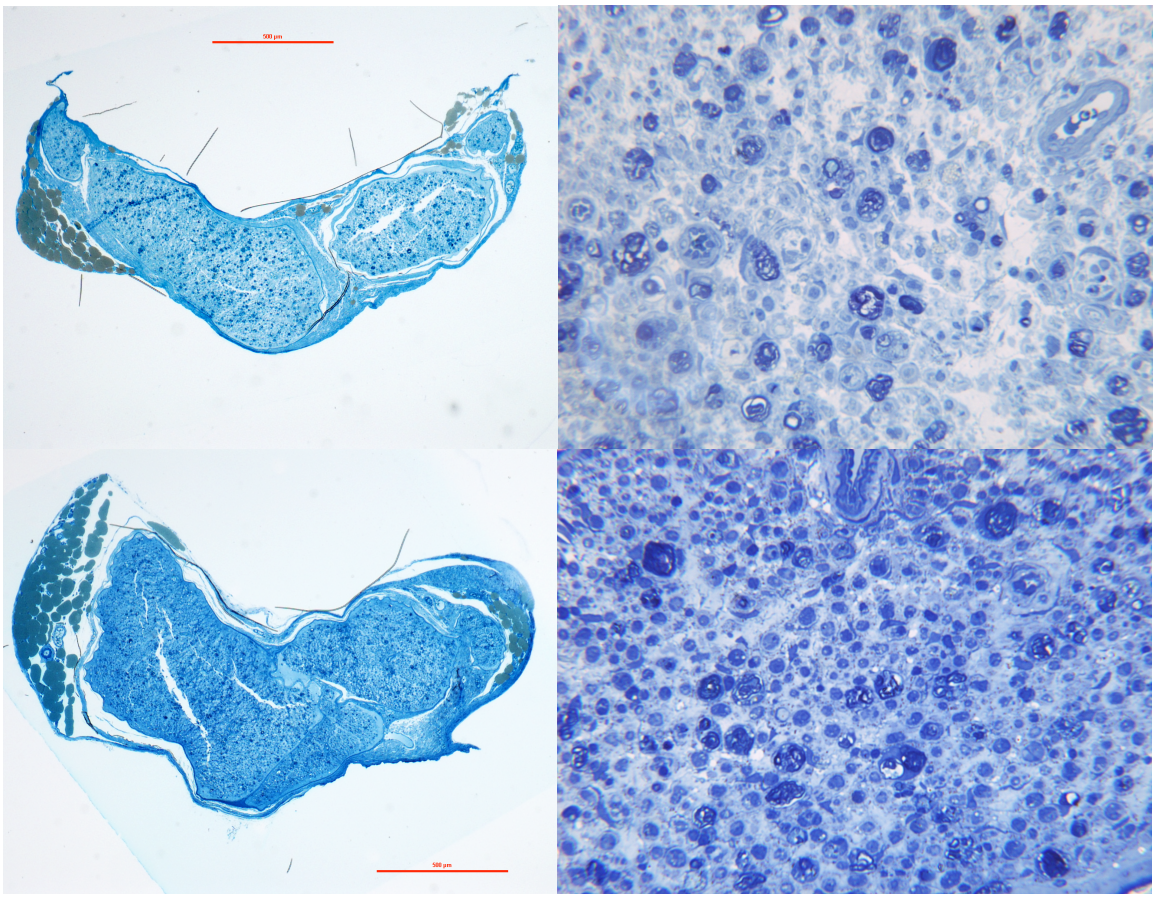

Figure 6. Toluidine blue stained sections of distal nerve segment of control (top) and NGF-eluting (bottom) nerve allografts at 3 weeks post-repair.

Discussion

Previous work has shown that diffusion tensor imaging is capable of visualizing degeneration and regeneration of peripheral nerves.[6], [8], [9] These studies have shown that FA and parallel diffusivity decrease in degenerating nerves and are recovered during regeneration. Diffusion tensor tractography has also been shown to have disrupted fiber tracking distal to the injury site in a crushed nerve model that recovers with regeneration. In Chapter IV, we observed similar decreases in FA and tract continuity in transected rodent sciatic nerves that were microsurgically repaired. The purpose of this study was to

characterize axon regeneration in acellular nerve allografts that were implanted into a rat sciatic nerve gap injury. Specifically, we performed *ex vivo* imaging of the NGF-eluting Sondell acellular nerve allograft and control Sondell nerve allografts that were presented in Chapter III.

Since we could not find any existing diffusion tensor imaging of acellular nerve allografts, we will compare our findings here with studies of axonotmetic nerve injuries. Similar to crush nerve injuries and our nerve transection findings in Chapter IV, we observed an initial decrease in FA and increase in radial diffusivity immediately after injury.[9] No difference was observed in parallel diffusivity at one week after injury, which may be in part due to cytotoxic edema and cellular infiltration.[2] There was no significant change in parallel diffusivity at 3 weeks, but greater variability was observed in control nerve allografts. Interestingly, radial diffusivity of NGF-eluting nerve allografts normalized by 3 weeks but continued to increase in control nerve allografts. Tractography also showed robust axon elongation in NGF-eluting nerve allografts at both 1 week and 3 weeks, but there was minimal tracking past the proximal seed ROI in control nerve allografts. This finding was supported by histology, which showed minimal Gap-43 neurite staining in mid-graft sections of the control nerve allografts and several Gap-43 positive regenerative neurite clusters within NGF-eluting nerve allografts.

Conclusion

This study provides strong evidence of the benefits of NGF-eluting acellular nerve allografts in nerve gap injury repair. Using diffusion tensor imaging, we have shown that NGF-eluting nerve allografts accelerate axonal outgrowth over control nerve allografts. Additionally, we have shown that diffusion tensor imaging and tractography can be used to monitor neurite outgrowth through acellular nerve allografts.

References

[1] C. Beaulieu, M. D. Does, R. E. Snyder, and P. S. Allen, "Changes in water diffusion due to Wallerian degeneration in peripheral nerve," *Magn. Reson. Med.*, vol. 36, no. 4, pp. 627–631, Oct. 1996.

[2] C. Beaulieu, "The basis of anisotropic water diffusion in the nervous system - a technical review.," *NMR Biomed.*, vol. 15, no. 7–8, pp. 435–55, Jan. .

[3] E. L. Whitlock, T. M. Myckatyn, A. Y. Tong, A. Yee, Y. Yan, C. K. Magill, P. J. Johnson, and S. E. Mackinnon, "Dynamic quantification of host Schwann cell migration into peripheral nerve allografts.," *Exp. Neurol.*, vol. 225, no. 2, pp. 310–9, Oct. 2010.

[4] M. Sondell, G. Lundborg, and M. Kanje, "Regeneration of the rat sciatic nerve into allografts made acellular through chemical extraction.," *Brain Res.*, vol. 795, no. 1–2, pp. 44–54, Jun. 1998.

[5] T. Takagi, M. Nakamura, M. Yamada, K. Hikishima, S. Momoshima, K. Fujiyoshi, S. Shibata, H. J. Okano, Y. Toyama, and H. Okano, "Visualization of peripheral nerve degeneration and regeneration: monitoring with diffusion tensor tractography.," *Neuroimage*, vol. 44, no. 3, pp. 884–92, Feb. 2009.

[6] H. C. Lehmann, J. Zhang, S. Mori, and K. A. Sheikh, "Diffusion tensor imaging to assess axonal regeneration in peripheral nerves," *Exp Neurol*, vol. 223, no. 1, pp. 238–244, 2010.

[7] A. Leemans, B. Jeurissen, J. Sijbers, and D. Jones, "ExploreDTI: a graphical toolbox for processing, analyzing, and visualizing diffusion MR data.," in *17th Annual Meeting of Intl Soc Mag Reson Med*, 2009, p. 3537.

[8] M. Bendszus, C. Wessig, L. Solymosi, K. Reiners, and M. Koltzenburg, "MRI of peripheral nerve degeneration and regeneration: correlation with electrophysiology and histology," *Exp Neurol*, vol. 188, no. 1, pp. 171–177, 2004.

[9] S. Morisaki, Y. Kawai, M. Umeda, M. Nishi, R. Oda, H. Fujiwara, K. Yamada, T. Higuchi, C. Tanaka, M. Kawata, and T. Kubo, "In vivo assessment of peripheral nerve regeneration by diffusion tensor imaging.," *J. Magn. Reson. Imaging*, vol. 33, no. 3, pp. 535–42, Mar. 2011.

CHAPTER VI

SUMMARY AND FUTURE DIRECTIONS

The primary aims of this dissertation were to study 1) the effects of Nerve Growth Factor and Glial-Derived Neurotrophic Factor as adjuvant therapies with state-of-the-art acellular nerve allografts for peripheral nerve repair (Chapter II), 2) the feasibility of sustained neurotrophic factor delivery using acellular nerve allografts as affinity-based delivery scaffolds (Chapter III), and 3) the characterization of peripheral nerve transection and repair using high-resolution diffusion tensor imaging (Chapter IV). I've included an additional aim on the characterization of NGF-eluting and control acellular nerve allografts using high-resolution diffusion tensor imaging (Chapter V). In the final chapter I will present our additional work on the topic of polyethylene glycol-fusion of transected peripheral nerves (Chapter VII).

In Chapter II, we found that NGF had significant pro-regenerative effects when combined as an adjuvant therapy with freeze-thaw decellularized and chrondrotinase-treated nerve allografts. In addition to increased total myelinated axon counts, we found that ChAT-positive motor axons were significantly increased and IB4-positive nociceptive neurons were reduced in NGF-treated allografts at 8 weeks post-repair. In Chapter III, we evaluated multiple nerve decellularization techniques for their extracellular matrix architecture, cellular clearance and NGF release profile. In this study, Sondell allografts were found to have the best extracellular matrix properties and retained NGF over 21 days *in vitro*. We then conducted an *in vivo* study of NGF-eluting and control Sondell nerve allografts and we found improved Gap-43 positive axon regeneration mid-graft in NGF-eluting allografts at 3 weeks post-repair.

We introduced diffusion tensor imaging in Chapter IV for characterization of acute microsurgically-repaired peripheral nerve transection. We found that fractional anisotropy and radial diffusivity were significantly changed immediately after nerve transection in an excised rodent sciatic nerve model. Using tractography, we also found a dramatic loss of continuous tracts through the injury site of transected and epineurally-repaired sciatic nerves. In Chapter V, we applied diffusion tensor imaging to characterize NGF-eluting and control Sondell acellular nerve allografts that were implanted in a rodent sciatic nerve gap injury model. Using DTI measurements and tractography, this study provides additional support for the pro-regenerative effects of NGF-eluting nerve allografts.

There are several future studies that I recommend to further advance the work performed in this dissertation. 1) Sprague-Dawley rats were the primary animal model used in this work, because they are well-established models of peripheral nerve repair and they have low breeding and housing costs. However, large animals provide a more accurate model of large nerve gap injury. Long-term survival studies in a large animal nerve gap model should be performed prior to human trials. 2) Quantitative proteomic analysis of acellular nerve allografts should be performed to fully characterize the effects of nerve processing on extracellular matrix composition. Although we performed quantitative analysis of the collagen, glycosaminoglycan, actin and myelin content of the allografts, we have not identified all potential NGF binding proteins present in the allografts. These data will be important for identifying additional growth factors that can be delivered using acellular nerve allografts and for fine-tuning the NGF release profile. 3) To fully understand the effects of NGF-eluting nerve allografts, additional long-term *in vivo* studies should be performed in a large animal model and characterized at multiple time points *in vivo* with diffusion tensor imaging and electrophysiology.

CHAPTER VII

SUPPLEMENT ON POLYETHYLENE GLYCOL MEDIATED FUSION OF PERIPHERAL NERVES

Overview of PEG Fusion Theory

Polyethylene glycol (PEG), a hydrophilic polymer composed of varying chain lengths of ethylene glycol monomers, has been known for several decades to have unique fusogenic effects with eukaryotic plasma membranes. This property of PEG has been widely used in generating hybridomas for production of antibodies. PEG has also been used for nuclear transfer in mammalian cloning. Although the detailed mechanism of lipid bilayer fusion remains unknown, PEG has been shown to cause agglutination and convergence of a variety of cell and microcell membranes.

Axonal fusion was first described in crayfish motor axons in the late 1960s. Following transection of motor neurons, central cell bodies of some neurons could be found to rejoin the distal neuron segment and immediately restore function.[1] Although axonal fusion does not spontaneously occur in mammalian neurons, fusion of mammalian cells has been performed in immunology laboratories for several decades using PEG or electrofusion. Krause and Bittner first showed PEG-mediated fusion of myelinated axons in an earthworm, Lumbricus terrestris, medial giant axon model 25 years ago.[2] Since then, PEG fusion has been investigated for its application to peripheral neurons using in vitro and in vivo mammalian models. Although the specific mechanism remains unknown, there is building evidence that closely apposed axon

endings in peripheral nerve repair can be fused with application of PEG producing immediate electrophysiological recovery.

This supplement includes publications that I have contributed to during my dissertation work that advance the existing knowledge of PEG-mediated axonal fusion. In the first study (JSR 2013), we examine the role of a specific ionotropic ATP receptor (P2x7) in axonal fusion and we evaluate an antagonist of this receptor in vitro and in vivo prior to the application of PEG. This study provides support that PEG fusion of axons requires blockage of calcium-mediated axolemmal sealing and can be enhanced by blocking post-injury inward calcium currents. In the second study (JNR 2014), we evaluate the use of PEG fusion of axons in fresh nerve allograft repair in vivo. This study provides initial evidence of the ability of PEG to mediate axonal fusion with interposition nerve allograft segments, immediately restoring nerve function and preventing Wallerian degeneration of the distal nerve stump.

[1] R. R. Hoy, G. D. Bittner, and D. Kennedy, "Regeneration in Crustacean Motoneurons: Evidence for Axonal Fusion," *Science (80-.).*, vol. 156, no. 3772, pp. 251–252, Apr. 1967.

[2] T. L. Krause and G. D. Bittner, "Rapid morphological fusion of severed myelinated axons by polyethylene glycol.," *Proc. Natl. Acad. Sci. U. S. A.*, vol. 87, no. 4, pp. 1471–5, Feb. 1990.

P2X7 RECEPTOR MODULATION IN PEG FUSION

Adapted from: C. L. Rodriguez-Feo, K. W. Sexton, R. B. Boyer, A. C. Pollins, N. L. Cardwell, L. B. Nanney, R. B. Shack, M. A. Mikesh, C. H. McGill, C. W. Driscoll, G. D. Bittner, and W. P. Thayer, "Blocking the P2X7 receptor improves outcomes after axonal fusion.," *J. Surg. Res.*, vol. 184, no. 1, pp. 705–13, Sep. 2013.

Abstract

Activation of the P2X7 Receptor on nerve cells causes the formation of pannexin pores, which allows the influx of calcium across the cell membrane. Polyethylene glycol (PEG) and methylene blue (MB) have previously been shown to delay Wallerian degeneration if applied during microsuture repair of the severed nerve. *Our hypothesis is that by modulating calcium influx via the P2X7 receptor pathway, we could improve PEG based axonal repair.* The P2X7 receptor can be stimulated or inhibited using bzATP or Brilliant Blue (FCF), respectively. A single incision rat sciatic nerve injury model was used. The defect was repaired using a previously described PEG, MB fusion protocol. Experimental animals were treated with 100 μL of 100 μM FCF solution (n=8) or 100 μL of a 30 μM bzATP solution (n=6). Control animals received neither FCF, bzATP, nor PEG. Compound Action Potentials (CAPs) were recorded prior to transection (baseline), immediately after repair, and 21 days post operatively. Animals underwent behavioral testing 3,7, 14, and 21 days post operatively. After sacrifice, nerves were fixed, sectioned, and immunostained to allow for counting of total axons. Rats treated with FCF showed an improvement as compared to control at all time points (n=8) ($p= .047, .044, .014$, and $.0059$ respectively). A statistical difference was also shown between FCF and bzATP at Day 7 ($p<.05$), but not shown with days 3, 14, and 21.

(p>.05). This study provides evidence that blocking the P2X7 receptor improves functional outcomes after PEG mediated axonal fusion.

Introduction

Current strategies for peripheral nerve repair include nerve grafts, nerve growth guides, and micro-sutures. (1) These techniques rely on the proximal outgrowth at a rate of 1mm/day toward the targeted tissues. The time needed for re-innervation of proximal injuries (measured in months) as compared to distal injuries (measured in weeks) allows for muscle atrophy causing repair failure. (2) Nerve fusion is an emerging technology that could prevent this atrophy seen after months allowing for a successful re-innervation by the proximal axonal outgrowth. (3) The impact of nerve fusion has lead to a great interest in mammalian models of peripheral nerve repair. (4,5,6) Polyethylene glycol (PEG) based fusion has been shown to fuse the axolemmal membranes of crushed/severed nerves, the most common nerve injuries after trauma. (4) *In vivo* experiments have shown improved behavioral outcomes and increased numbers of axons in the distal, reattached segment. (4,5) The obstacles of nerve fusion include delaying and inhibiting the process of Wallerian degeneration, preventing the sealing of the proximal nerve end, and reestablishing the morphology and functionality of the nerve. (7)

In an attempt to further enhance the efficiency of PEG based axonal fusion, which has been shown to be calcium dependent (8), we attempted to modulate calcium influx at the cellular level through selective activation or inhibition of calcium channels. Activation of the purinergic P2X7 receptor causes the formation of pannexin pores. (9,10) These holes allow for the efflux of ATP and the influx of calcium across the cell membrane. For injured neurons, this has been reported to play a role in the initiation of Wallerian degeneration. (8,11) PEG and MB have previously been shown to delay Wallerian degeneration through a receptor-independent manner if applied during microsuture repair of the severed nerve. (4,7,5)

Calcium modulation is a critical part of the PEG based axonal repair because once calcium enters the axon, the cut nerve ends seal preventing PEG based axonal fusion. Our hypothesis is that by modulating calcium influx via the P2X7 receptor pathway, that we could improve outcomes after PEG based axonal repair. Specifically, by blocking the p2x7 pathway with (FCF), a purinergic specific blocker of the p2x7 pathway, or activating with (bzATP), a nonspecific activator of the p2x7 pathway, in combination with PEG mediated fusion, we can modulate the progress of Wallerian degeneration in a rat model. (10)

Materials and Methods

All experimental procedures were approved by and performed in accordance with the standards set forth by the Institutional Animal Care and Use Committee at Vanderbilt University.

Surgical procedures

Female Sprague-Dawley rats were anesthetized with inhaled isoflourane, their left hind limb was shaved with clippers, and the surgical site was prepped aseptically. A two cm incision was made parallel, and approximately 1 cm caudally from the femur. Using sharp dissection, the biceps femoris was bisected along the plane of muscle fibers overlaying the sciatic nerve. The muscle fibers were then retracted exposing the left sciatic nerve. The exposed nerve was then dissected free of perineural tissue using sharp dissection and minimal retraction. The exposed nerve was bathed in Plasma-lyte A® (Baxter: Deerfield, IL) and electrophysiological testing was performed. Plasma-lyte A® is a calcium free solution containing

the following (in mEq/L): (Na 140, K 5, Mg 3, Cl 98, Acetate 27, Gluconate 23) at pH 7.4 containing 294 mOsm/L.

The sciatic nerve was transected prior to the trifurcation followed by irrigation with Plasma-lyte A®. The proximal and distal nerve ends were then bathed in a 100 microliters of 100 microMolar FCF solution (Sigma-Aldrich; St. Louis, MO)(12) or a 100 microliters of a 30 microMolar bzATP (Sigma-Aldrich; St. Louis, MO) solution. Using standard microsurgical techniques, with careful attention paid to maintain orientation using the epineural blood vessels, the two ends were sutured in place using 9-0 Ethilon (Ethicon, Sommerville, NJ). Once the nerve was rejoined in an end-to-end fashion using an interrupted suturing technique and microscopic magnification, a hypotonic 1% solution of MB (Acros Organics; Morris Plains, NJ) in sterile water was applied to the coaptation site for one minute. A 50% by weight solution of PEG (3.35kD molecular weight, Sigma-Aldrich; St. Louis, MO) in sterile water was then applied to the coaptation sites for 1 minute in experimental animals. Additional animals received the surgical protocol with FCF or BzATP, but they did not receive the PEG treatment. Control animals received only the MB solution.

The wound was then irrigated with Lactated Ringers (Hospira; Lake Forest, IL) and electrophysiological testing was repeated. Lactated Ringers contains the following (in mEq/L): Na 130, K 4, Ca 2.7, Cl 109, and Lactate 28. This isotonic, calcium-containing solution is at pH 6.5 and has 273 mOsm/L. The retractor was removed and the muscle was sutured back together in the appropriate orientation using 5-0 monocryl suture (Ethicon, Sommerville, NJ). The skin was approximated using a running subcuticular 5-0 monocryl suture (Ethicon, Sommerville, NJ). All control and experimental animals were then given a subcutaneous injection of ketoprofen (5mg/kg) and allowed to emerge from anesthesia. Ketoprofen is almost completely excreted by 24 hours postoperatively, having minimal, if any, impact on behavioral testing occurring after that time point. (13)

At 3, 7, 14, and 21 days postoperatively, behavioral testing was performed. After behavioral testing on the 21 day postoperatively, the rats were again anesthetized with inhaled isoflourane and the left hind limb was prepared as previously described. Using the same exposure technique, the left sciatic nerve was exposed. The wound was irrigated with Plasma-lyte A® and electrophysiological testing was repeated.

The rat was then sacrificed via intracardiac injection of Fatal-Plus Solution (Vortech, Dearborn, MI). The injured nerve was harvested immediately after sacrifice and placed into 10% neutral buffered formalin. For electrophysiological testing and behavioral testing, 4 rats were in the FCF experimental group, 4 rats were in the BzATP experimental group, and 12 rats were in the baseline group. For histological testing, 8 rats were used in the FCF experimental group, 6 rats were used in the BzATP experimental group, and 7 rats were used in the control group.

Electrophysiology testing

Compound Action Potentials (CAPs) are a measure of axonal continuity and all were obtained using a Powerlab Data Acquisition System (ADInstruments; Colorado Springs, CO) interfaced with Scope™ 4 (ADInstruments; Colorado Springs, CO). One dual-terminal hook electrode was placed under both the proximal and distal end of the exposed nerve. The proximal electrode was used to deliver an electrical stimulus and the distal electrode was used to record the stimulus and CAPs. CAPs were recorded prior to nerve transection (baseline), immediately after repair with solution therapy, and at 21 days postoperatively.

Behavioral testing

Behavioral assessments were performed at 3, 7, 14, and 21 days postoperatively. Animals were not tested earlier to allow for adequate recovery from anesthesia and to minimize any confounding effects of ketoprofen administration at the time of surgery.

Foot fall asymmetry score

Animals were allowed to roam freely on a mesh grid measuring 45 cm x 30 cm, with square openings measuring 2.5 cm x 2.5 cm. The grid was elevated 2 cm above a solid base. Trials for each animal were recorded for 50 total steps per hindlimb. A foot fault was scored when the stepping hind-limb fell through an opening in the grid, touching the floor. If the hindlimb was retracted after falling through the grid opening, but prior to touching the floor, the step was scored as a partial fault. A composite score was calculated using the previously reported methods and the following equation (4,14):

1) Composite Foot Fault score = (# Partial Faults x 1) + (# Full Faults x 2)
2) % Foot Fault = (Composite Foot Fault score/ total number of steps) x 100%
3) Foot Fault Asymmetry Score = % Foot Fault (normal hindlimb) - % Foot Fault (surgical hindlimb)

Histology

Immunohistochemistry

Immunohistochemical staining was performed using commercial antibodies specifically directed against Myelin Basic Protein (MBP) (Abcam, Cambridge, MA) and S100 alpha (S100a) (Abcam, Cambridge, MA). Formalin-fixed paraffin embedded tissues were sectioned at 5 μm, placed on slides and warmed overnight at 60°C. Slides were deparaffinized and rehydrated with graded alcohols ending in

Tris buffered saline (TBS-T Wash Buffer, LabVision, Freemont, CA). For both, heat mediated target retrieval was performed in 1X Target Retrieval Solution (pH 6.0, DAKO, Carpenteria, CA). Endogenous peroxidases and non-specific background were blocked by subsequent incubations in 3% H_2O_2 (Fisher, Suwanee, GA) in TBS-T and serum-free Protein Block (RTU, DAKO). Primary antibodies to MBP and S100A were used at 1:800 and 1:1,600, respectively for 1 hour, followed by incubation in EnVision+ HRP Labelled Polymer (RTU, DAKO). Slides were rinsed with TBS-T between each reagent treatment and all steps were carried out at room temperature unless otherwise noted. Visualization was achieved with DAB+ chromogen (DAKO). Slides were counterstained with Mayer's hematoxylin, dehydrated through a series of alcohols and xylenes, and then coverslipped with Acrytol Mounting Media (Surgipath, Richmond, IL).

Light Microscopy

All stained slides were examined using an Olympus Vanox-T AH-2 light microscope (Olympus, Center Valley, PA) interfaced to Pixera Pro 600 HS digital camera (Pixera Corporation; Santa Clara, CA). Multiple digital photomicrographs were captured through a 10x objective using Viewfinder V3.0.1 (Pixera Corporation; Santa Clara CA). For each nerve processed, representative cross sections were photographed distal to the site of injury and distally from the sciatic nerve. To count axons the number of stained axons on each photomicrograph, ImageJ v1.45 software combined with the Wright Cell Imaging Facility plug-in package was used in a method that has been previously reported. (15, 16) Equivalent detection thresholds were used for counting axons in each photomicrograph. The total number of axons per cross section was determined by adding the axon totals from all representative photomicrographs or a given cross section; care was taken to avoid duplicate counting of axons.

Statistical analyses

All statistical analyses were performed using GraphPad Prism 5 (GraphPad Software; San Deigo, CA). To compare CAPs from all groups a Kruskal-Wallis test with Dunn's multiple comparison test was performed. Specific CAPs comparisons were completed with an unpaired student's t-test, where appropriate. With regard to foot fault asymmetry scores, a two way ANOVA with Bonferroni's multiple comparison test was employed to specifically compare treatment and control groups. For comparison of axon counts Student's t-test was used to compare specific groups. All p values were 2-tailed and significance was determined at $p < .05$.

In vitro sealing

B104 cells

B104 cells derived from a CNS neuroblastoma of hippocampal origin (17) were used as a model system to study neuronal function *in vitro* (17). B104 cells have easily identifiable cell bodies and axon-like neurites, allowing each cell to be precisely transected and uniquely and individually identified (17). Data on sealing of B104 cells are consistent with data on plasmalemmal sealing from at least 20 other preparations from many phyla and different cell types *in vitro* and *in vivo*.

Cell culture

As previously reported (17), B104 cells were grown in 75 cm^2 vented cap flasks (BD-Falcon, Franklin Lakes, NJ) in a humidified incubator at 37˚C in 5% CO_2 in 4 mL of "cell-growth media," which

consists of a 1:1 mixture of Dulbecco's Modified Eagle's Media and Ham's F12 (DMEM:F12, HyClone, Logan, UT), supplemented for growth with 10% heat inactivated fetal bovine serum (FBS, Hyclone, Logan, UT), and containing 1% antibiotics (10,000 Units of Penicillin/mL and 10 mg/mL of streptomycin, Sigma-Aldrich, St. Louis, MO). Cell-growth media was changed every 2 days and cultures passaged at 80% confluency. Cells were then either sub-cultured in a vented cap flask or seeded at approximately 2000 cells/cm^2 in cell-growth media on Petri dishes coated with Poly-D-lysine (Sigma-Aldrich, St. Louis, MO) to prevent cells from detaching during solution changes and/or neurite transections. After 24 hours, the cell-growth media was replaced with serum-free DMEM:F12 (Hyclone, Logan, UT) in which B104 cells then differentiate. B104 neurites were typically transected 24-48 hours after replacing the cell-growth media with serum-free DMEM:F12.

Transection of neurites of B104 cells

Prior to transection, the differentiation medium was washed out of the dishes twice with Ca^{2+}-free phosphate buffered saline (referred to as "Ca^{2+}-free saline", PBS -/-, HyClone, Logan, UT) and replaced with Ca^{2+}-free saline. Unless stated otherwise, all neurites were transected in Ca^{2+}-free saline using a sharpened, pulled-glass micro-capillary tube ("micro-knife"), which was placed on a micro-manipulator (Narishige Instruments, East Meadow, NY) and quickly drawn across the surface of the Petri dish, etching a score line that showed the path of the knife. We were able to uniquely and individually identify each transected cell by the relation of the transected neurite to its soma and to the score mark on the plate (17). Cells were exposed to Ca^{2+}-free saline for a maximum of ten minutes. The Ca^{2+}-free saline was then replaced with a phosphate buffered saline containing 1 mM Ca^{2+} ("Ca^{2+}-saline", PBS+/+, HyClone, Logan, UT) to initiate the sealing process (17). Cells were exposed to Ca^{2+}-saline for five minutes prior to assessment of sealing.

Assessment of plasmalemmal sealing

Dye exclusion is the most reliable and reproducible measure of plasmalemmal sealing (17). Other methods of evaluating sealing often have ambiguous or un-interpretable results (17). Membrane bound structures are often damaged during fixation for electron microscopy, thereby preventing accurate observations of vesicle accumulation at the damage site (17).

We added a fluorescent dye, 3 kDa Texas Red dextran (Molecular Probes, Eugene, OR), to the Ca^{2+}-free saline as an indicator of rapid plasmalemmal sealing. For all experiments, the dye was thoroughly washed out with Ca^{2+}-saline after a 10 min exposure to Texas Red dextran and sealing was assessed. Transected cells that excluded dye were counted as "sealed". Cells that did not exclude dye were counted as "not sealed". We consistently used 3 kDa Texas Red dextran to assess sealing in all other experiments reported herein to avoid any variation in sealing time due to differences in dye molecular weight (17).

B104 cells were observed under an inverted Zeiss Axio Vert A1 fluorescent microscope with a 40X, long focal length lens and illuminated by a Lumen Dynamics X-Cite series 120Q light source. We transected 10-30 uniquely identifiable cells within 5-10 min in a Petri dish containing the Ca^{2+}-free saline, Texas Red Dextran and, in some, bzATP. Sealing of individually identified cells transected nearer to (< 50 μm), and farther from (> 50 μm), the soma were typically observed on the same Petri dish. For this paper, we only counted cells with neurites transected farther from the soma. To insure that transections "farther from the soma" were greater than 50 μm, other cells were purposefully cut as far from the cell body as possible (typically 80-100 μm). At least 44 cells total were cut using at least two Petri dishes with an average of 64. Cells with transection distances not obviously "farther from" the soma were not included in dye exclusion counts.

Pharmacological Reagents and Toxins

All pharmacological agents were dissolved in distilled water, unless otherwise noted.: [2'(3')-O-(4-Benzoylbenzoyl)adenosine 5'-triphosphate triethylammonium salt : BzATP ,Sigma B6396), Texas Red Dextran, 3000 MW, Neutral (Invitrogen D3329).

Statistical analyses

For each experimental treatment group, at a given PC time, the data were pooled for all cells (n) from all Petri dishes (N). "Sealing probability" was defined as the percent of a set of individually-transected and uniquely identified cells that excluded 3 kDa Texas Red dextran (sealed) at a given PC time. This value was obtained by dividing the total number of sealed cells by the total number of transected cells. Therefore, a "sealing probability" of 30% means that 30% of transected cells completely excluded dye at a given PC time.

The Cochran-Mantel-Haenszel χ^2 (CMH X^2) test for independence was used as the most appropriate statistical test to determine whether differences between sealing probabilities at a given PC time for different experimental treatments were statistically significant ($p < 0.05$), as previously described (17). Briefly, the CMH X^2 test for independence is used to compare data separated into two by two contingency tables (sealed or not sealed, and control vs. experimental data sets). Furthermore, the CMH X^2 test requires binary outputs, which applies to our sealing assay (sealing is treated as a "yes" or "no" event at a given PC time). Since sealing of a given cell and, but not each Petri dish (sometimes containing over 100 transected cells), are independent events, measures of variance (such as SE or SD) are not applicable.

Results

Electrophysiology data

Electrophysiological testing immediately post-repair revealed a difference between baseline (mean 4.965 n = 12) and FCF (mean 0.8225, n = 4) (p=0.0091) (**Figure 1**). A difference was also seen between BzATP (mean 5.045 n = 4) and FCF (mean 0.8225, n = 4) (p = 0.0208), but no difference was seen between Baseline and BzATP (**Figure 1**). Baseline CAPs were present in all animals (mean 4.965 $\pm$ 2.032 mV, minimum 1.360 mV, maximum 8.240 mV; n= 12) and the combined results are shown (**Figure 1**). Individually, no statistically significant differences were detected between baseline CAPs in the experimental control groups (Use One-way Anova): FCF (mean 5.230 $\pm$ 2.608 mV, min 1.940 mV, max 8.240 mV), experimental BzATP (mean 5.032 $\pm$ 2.631 mV, min 1.360 mV, max 7.500 mV), experimental oATP (mean 4.633 $\pm$ 1.081 mV, min 3.490 mV, max 5.600 mV), or control groups (data not shown) prior to neurotomy. After nerve transection and repair CAPs were obtained for most animals within the experimental groups. Controls for PEG fusion (n = 6), FCF without PEG (n = 6), and BzATP without PEG (n = 6) had no CAPs immediately after repair or 21 days post-repair. By contrast, 21 day post-repair CAPs were found in FCF-treated animals (n = 6) and not in the BzATP (n = 6) treated animals. Values for the FCF treated animals were statistically smaller than baseline values (p = 0.0012). (**Figure 2**) 3 week FCF CAP values were mean 1.105 ± 1.713, min 0.000, max 3.400, n = 6. Thus, the FCF treated group was the only group that exhibited CAPs at 21 days, as compared to control and BzATP. While there was no statistically significant difference between baseline and immediate BzATP-treated CAPs (p = 0.9567), CAPs could not be obtained in the BzATP with PeG, BzATP without PEG, FCF without PEG, or the Control groups at 21 days. (**Figure 2**)

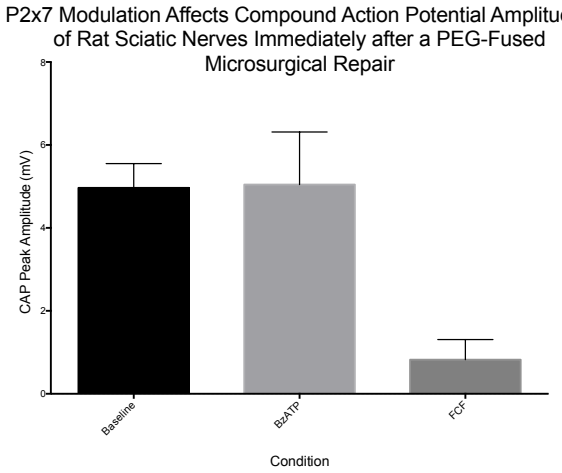

Figure 1. FCF treatment groups demonstrated a statistically significant decrease in Compound Action Potential Amplitudes as compared to Baseline and BzATP treatment groups immediately after PEG-based Nerve Fusion (50% PEG 3.35kD). ($p < 0.0091$ and $p < 0.0208$). Baseline n=12, BzATP n=4, FCF n=4.

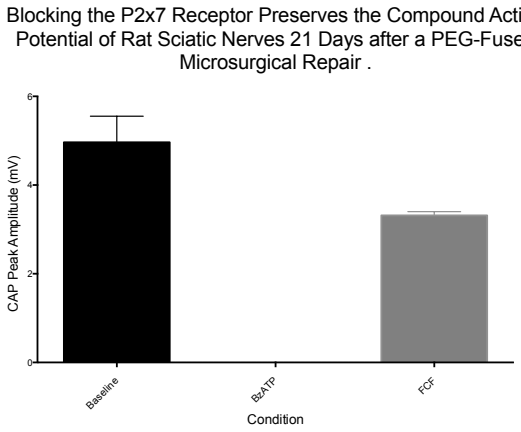

Figure 2. FCF treatment groups maintained a Compound Action potential at 21 days while the BzATP and Control Treatments groups did not. The CAP recorded for the FCF treatment group was statistically less than baseline. ($p < 0.0012$) FCF n=6, Baseline n=12

Behavioral Data

Foot Fall Asymmetry Score

Footfall asymmetry scores were significantly improved for FCF treatment group compared to FCF without PEG at 7, 14, and 21 days postoperatively ($p<.05$). (**Figure 3**). The FCF treatment group was improved compared to control at 3, 7, 14, and 21 days ($p<.05$)There was a difference seen on Day 7

between FCF with PEG and BzATP with PEG ($p<.05$), but that trend was not seen on day 3, 14, and 21 ($p>.05$). On days 3, 7, and 14 BzATP with PEG was statistically better than BzATP without PEG ($p<.05$). (**Figure 3**) FCF with PEG Treated values for footfall asymmetry scores for postoperative day 3 had a mean value of -75.25 $\pm$ 21.75 (min -116, max -42, n = 8), postoperative day 7 had a mean value of -66.25 $\pm$ 5.020 (min -86, max -46, n = 8), postoperative day 14 had a mean value of -52.75 $\pm$ 3.890 (min -74, max -42, n = 8), and postoperative day 21 had a mean value of -55.50 $\pm$ 6.276 (min -80, max -22, n = 8). BzATP with PEG Treated values for footfall asymmetry scores for postoperative day 3 had a mean value of -81 $\pm$ 17.29 (min -108, max -64, n = 6), postoperative day 7 had a mean value of -90.00 $\pm$ 4.517 (min -106, max -78, n = 5), postoperative day 14 had a mean value of -68.00 $\pm$ 7.616 (min -90, max -44, n = 5), and postoperative day 21 had a mean value of -68.80$\pm$ 5.499 (min -88, max -58, n = 5). FCF without PEG values for footfall asymmetry scores for postoperative day 3 had a mean value of -102.0 $\pm$ 7.155 (min -116, max -96, n = 6), postoperative day 7 had a mean value of -99.67 $\pm$ 9.416 (min -116, max -90, n = 6), postoperative day 14 had a mean value of -95.33 $\pm$ 11.84 (min -118, max -86, n = 6), and postoperative day 21 had a mean value of -69.33 $\pm$ 15.42 (min -86, max -42, n = 6). BzATP without PEG values for footfall asymmetry scores for postoperative day 3 had a mean value of -121.0 $\pm$ 8.075 (min -130, max -112, n = 6), postoperative day 7 had a mean value of -118.3 $\pm$ 10.07 (min -128, max -100, n = 6), postoperative day 14 had a mean value of -117.7 $\pm$ 12.23 (min -138, max -102, n = 6), and postoperative day 21 had a mean value of -86.00 $\pm$ 12.96 (min -102, max -66, n = 6). Control values for footfall asymmetry scores for postoperative day 3 had a mean value of -98.4 $\pm$ 8.877 (min -114, max -92, n = 5), postoperative day 7 had a mean value of -88 $\pm$ 4 (min -102, max -72, n = 8), postoperative day 14 had a mean value of -72.75 $\pm$ 3.228 (min -92, max -62, n = 8), and postoperative day 21 had a mean value of -80.29 $\pm$ 3.637 (min -94, max -66, n = 7).

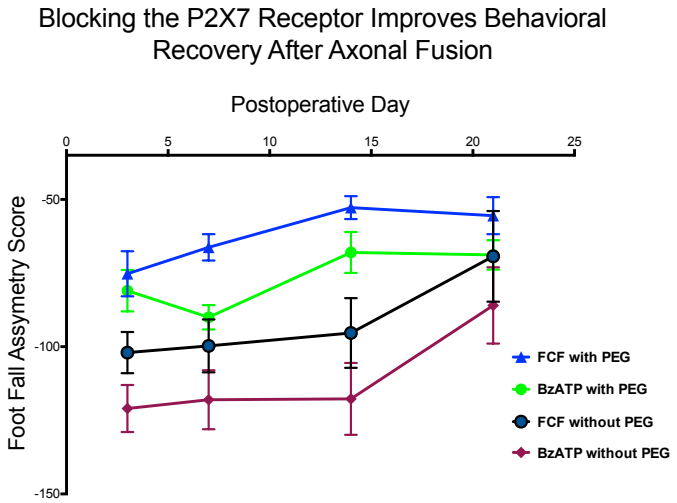

Figure 3. The P2x7 receptor is activated by BzATP, an ATP analog, and competitively antagonized by FCF. At 7 days and 14 days FCF with PEG was statistically improved compared to FCF without PEG ($p<.05$). On day 7, FCF with PEG was improved compared to BzATP with PEG ($p<.05$), however, on days 3, 14, and 21 there were no differences seen statistically. On day 3, day 7, day 14 BzATP with PEG was statistically better than BzATP without PEG ($p<.05$).

In vitro sealing

Figure 4 shows the ratios of sealed to unsealed neurons where different concentrations of BzATP were used. Neurons treated with 0.3 μM, 3 μM, 30 μM, and 300 μM had a sealed to unsealed ratio of 0.2558±0.4415, 0.4833±0.5039, 0.4714±0.5028, and 0.3205±0.4697 respectively. There was a statistical difference between 3 μM and 0.3 μM ($p=.0245$) as well as 30 μM and 0.3 μM ($p=.0289$). There was so difference between 3 μM, 30 μM, and 300 μM concentrations.

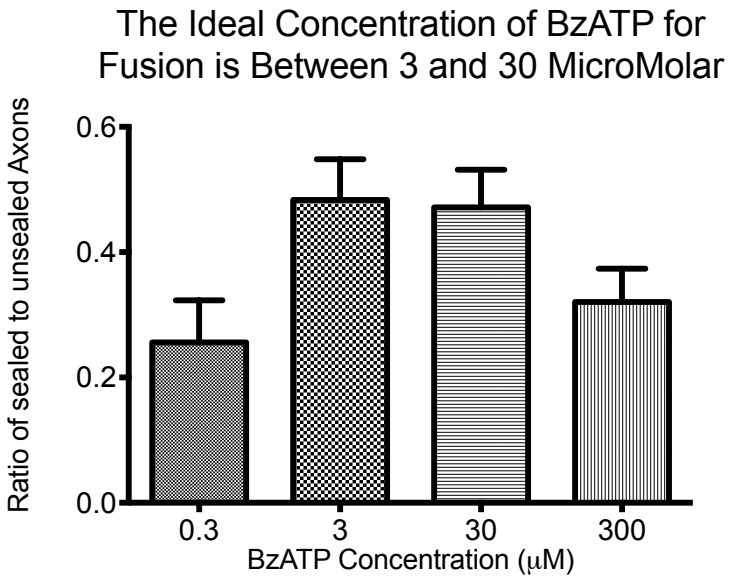

Figure 4. Ideal concentrations were determined to be between 3 and 30 μM. There a statistical difference between 3 μM and 0.3 μM as well as 30 μM and 0.3 μM ($p<.05$). No statistical difference was shown between 300 μM and the other groups.

Histological data

Figure 5 shows representative nerve sections staining for axons using antibodies specific for myelin basic protein 21 days after injury. Nerves treated with FCF did show a trend of increased myelinated axonal counts (1830±351.1, n=8) compared to BzATP (1690±166.5, n=6), or control (1614±237.4, n=5), but this trend did not reach statistical significance (p=.3853, p=.2971), however, this could be confounded by axonal outgrowth because axons could have grown over 2cm from the neurorrhaphy site in this timeframe.

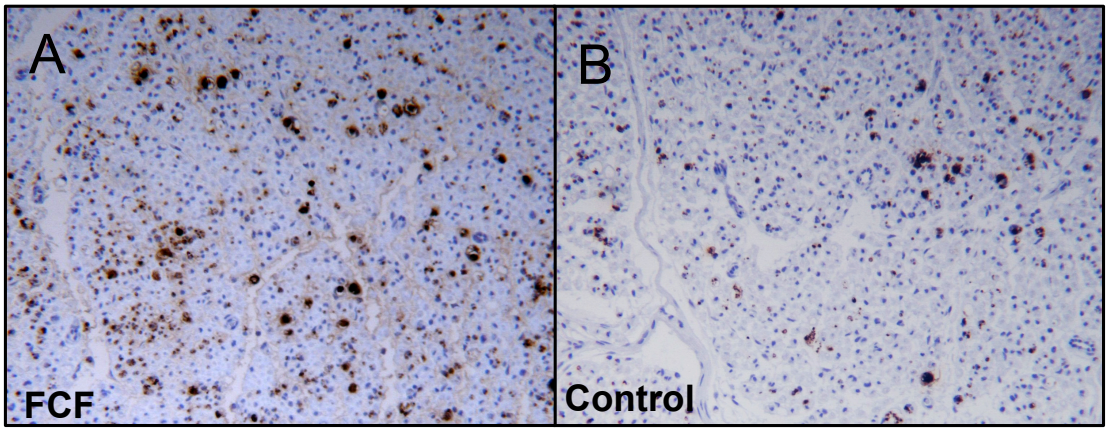

Figure 5. Representative photomicrographs of nerve cross sections comparing the FCF Treatment group versus Control. A) FCF treated nerve stained with myelin basic protein 21 days postoperatively, distal. B) Control nerve stained with myelin basic protein 21 days postoperatively, distal

Discussion

Peripheral nerve injury is common, occurring in over 17,500 cases annually in the United State. (18,19) Techniques such as nerve grafts, tissue matrices, and nerve growth guides have been designed to enhance the number of axons regenerating by outgrowths from surviving distal stumps. (3) Regardless of repair strategy, regenerating axons may take months to reach the denervated target tissues when injuries are proximal which results in poor outcomes. (3, 20) Electrophysiological studies of distal nerve segments after cut severance in rats revealed that distal stumps, when stimulated directly, most will fail to conduct CAPs by 24 hours and all failed to conduct CAPs at 36 hours even if repaired. (21) In our prior reports on PEG fusion, we demonstrated that PEG fusion of severed nerves can delay this process and behavioral studies also showed that PEG fused nerves improved functional outcomes after nerve transection. (7,5)

Calcium modulation is a critical part of PEG based axonal repair because once calcium enters the axon, the cut nerve ends seal preventing PEG based axonal fusion. (7) In an attempt to further enhance the

efficiency of PEG based axonal fusion (7), we attempted to modulate calcium influx after injury at the cellular level through selective activation or inhibition of channels that allow calcium influx after injury. P2X receptors are a family of ligand-gated ion channels consisting of proteins with intracellular amino and carboxy termini and a large extracellular loop between 2 hydrophobic segments that bind extracellular ATP. (10) Seven different subtypes of this receptor have been cloned, the first isolated from smooth muscle and the remaining from nervous tissue. (22) Activation of this receptor has been shown to increase calcium influx by causing the formation of pannexin pores after nerve injury. (23,24,25). These holes allow for the influx of calcium across the cell membrane. **Figure 6** and **Figure 7** demonstrate the proposed effects of P2X7 on intracellular calcium. For injured neurons, this is believed to play a role in the initiation of Wallerian degeneration. (8,11) Blocking the P2X7 pathway with Brilliant Blue (FCF), a purinergic specific blocker of the P2X7 pathway, or activating with (bzATP), a nonspecific activator of the P2X7 pathway, (25) in combination with PEG mediated fusion, we can enhance, with FCF, or reduce, with bzATP, the post PEG fusion compound action potentials. We believe this smaller current of calcium ions crossing the plasmalemmal membrane is due to closed pannexin pores caused by the Antagonist effects of FCF. (**Figure 1**) **Figure 2**, however, shows that fused axons treated with FCF are more likely to maintain the ability to support CAP transmission after 3 weeks compared to either control, or BzATP treated axons. **Figure 3** shows the progression of behavioral function over 21 days. Remarkably, rats treated with FCF, which blocks the P2X7 pathway, showed significant improvement compared to control points (n=8). A statistical difference was also shown between FCF and bzATP at Day 7 ($p = .008$), but not shown with days 3, 14, and 21. ($p=.60$, .0733, and .1724, respectively). This data implies that blocking the P2X7 receptor improves functional outcomes compared to controls. Footfall behavioral data is a more specific test for sciatic nerve function whereas CAPs are more sensitive for sciatic nerve function. This could potentially explain the discrepancy seen in Footfall data versus CAPs at 3 weeks.

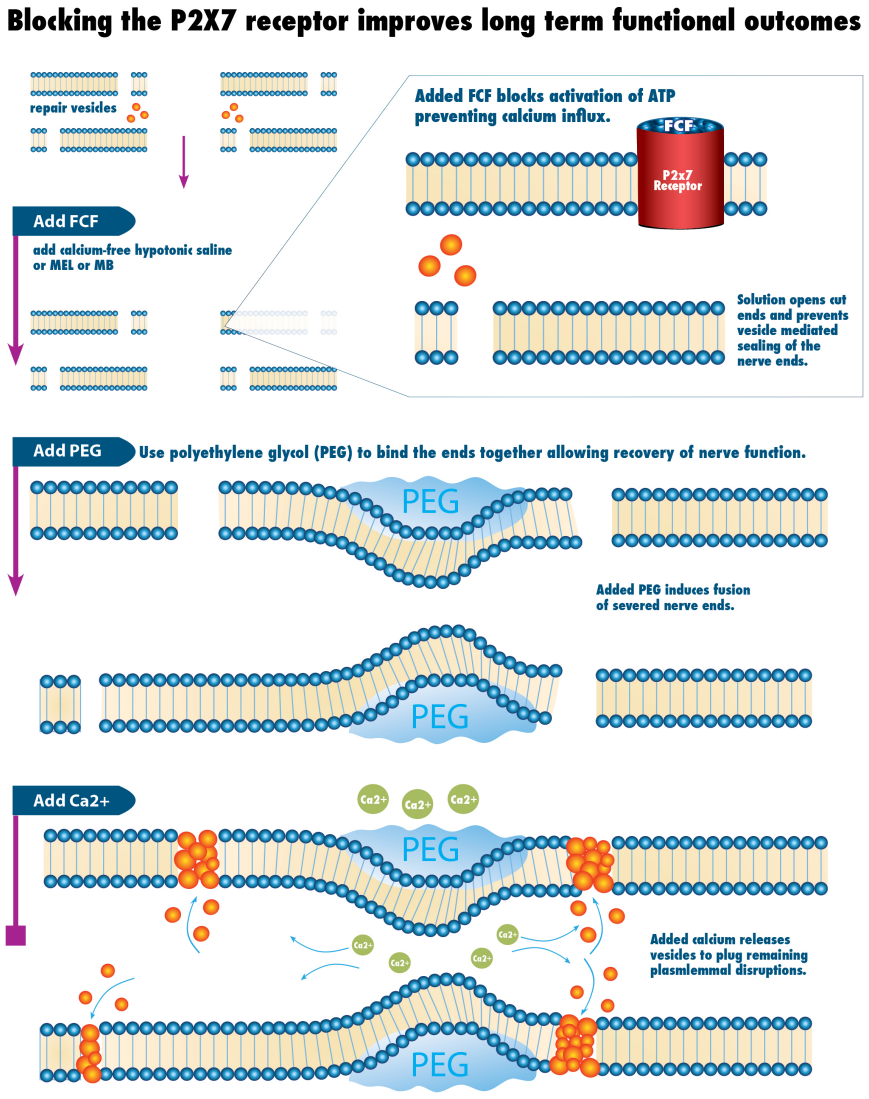

Figure 6. Proposed mechanism of the effects of P2x7 receptor blockade in PEG fusion of peripheral nerve axons.

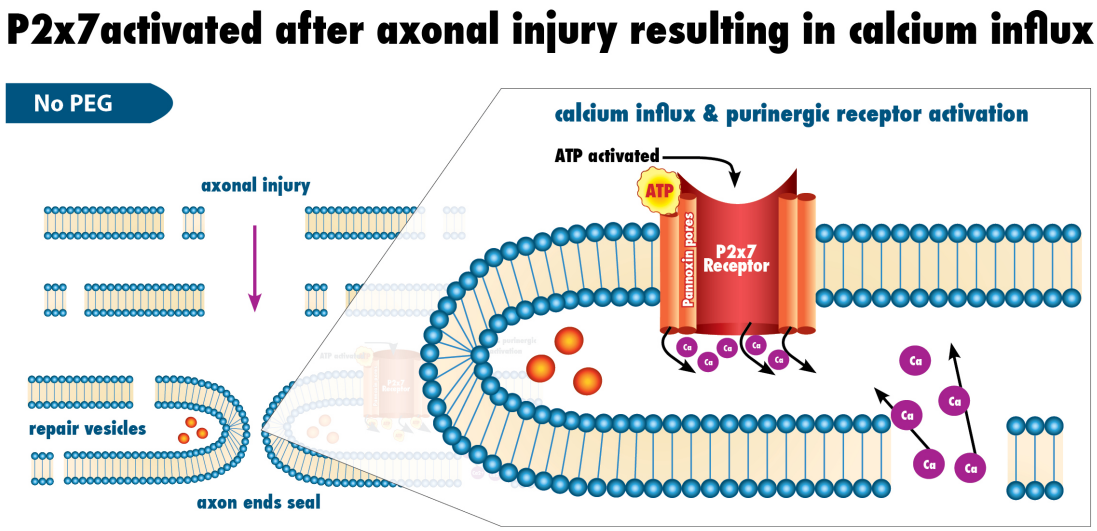

Figure 7. Proposed mechanism of axonal sealing following axotomy and activation of the P2x7 receptor.

Interestingly, *in-vitro* studies using bzATP and our B104 neurite axonal injury model have shown that bzATP can enhance sealing in a dose dependent fashion (Fig 4). Although at high doses, bzATP becomes toxic to cells (data not shown), lower doses in the 3-30uM range statistically increase sealing of transected neurites. We believe this premature sealing prevents PEG based fusion and explains why the bzATP PEG fused animal behavior models that of no PEG fusion control (Figure 3). Interestingly, this is one of the first reports of increased sealing of transected B104 neurites in the absence of calcium. Possible explanations for this bzAPT / P2X7 mediated sealing after axon injury include alteration of intracellular calcium stores to augment fusion, or could even imply an alternative, calcium independent, mechanism of axonal sealing after injury.

We also noted a trend toward improvement in axon survival noted in immunohistochemical studies at 3 weeks after nerve transection and repair. Taken together, these data give evidence that receptor based modulation of calcium entry after nerve injury can enhance outcomes after PEG based

axonal fusion in a rat model. We believe that this is most likely due to prevention of P2X7 mediated calcium influx after axonal injury and could have implications for this and other nerve repair strategies.

Historically, experimental models of nerve injury have shown that calcium modulation can improve nerve recovery. (26,27) These authors demonstrated that nerve outgrowth and recovery could be increased through calcium channel modulation. These elegant animal studies were followed by a remarkable case report in which calcium channel blockade with nimodipine resulted in advanced recovery after laryngeal nerve transection in a human patient. (26) Our work lends further evidence that calcium modulation may be beneficial after peripheral nerve injury. Treatment with FCF can improve early functional outcomes after PEG fusion of acutely transected nerves. (**Figure 3**) Fusion of transected axons after injury or resection could revolutionize nerve repair strategies. If these strategies demonstrate progress in larger animal models where the distance between end organs and nerve injury site are larger, we envision that this line of investigation will eventually find its application in human nerve injury. For patients with proximal nerve injuries or brachial plexus injuries, these advancements might mean more than just earlier recovery, but might allow for recovery of muscle function that is not possible using current nerve repair strategies. Since the rate of axonal outgrowth after standard neurorrhaphy techniques is only 1 mm per day, for proximal neuronal injuries that are over 30 cm from the motor endplate, reinnervation occurs too late for functional recovery. By avoiding the current delays in recovery associated with axonal outgrowth, patients may experience more immediate and overall improved outcomes.

Future Directions

Since nerve repair is often not available immediately at the time of injury, we will expand our trials to include techniques that may increase our ability to fuse severed axons in a delayed nerve repair model. We have evidence that we can successfully delay nerve repair up to 24hrs after injury and still

fuse the severed axons, but note that if the repair is delayed beyond 3 days that nerve degeneration will reduce our ability to fuse-repair severed axons. (data not shown) Interestingly, we note a trend that behavioral outcomes only improved roughly 25% in the 24 hour delayed nerve injury experiment compared over 50% improvement typically seen at similar post fusion times (data not shown) for animals that underwent nerve severance with immediate repair. As noted in this report, we have been able to demonstrate that modulation of calcium influx into the injured axons by treating the wound bed with FCF at the time of injury, and immediately before fusion repair improves outcomes (**Figure 3**). We plan to use FCF to see if we can improve outcomes in a delayed nerve repair model where animals have their sciatic nerves injured, then repaired 24hr later to try to bolster outcomes to the level seen when the fusion repair is performed immediately at the time of injury.

Limitations

Larger animal model should be studied in order to confirm that both the PEG fusion effect and the calcium modulation effect of FCF are maintained and are relevant to human nerve injuries. In our small animal model, 8 weeks after nerve repair axonal outgrowth in control groups that have appropriate neurorrhaphy typically improve and this may confound our ability to assess differences in treatment groups. Also, we do not know how many axonal segments are PEG-fused or the specificity of the motor or sensory proximal-distal axonal fusions. Misalignments can be compounded when using nerve grafts to repair gaps, or when mixed nerves, as opposed to purely motor or sensory nerves are repaired. If outcomes in future large animal studies are suboptimal, rotational studies may be required to evaluate functional outcomes in situations where nerve fascicles are purposely misaligned. If this is a persistent problem in our nerve repairs, fascicular based fusion or more microsutures may be required to improve alignment and minimize the effects of rotation.

In summary, we report that combination therapy of PEG fusion and calcium modulation technique can improve electrophysiologic and behavioral outcomes after nerve transection. Future studies to include the testing with larger animal models and even nerve grafts for nerve injuries with nerve gaps allografts to build on the foundational work reported in this manuscript.

References

1. Kalbermatten, D. F., J. Pettersson, et al. (2009). "New fibrin conduit for peripheral nerve repair." J Reconstr Microsurg **25**(1): 27-33.

2. Lago, N. and X. Navarro (2006). "Correlation between target reinnervation and distribution of motor axons in the injured rat sciatic nerve." Journal of Neurotrauma **23**(2): 227-240.

3. Evans, P. J., J. R. Bain, et al. (1991). "Selective reinnervation: a comparison of recovery following microsuture and conduit nerve repair." Brain Res **559**(2): 315-321.

4. Britt, J. M., J. R. Kane, et al. (2010). "Polyethylene glycol rapidly restores axonal integrity and improves the rate of motor behavior recovery after sciatic nerve crush injury." J Neurophysiol **104**(2): 695-703.

5. Sexton, K. W., A. C. Pollins, et al. (2012). "Hydrophilic polymers enhance early functional outcomes after nerve autografting." The Journal of surgical research.

6. Donaldson, J., R. Shi, et al. (2002). "Polyethylene glycol rapidly restores physiological functions in damaged sciatic nerves of guinea pigs." Neurosurgery **50**(1): 147-156; discussion 156-147.

7. Bittner, G. D., C. P. Keating, et al. (2012). "Rapid, effective, and long-lasting behavioral recovery produced by microsutures, methylene blue, and polyethylene glycol after completely cutting rat sciatic nerves." Journal of neuroscience research **90**(5): 967-980.

8. Yoo, S., M. P. Nguyen, et al. (2003). "Plasmalemmal sealing of transected mammalian neurites is a gradual process mediated by Ca(2+)-regulated proteins." J Neurosci Res **74**(4): 541-551.

9. Chessell, I. P., J. P. Hatcher, et al. (2005). "Disruption of the P2X7 purinoceptor gene abolishes chronic inflammatory and neuropathic pain." Pain **114**(3): 386-396.

10. Arbeloa, J., A. Perez-Samartin, et al. (2012). "P2X7 receptor blockade prevents ATP excitotoxicity in neurons and reduces brain damage after ischemia." Neurobiology of disease **45**(3): 954-961.

11. Lee, S. K. and S. W. Wolfe (2000). "Peripheral nerve injury and repair." J Am Acad Orthop Surg **8**(4): 243-252.

12. Brophy et al. (2011) “Methods and Compositions for Vein Harvest and Autografting” United States Patent Application Publication. US2011/0190572A1.

13. Kantor, T. G. (1986). "Ketoprofen: a review of its pharmacologic and clinical properties." Pharmacotherapy **6**(3): 93-103.

14. Sedy, J., L. Urdzikova, et al. (2008). "Methods for behavioral testing of spinal cord injured rats." Neurosci Biobehav Rev **32**(3): 550-580.

15. Abràmoff, M.D., Magalhães, P.J. & Ram, S.J. Image processing with ImageJ. *Biophotonics international* **11**. 36-42 (2004).

16. Marina N, Bull ND, Martin KR. A semiautomated targeted sampling method to assess optic nerve axonal loss in a rat model of glaucoma. Nat Protoc 2010; 5:1642.

17. Spaeth, C. S., T. Robison, et al. (2012). "Cellular mechanisms of plasmalemmal sealing and axonal repair by polyethylene glycol and methylene blue." J Neurosci Res **90**(5): 955-966.

18. Wolfe SW, Hotchkiss RN, Pederson WC, Kozin SH. Green's Operative Hand Surgery. Churchill Livingstone. 2011;5.

19. Kang, J. R., D. P. Zamorano, et al. (2011). "Limb salvage with major nerve injury: current management and future directions." J Am Acad Orthop Surg **19 Suppl 1**: S28-34.

20. Eidelberg, E., D. Straehley, et al. (1977). "Relationship between Residual Hindlimb-Assisted Locomotion and Surviving Axons after Incomplete Spinal-Cord Injuries." Experimental Neurology **56**(2): 312-322.

21. Miledi, R. and C. R. Slater (1970). "On the degeneration of rat neuromuscular junctions after nerve section." J Physiol **207**(2): 507-528.

22. Riley, D. A., J. R. Sanger, et al. (1988). "Identifying motor and sensory myelinated axons in rabbit peripheral nerves by histochemical staining for carbonic anhydrase and cholinesterase activities." Brain Res **453**(1-2): 79-88.

23. Schemann, M., H. Sann, et al. (1993). "Identification of cholinergic neurons in enteric nervous system by antibodies against choline acetyltransferase." Am J Physiol **265**(5 Pt 1): G1005-1009.

24. Nichols, C. M., T. M. Myckatyn, et al. (2005). "Choosing the correct functional assay: a comprehensive assessment of functional tests in the rat." Behav Brain Res **163**(2): 143-158.

25. Zhang, Z., E. O. Johnson, et al. (2006). "Long-term evaluation of rabbit peripheral nerve repair with end-to-side neurorrhaphy in rabbits." Microsurgery **26**(4): 262-267.

26. Mattsson, P., A. M. Janson, et al. (2001). "Nimodipine promotes regeneration and functional recovery after intracranial facial nerve crush." J Comp Neurol **437**(1): 106-117.

27. Gomez, T. M. and N. C. Spitzer (1999). "In vivo regulation of axon extension and pathfinding by growth-cone calcium transients (vol 397, pg 350, 1999)." Nature **399**(6731): 84-84.

PEG FUSION OF NERVE ALLOGRAFTS

Adapted from: D. C. Riley, G. D. Bittner, M. Mikesh, N. L. Cardwell, A. C. Pollins, C. L. Ghergherehchi, S. R. Bhupanapadu Sunkesula, T. N. Ha, B. T. D. Hall, A. D. Poon, M. Pyarali, R. B. Boyer, A. T. Mazal, N. Munoz, R. C. Trevino, T. Schallert, and W. P. Thayer, "Polyethylene glycol-fused allografts produce rapid behavioral recovery after ablation of sciatic nerve segments.," *J. Neurosci. Res.*, Nov. 2014.

Abstract

Restoration of neuronal functions by outgrowths regenerating at ~1mm/d from the proximal stumps of severed peripheral nerves takes many weeks or months, if it occurs at all, especially after ablation of nerve segments. Distal segments of severed axons typically degenerate in 1-3 days. The purpose of this study was to show that Wallerian degeneration could be prevented or retarded and lost behavioral function restored following ablation of 0.5 – 1 cm segments of rat sciatic nerves in host animals. This is achieved using 0.8 – 1.1cm microsutured donor allografts treated with bioengineered solutions varying in ionic and polyethylene glycol (PEG) concentrations (modified PEG-fusion procedure), being careful not to stretch any portion of donor or host sciatic nerves. Our data show that PEG-fusion permanently restores axonal continuity within minutes as initially assessed by action potential conduction and intracellular diffusion of dye. Behavioral functions mediated by the sciatic nerve are largely restored within 2 - 4 wk as measured by the Sciatic Functional Index (SFI). Increased restoration of sciatic behavioral functions after ablating 0.5 – 1 cm segments is associated with greater numbers of viable myelinated axons within, and distal to, PEG-fused allografts. Many such viable myelinated axons are almost-certainly spared from Wallerian degeneration by PEG-fusion. PEG-fusion of donor allografts may produce a paradigm-shift in the treatment of peripheral nerve injuries.

Introduction

Behavioral recovery after severing PNS axons in mammals and invertebrates

Rapid and effective repair of peripheral nerve injuries to restore lost behavioral functions, especially after ablation of ≥ 0.5 – 2 cm segments, remains an unattained goal of clinicians and neuroscientists (Birch et al., 1998; Allan, 2000; Bittner et al., 2000, 2012; Campbell, 2008).

Severed mammalian peripheral axons naturally regenerate by slow (~1mm/d) outgrowths from severed proximal stumps while their severed distal stumps usually degenerate within 1 - 3d (Wallerian degeneration) (Ramon y Cajal, 1928; Campbell, 2008). Regenerating axons often do not remake functional connections after a simple transection, and behavioral recovery is rarely fully restored. Even the best current techniques to re-appose cut ends by microsutures through the epineurium or tubular conduits do not re-establish axonal continuity, produce rapid functional recovery or prevent Wallerian degeneration (Campbell, 2008). Furthermore, behavioral recovery is much worse and sometimes non-existent if the cut ends cannot be directly re-apposed after loss of a segment of a PNS nerve in humans (Allan, 2000) and rats (Bittner et al., 2012). In contrast to the slow and often inadequate regeneration-repair of severed mammalian peripheral nerves, severed PNS (and some CNS) axons in many phyla naturally, rapidly and effectively restore lost behaviors by outgrowths from proximal stumps that functionally activate or specifically fuse with their own surviving distal axonal segments so that the two severed axonal halves function as one continuous axon within days after lesioning (Hoy et al., 1967; reviewed by Bittner et al., 2000).

Development of PEG-fusion procedures to repair singly crushed or cut axons

Polyethylene glycol (PEG) as an artificial membrane fusogen was initially used to rapidly and permanently reconnect (PEG-fuse) the severed proximal and distal ends of giant invertebrate axons (Krause and Bittner, 1990; Lore et al, 1999). We and others subsequently described cellular pathways that induce sealing

(repair) of plasmalemmal holes or axonal transections and identified many substances such as calcium and methylene blue that promote or inhibit, respectively, vesicle formation and membrane repair (Krause et al.,1994; Steinhardt et al, 1994; Spaeth et al, 2012). Consequently, PEG-fusion success was greatly enhanced if the cut ends were opened and vesicle formation at cut ends inhibited by calcium-free hypotonic salines containing methylene blue or melatonin (Krause and Bittner, 1990; Lore et al, 1999; Britt et al., 2010).

A PEG-fusion technique consisting of a well-defined sequence of bioengineered solutions could rapidly and permanently (12 weeks postoperatively) restore up to 80% of lost behavioral function as measured by the Sciatic Functional Index (SFI) in rats with singly crushed sciatic nerves severed and repaired in *calcium-free* salines (Britt et al, 2010). By using microsutures to closely appose cut axonal ends that separate by several mm, lost behavioral function could be similarly restored when all procedures were again performed in *calcium-free* salines (Bittner et al., 2012). Sciatic nerves cut in calcium-containing solutions or extracellular fluids could also be repaired, although the animals were only tested for action potential through-conduction immediately postoperatively (Bittner et al., 2012) or followed for 1 week behaviorally (Rodriguez-Feo et al., 2013). In the course of these procedures, we noted that careful trimming of cut axonal ends in Ca-free hypotonic salines enhanced their close apposition and the PEG-fusion of cut ends. However, cut-end trimming increased the separation between cut ends and stretching or pulling on nerves greatly reduced behavioral recovery after their PEG-fusion. Furthermore, crushes made in calcium-containing salines were infrequently repairable because the crushed segment had to be cut out (ablated) and the nerve stretched for PEG-repair with microsutures.

Development of PEG-fusion procedures to repair ablated axonal segments

Repair of 0.5cm segments of rat sciatic nerves ablated in *calcium-containing* extracellular fluids could be achieved by re-inserting the segment (an autograft) and repairing both cut ends with microsutures and PEG-fusion (Sexton et al., 2012). At three post-operative days, animals with PEG-fused autografts had (1) action potentials

conducting across the autograft, (2) significantly more sensory and motor axons surviving within, and distal to, the autograft, and (3) significantly better SFI scores compared to negative control animals with autografts that were not PEG-fused. However, microsuturing during PEG-fusion stretched axons in the donor autograft and host sciatic nerve and PEG-fused autografts might pull apart or otherwise fail after 3d. Furthermore, in almost any clinical setting, an ablated nerve segment is not recoverable for subsequent use as an autograft. Autografts taken from other nerves to repair a major nerve are also often associated with significant donor site morbidity (Birch et al., 1998; Allan 2000; Campbell 2008) and are much smaller in diameter than the sciatic nerves, making PEG-fusion repair difficult or impossible. Clinicaly, there has been increased interest in using nerve allografts to avoid donor site morbidity. In contrast, sciatic nerves (potential allografts) stored for 4 days *ex-vivo* at 6 - 9ºC exhibited good PEG-fusion repair un-stretched *ex vivo* (Marzullo et al, 2001). Finally, in a speculative pilot study using allografts stored for 2 days at 7ºC for six rats having micro-sutured, un-stretched PEG-fused sciatic nerves at 7 post-operatve days, we observed significant behavioral recovery compared to six negative control animals. At 7 postoperative days, we also observed retardation of Wallerian degeneration within, and distal to the allograft, in three PEG-fused animals compared to the same regions of the sciatic nerve in three negative control animals**.**

Given these findings, we developed a modified PEG-fusion procedure that uses 0.8 -1.1 cm long sciatic allografts excised in calcium-containing fluids from donor Sprague-Dawley rats and stored at 7ºC for 30min – 4 hr. The donor allograft is placed in a host Sprague-Dawley rat having a complete ablation of a 0.5-1cm long segment of its sciatic nerve in *calcium-containing* extracellular fluids. All severed axonal ends are carefully trimmed in calcium-free salines and microsutured to enhance close apposition of un-stretched cut axonal ends that are opened, and vesicle formation inhibited, by a hypotonic calcium-free saline containing methylene blue. PEG is then applied in a hypotonic calcium-free saline to induce axolemmal continuity. PEG is washed off with a calcium-containing isotonic saline to seal any remaining axolemmal discontinuities (Britt et al., 2010; Bittner et al., 2012).

Our data collected from two separate laboratories show that axolemmal function and axoplasmic continuity is rapidly (within minutes) restored in animals with successful PEG-fusion of allografted, un-stretched, sciatic

nerves. Significant behavioral function is restored within 3 -14d and is correlated with increased axonal viability of myelinated sensory and motor axons within, and distal to, the allograft, i.e., Wallerian degeneration is prevented or retarded. Furthermore, greater restoration of behavioral function is correlated with greater numbers of viable axons within, and distal to, PEG-fused allografts. Finally, this modified PEG-fusion procedure developed in an animal model uses concepts, techniques, and chemical substances that should be readily translatable to clinical procedures (Campbell, 2008; Williams et al., 2008; Burch, 2011).

Materials and Methods

Study design

We used 250-300 g Sprague-Dawley rats. Sprague-Dawley rats are not genetically homogeneous, i.e., there is genetic variation but not to the extent that might occur between different species. We used two groups of animals. One group received all PEG fusion procedures described below (PEG-fused animals) and the other group all procedures except application of PEG to closely apposed cut ends (negative control animals). All animals in both groups were initially tested for through-conduction of action potentials from the upper to lower thigh before and after lesioning and allograft repair. For the main study, at VU, 12 "negative control" rats received donor allografts that were not PEG-fused as did 6 negative control rats at UT; 13 rats received donor allografts that were PEG-fused at VU and 6 PEG-fused animals were produced at UT. VU animals were behaviorally tested at 3 and 7d postoperatively to determine whether there were any initial effects of PEG-fusion. UT animals were behaviorally tested at 3, 7, 14, 21, 28, 35 and 42 d postoperatively to confirm short-term effects and determine longer-term effects and sciatic nerves taken for histological analyses at 42 postoperative days. In a pilot study at VU, six PEG-fused and six negative control animals were behaviorally tested at 7 postoperative days and sciatic

nerves taken from three of these animals for histological analyses.

We used 5 or more animals per group because power analyses and our previous data (Britt et al, 2010; Bittner et al, 2012; Rodriguez-Feo et al, 2013) had shown that such sample sizes allowed us to detect SFI differences of 15 - 20% at $p < 0.05$ with Student's T-test. We used a larger number (12 - 13) of animals maintained for 1 wk to identify a statistically significant initial effect with more certainty. Once that was determined, power analyses of the data and our previously published data showed that we could use a smaller number (6) of animals to follow the effects for 6wk. We chose 6wks because 42 days should be beyond tissue rejection times and because previous studies on singly cut nerves had shown a plateau in behavioral recovery at 6wks that was maintained for 6 - 12wk thereafter (Bittner et al., 2012). Whether or not animals received PEG was determined by a pre-determined schedule. Animals were tested by those blinded to the conduct of the experiment. All experimental procedures were approved by and performed in accordance with the standards set forth by the Institutional Animal Care and Use Committees at VU and UT.

Surgical procedures for the modified PEG-fusion protocol

Female Sprague-Dawley rats were anesthetized with inhaled isoflurane (2%) and the left hind limb shaved with clippers. A three cm incision was made parallel, and just posterior, to the femur of the left leg. Using micro-scissors, a clean transection was made through the biceps femoris, parallel to the muscle fibers in order to minimize muscle damage under a surgical microscope at 10-30x (VU) or a dissecting microscope at 10-30x magnification (UT). CAPs were recorded in isotonic extracellular fluid by stimulating the entire sciatic nerve in the upper thigh and recording action potentials extracellularly from the entire sciatic nerve in the lower thigh.

A 0.5 - 1cm segment of sciatic nerve was removed (ablated) and replaced with a slightly longer segment of sciatic nerve from a donor Sprague-Dawley rat in calcium-containing extracellular fluid, sometimes washed

with calcium-containing isotonic saline. This procedure took 15 - 30 min. The donor segment was excised in calcium-containing extracellular fluids, occasionally washed with calcium free-containing isotonic saline, and stored at 7ºC for 30min - 4 hr in Plasma-lyte A® (Baxter: Deerfield, IL), which is calcium free and isotonic. The exposed, severed nerve in the host animal was then rinsed in Plasma-lyte A® (Baxter: Deerfield, IL). The donor segment was positioned carefully to maintain fascicle orientation and sized to insure that neither host nor donor nerves would be stretched at any step of the PEG-fusion procedure. Sciatic nerve ends of both donor and host animal were neatly trimmed flush to the epineural tissue and a hypotonic solution of 1% Methylene Blue (Acros Organics; Morris Plains, NJ) in sterile distilled water was applied to coaptation sites. Using standard microsurgical techniques, the allograft was sutured into place using 9-0 Ethilon (Ethicon, Sommerville, NJ) so that all cut ends were apposed (touching) without stretching the proximal, allograft, or distal axons. Once both ends were approximated and held in place by microsutures, a hypotonic 50% by weight solution of PEG (3.35kD molecular weight, Sigma-Aldrich; St. Louis, MO) in sterile water was applied to the coaptation sites for 1 minute in PEG-fused animals. Negative control animals did not receive PEG.

The wound was then flushed with isotonic Lactated Ringer (Hospira; Lake Forest, IL), which contains calcium, and tested for through- conduction of CAPs stimulated proximal to the allograft and recorded distal to the allograft. The cut thigh muscles were re-apposed by horizontal mattress sutures. The skin was re-approximated using a running subcuticular 5-0 monocryl suture (Ethicon, Sommerville, NJ). All animals received a subcutaneous injection of ketoprofen (5mg/kg) and were allowed to recover from anesthesia under careful monitoring

Electrophysiological testing

Extracellular recordings of Compound Action Potentials (CAPs) are a measure of axonal continuity between the stimulating and recording electrodes (Lore et al, 1999; Bittner et al., 2012). All CAPs were obtained using a

Powerlab Data Acquisition System (AD Instruments; Colorado Springs, CO) interfaced with LabChart 7 (AD Instruments; Colorado Springs, CO). The stimulating dual terminal electrode was placed under the sciatic nerve, proximal to the allograft. The recording electrode was placed under the sciatic nerve, distal to the allograft. CAPS were recorded prior to nerve segment removal (pre-injury) and immediately after application of isotonic Ca^{2+}-containing saline (post-PEG-fusion for experimental animals).

Intra-axonal dye diffusion across lesion sites

To assess morphological continuity in PEG-fused and negative control sciatic nerves, intra-axonal dye diffusion was observed for 12 sciatic nerves excised from the animal immediately after surgery at UT. After confirmation of physiological continuity through CAP conduction, a 3-4cm segment of sciatic nerve, including the graft site, was excised from the animal within 2hr. The proximal end of the sciatic nerve segment was placed within a watertight ring of petroleum jelly (Vaseline) containing Plasma-lyte A® and 50µl of 2kDa Texas red dextran (Lore et al., 1999; Bittner et al, 2012; Spaeth et al, 2012). The remainder of the nerve, including the proximal and distal lesion sites of the graft, was bathed in Plasmalyte A outside of the ring. The nerve was refrigerated for about 24hr at 4°C to allow time for dye to diffuse intracellularly through the length of the nerve. Nerves were examined for intra-axonal diffusion of fluorescent dye beyond the graft site using a Leica SP2 AOBS Confocal Microscope. Images were then stitched together using Adobe Photoshop in order to visualize the diffusion of dye through the entire length of the nerve.

***Behavioral testing using the Sciatic Functional Index (SFI)**:*

The SFI is a well-accepted measure of sciatic function that includes both appropriate sensory feedback and precise motor control, particularly for distal muscle masses that determine lower leg and toe position and movement (Mediniceli et al., 1982; Bittner et al, 2000, 2012; Britt et al, 2010). Behavioral assessments were at 3d and then weekly intervals up to 6wk post-operatively. Animals were not tested earlier to allow adequate recovery time from the effects of ketoprofen administration at the time of surgery. Rats were trained to walk up an inclined beam to a cage. After these habituation trials, the rats navigated the beam to the cage without hesitation. For each trial run, a strip of white receipt paper was secured to the wooden beam for data collection. The hind limbs were inked such that blue designated the surgical limb and red the un-operated limb before the animals were placed on the end of the beam farthest from the cage.

As previously reported (Medinaceli et al., 1983; Britt et al., 2010; Bittner et al,. 2012) the SFI was scored as follows: Three consecutive footprints from each limb were used to measure normal print length (NPL), normal toe spread (NTS), normal intermediary toe spread (NIS), experimental print length (EPL), experimental toe spread (ETS), and experimental intermediary toe spread (EIS). Intermediary toe spread was measured from toes 2 - 4, toe spread toe 1-5, and print length from the heel to end of toe 3. SFI scores were then calculated using mean values by:

$$SFI = -38.3((EPL-NPL)/NPL) + 109.5((ETS-NTS)/NTS) + 13.3\ ((EIT-NIT)/NIT) - 8.8$$

Behavioral function was assessed by those blind by to the treatment. SFI scores of -100 or less indicate complete loss of sciatic nerve function and scores of ± 10 indicate normal sciatic nerve function.

Histology

For toluidine blue stains at UT of viable myelinated axons, rats were deeply anesthetized with ketamine/xylazine and perfused transcardially with 0.1M sodium cacodylate buffer, pH 7.4, followed by the same buffer containing 2% paraformaldehyde and 3% glutaraldehyde. Sciatic nerves were dissected and pinned into a Sylgard-coated dish and fixed overnight in the same fixative. The following day, nerves were washed in cacodylate buffer, trimmed into regions of interest, stained en bloc in 1% osmium tetroxide with 1% ferrocyanide with in cacodylate buffer, washed in water, stained en bloc in 1% uranyl acetate in water, then washed and stored in water. Nerves were dehydrated through graded alcohols, exchanged to acetone, and embedded in Hard Plus Resin 812 (Electron Microscopy Sciences). Thick sections were cut on a Leica Ultracut UCT ultramicrotome and stained with toluidine blue, coverslipped, and imaged.

For immunohistochemical stains at VU as previously described (Sexton et al., 2012; Rodriguez-Feo et al, 2013), rats were deeply anesthetized with ketamine/xylazine and perfused transcardially with PBS. Nerves were pinned into a Sylgard dish with 4% paraformaldehyde overnight, then dehydrated and embedded in paraffin. Immunohistochemical staining was performed using commercial antibodies specifically directed against carbonic anhydrase II (Abcam, Cambridge, MA) to identify viable myelinated sensory axons and choline acetyltransferase (Millipore, Temecula, CA) to identify viable myelinated motor axons. For carbonic anhydrase II marker, heat mediated target retrieval was performed in 1X Target Retrieval Buffer, pH 9.0 (DAKO, Carpenteria, CA). Endogenous peroxidases and non-specific background were blocked by subsequent incubations in 3% H2O2 (Fisher, Suwanee, GA) in TBS-T and serum-free Protein Block (RTU, DAKO). For choline acetyltransferase marker, heat mediated target retrieval was performed in 1X Target Retrieval Buffer (DAKO). Endogenous peroxidases were blocked and non-specific background, secondary, and tertiary labeling of target was accomplished by use of Vector's ABC Elite Goat IgG kit (Vector Laboratories, Burlingame, CA) (Sexton et al., 2012). Visualization was achieved with DAB+ chromogen (DAKO). Slides were counterstained with Mayer's hematoxylin, dehydrated through a series of alcohols and xylenes, and then coverslipped with Acrytol Mounting Media (Surgipath, Richmond, IL).

For light microscopic observations at UT, slides were imaged at 10x or 20x on a Zeiss Axiovert A.1 or 200M with a digital Axiocam. Images for axon counts were montaged in Photoshop and counted in ImageJ. Viable myelinated axons within the sciatic epineural sheath that had an intact, non-collapsed myelin sheath and axoplasm with no dense staining were then counted manually. [Coagulated degenerating axoplasm stains densely.] At VU, all slides were examined using an Olympus Vanox-T AH-2 light microscope (Olympus, Center Valley, PA) interfaced to Pixera Pro 600 HS digital camera (Pixera Corporation; Santa Clara, CA). Digital photos were captured at 10x and 20x using Viewfinder V3.0.1 (Pixera Corporation; Santa Clara CA). For each nerve processed a cross section was photographed proximal to the site of injury, from the allograft, and distally from the sciatic nerves. Axon counts were made manually. For axonal counts, counters used 10x images of sciatic nerve cross sections. Viable myelinated axons within the sciatic epineural sheath that had an intact, non-collapsed myelin sheath and no dense-staining axoplasm were then counted manually in ImageJ (http://imagej.nih.gov/ij/) using the cell counter plugin.

Statistical Tests

We performed all statistical analysis using GraphPad Prism5 for PC (GraphPad Software, San Diego, CA). Comparisons between mean and SE values for SFI scores on a given postoperative day (or between experimental and negative control axon counts at 7 days for pilot data) were made using a two-tailed Student's T-test. For comparison of axonal counts, we also used an ANOVA. All p-values were two-tailed and significance was determined at $p < 0.05$, $p<0.01$, and $p<0.001$, typically indicated in graphs by symbols *, **, and ***, respectively.

Results

Electrophysiological and morphological evidence of rapid restoration of axonal continuity

Our electrophysiological data obtained at both VU and UT for both the main and the pilot study consistently showed that CAPs generated by stimulating the entire intact sciatic nerve in the upper thigh were conducted to the lower thigh in all animals sampled prior to any experimental procedure (Fig. 1A: Pre Injury traces). These CAPs, produced a twitch of the muscles they innervated in the calf and foot. This through-conduction of CAPs was lost after ablating a 0.5-1cm segment in the mid-thigh and was *not* restored by inserting a 0.8 – 1.1cm microsutured donor allograft (Fig. 1A), *unless* that allograft was also PEG-fused (Fig. 1A: PEG Post Repair). Within minutes, such PEG-fusion of both ends of the allograft restored through-conducting CAPs from upper thigh to lower limb, as well as twitching of muscles in the calf and foot. CAP amplitudes after PEG-fusion were typically not as large when compared to CAPs initially recorded from the intact nerve (Fig. 1A, B). CAP amplitudes were 0 mv (CAPs could not be detected) in negative control animals, i.e., if the donor allograft was not PEG-fused. These data suggest that PEG-fusion restored axolemmal continuity to some, but not all, sciatic axons from proximal to distal of the allograft. While PEG-fusion restores electrophysiological continuity to some axons, PEG-fusion almost-certainly does *not* specifically reconnect the distal and proximal portions of sensory with sensory axons and motor with motor axons, much less specific motor or specific sensory axons.

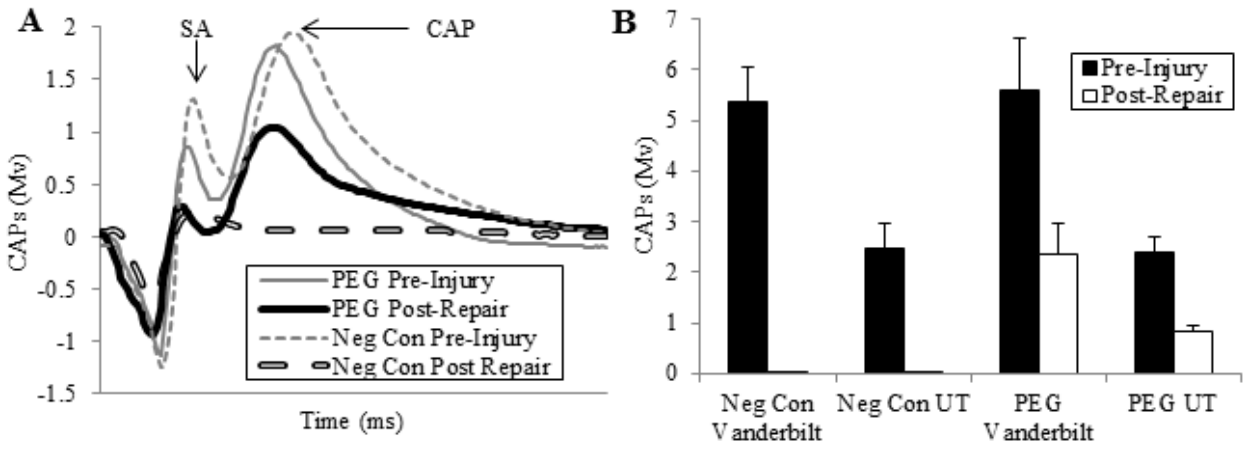

Figure 1. Electrophysiological assessment of sciatic nerve function shortly after allograft repair with and without PEG-fusion.

A. Representative CAP (mV) recordings from a negative control (dashed lines) and a PEG fused (solid lines) allograft pre-injury (thinner lines) and within 5 min after ablation of a 1 cm segment, insertion of a 1 cm donor segment without (negative control: thicker dashed line) or with PEG-fusion (thicker solid line) of both severed ends microsutured to the proximal or distal ends of the host sciatic nerve. SA = arrow points to peak of stimulus artefact. CAP: arrow points to peak amplitude of compound action potential

B. CAPs (mV, mean ± SE) recorded pre-injury and immediately post-repair plotted for 4 groups: Negative controls recorded at VU (n=12), and UT (n=6), PEG-fused at VU (n=13) and UT (n=6).

Our morphological data taken *ex vivo* begun within 2hr and examined 1d after allograft insertion showed that fluorescent dye intracellularly-loaded (Lore et al., 1999; Britt et al., 2010; Bittner et al., 2012; Spaeth et al., 2012) proximal to a microsutured allograft did *not* diffuse across the allograft (Fig. 2A), unless the allograft was also PEG-fused (Fig. 2B). These results were the same for each of 6 negative control and 6 PEG-fused sciatic nerves sampled at UT. These results suggest that PEG-fusion rapidly restores axoplasmic and axolemmal morphological continuity from proximal to distal of the allograft for many sciatic axons.

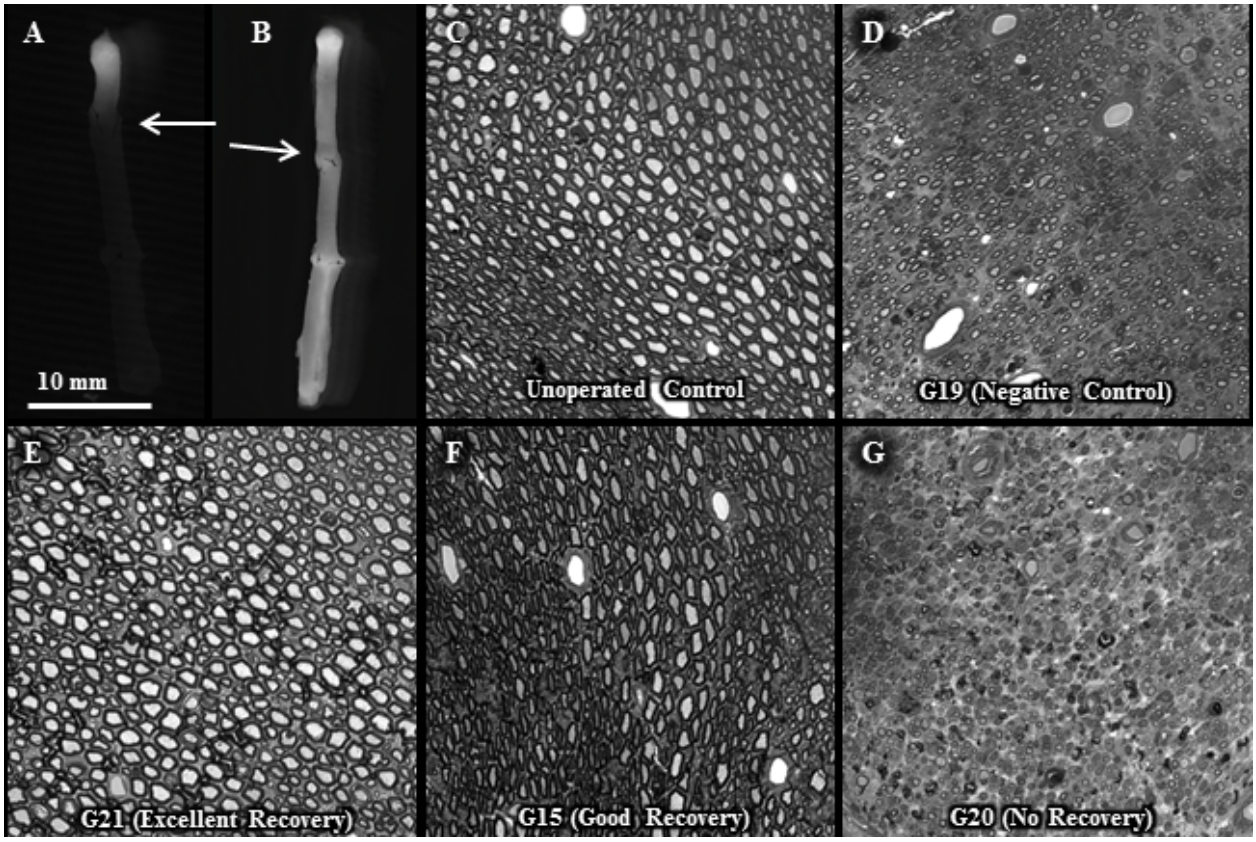

Figure 2. Morphological evidence of myelinated axon viability with and without allograft PEG-fusion 1d or 6w postoperatively

A, B. Intra-axonal dye diffusion of Texas Red at 1d postoperatively in a negative control (**A**) or PEG-fused (**B**) sciatic nerve. Arrow: site of proximal cut end of host sciatic nerve microsutured proximal end of donor sciatic allograft. Note that dye does not diffuse from the proximal segment of the host nerve into the donor allograft in the negative control sciatic nerve, but does diffuse into the allograft in the PEG-fused nerve.

C - G. Viable myelinated axons in toluidine-blue, plastic embedded sections of sciatic nerves viewed at 20x for an un-operated control (**C**) and the mid-allograft region at 6wk postoperatively for a negative control (**D,** animal # G-19) and PEG-fused sciatic nerves showing excellent (**E,** animal G-21), good (**F,** animal G-15) or no (**G,** animal G-20) behavioral recovery at 6wk postoperatively.

SFI-assessed behavioral function rapidly restored

While electrophysiological and morphological measures of restored axonal functions post-severance injury are

important, behavioral measures are the most critical assessments of restored axonal function (Bittner et al, 2000, 2012), because regenerating axonal outgrowths or PEG-fused (repaired) axons may never establish or maintain functional connections. SFI scores at 7 post-operative days for the pilot study at VU were significantly better ($p < 0.05$) for 6 negative control animals (65 ± 8 SE) versus -90 ± 8 SE for six animals with PEG-fused sciatic allografts. SFI measurements for the main study (Fig. 3) at 3d and 1wk at VU and from 3d - 6wk at UT were initially performed on all animals before they received any operative procedure to establish a baseline for each animal; i.e., each animal served as its own control. The baseline SFI scores of individual animals varied from -23 to + 16 with an average of 0.8 for all animals (dotted line in Fig. 3A) and +3.7 for UT animals (dotted line in Fig. 3B). After a sciatic nerve was ablated, the SFI scores for negative control animals varied between -119 and -81 with a mean value of -99.5 ± 3.7SE at 3 days (n=18) and showed no significant trend of recovery or decline 1-6wk post-operatively (Fig. 3A). In contrast, SFI measurements of PEG-fused animals showed significant ($p < 0.05$ to $p< 0.001$) behavioral recovery at 3d and 1wk at both UT (n=6) and VU (n=13). SFI scores for negative control animals at UT and VU did not differ significantly ($p > 0.05$, Student's T-test) from each other. That is, data from both laboratories were very similar (Fig. 3A). Behavioral recovery as measured by the SFI for PEG-fused animals at 1w was not significantly better compared to 3d at UT or VU.

SFI measures of behavioral recovery for most (5/6) PEG-fused animals at UT in the main study dramatically increased by 2 - 3 wk post-operatively and then plateaued through 6wk (Fig. 3A,B). As described in the legend of Figure 3B individual PEG-fused animals were classified as showing excellent (animals G-18, G-21, G-22), good (G-15), poor (G-16) or non-existent (G-21) behavioral recovery as defined by their pattern of SFI scores. The mean SFI's of PEG-fused animals were not significantly different at 2wk compared to 3 - 6wk (Fig. 3A). The mean SFI's for PEG-fused animals at 2 – 6wk were significantly better ($p < 0.05 – p <0.001$) than negative controls for each time point (Fig. 3A). On average, PEG-fused animals recovered about 70% of the SFI behavioral score attained by un-operated animals. The UT data for one PEG-fused animal (G-20) showed no behavioral recovery, possibly because the PEG-fusion procedure was unsuccessful for this animal, consistent with few viable axons observed distal to the proximal severance site (see below). All other (5/6) PEG-fused animals

showed much more SFI behavioral recovery of ~80% to baseline values compared to un-operated animals having little or no recovery, with two PEG-fused animals showing 90-95% recovery. Qualitative visual observations of movements of successfully PEG-fused rats in their cages were often very difficult to distinguish from movements of un-operated rats at 2-6wk postoperatively.

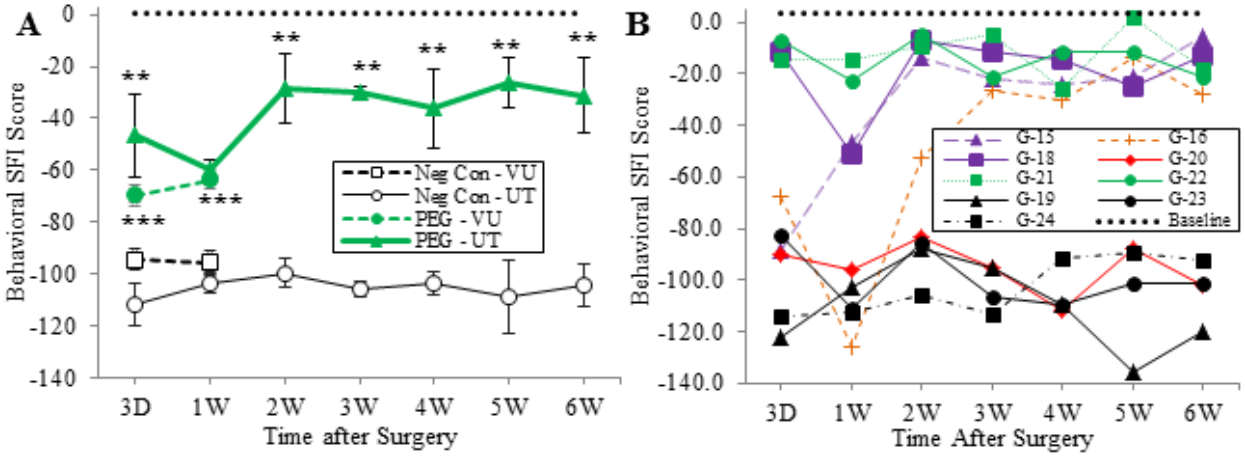

Figure 3. Behavioral assessments of sciatic nerve function with and without allograft PEG-fusion.

A. SFI score (mean ± SE) assessed at 3d to 6wk post-operatively at VU and UT. Groups and symbols as follows; unfilled circle: negative control UT, unfilled square: negative control VU, green filled triangle: PEG fused UT, green filled circle: PEG fused VU. The average baseline SFI value for all UT and VU animals is indicated by a horizontal dotted line. Significance comparisons between PEG-fused versus negative control SFI values at each time point for each data point calculated using Student's T-test (two tailed) indicated by *, **, *** for $p < 0.05$, 0.01, and 0.001 respectively, in this and other figures.

B. SFI data for individual negative control and PEG -fused animals at UT. Negative control animals (G-19, G-23, and G-24) showing no behavioral recovery indicated by black filled symbols. Behavioral recovery during first two weeks for PEG-fused animals were classified as excellent (green symbols: G-21and G-22), good (purple symbols: G-15 and G-18), poor (orange symbols: G-16) or no (red symbols: G-20) behavioral recovery. PEG fused animals classified as excellent showed -30 or better SFI scores at 3d that were maintained for 6wk. PEG-fused animal classified as good showed -30 or better SFI scores at 2 weeks that were maintained for 6wk. The PEG-fused animal classified as poor showed -30 or better SFI scores at 3 weeks that were maintained for 6wk. The PEG-fused animal classified as having no behavioral recovery (animal G-20) showed SFI scores of -80 to -110 from 3d - 6wk with no improvement. These SFI values were within the range of values observed for negative control animals (black filled symbols). The average baseline SFI value for all UT animals is indicated by a horizontal dotted line.

Increased numbers of viable myelinated axons at six weeks after injury

For the main study prior to fixation, nerves were assessed for gross anatomical features using a dissecting microscope at 10-50X. Suture sites on all negative control and most PEG-fused nerves showed some enlargement that was more prominent in negative controls. The sciatic nerve from PEG-fused animal G21 (excellent SFI recovery) was distinguishable from an un-operated nerve only by the presence of sutures. The nerve from PEG-fused animal G20 (no SFI recovery) was the most enlarged at the suture site and throughout the allograft.

For the main study, the morphological status of myelinated sciatic axons at 6wk postoperatively was assessed using several histological techniques. The number of total viable myelinated axons in toluidine-blue, plastic embedded sections viewed at 10x for the mid-allograft region of PEG-fused sciatic nerves with excellent SFI recovery at 6wk postoperatively was less than the number of total viable axons in un-operated sciatic nerves, but more than the negative control sciatic nerves (Figs .2C - G, 4A). The number of viable myelinated axons in animals having PEG-fused sciatic allografts associated with excellent (G-21) or good behavioral recovery (G-15) as measured by the SFI was greater than the number of viable myelinated axons in a PEG-fused sciatic nerve resulting in no behavioral recovery (G-20). In fact, the PEG-fused animal showing no behavioral recovery had fewer surviving axons in the allograft than the negative control animal (Figs .2C - G, 4A). We saw evidence of tissue rejection such as lymphocytic infiltration, tissue destruction, or vessel injury in negative controls or unsuccessful PEG-fusions at 6wk, but not in animals with successful PEG-fusion (Figs. 2C- G).

For the pilot study at VU, the sciatic nerves of three PEG-fused animals and three negative control animals were taken for histological analyses of total axonal number. The number of viable myelinated sciatic axons proximal the allograft (985 ± 61 SE) for the PEG-fused animals was not significantly different ($p = 0.57$ by Student's T-test) from the number for the negative controls (1072 ± 128). As reported for the main study, the PEG-fused animals had more viable axons (634 ± 85 SE) within the allograft compared to the negative controls (331 ± 92; $p = 0.072$). Distal to the allograft, the three animals with PEG-fused sciatic nerves had significantly more ($p = 0.0034$) viable myelinated axons (393 ± 35) compared to the negative control animals (119 ± 27). The total

number of viable myelinated axons always decreased in the allograft compared to the proximal sciatic nerve and always further decreased distal to the allograft, but the decrease was less in all cases for the PEG-fused animal.

For the main study, counts of myelinated sensory axons stained for carbonic anhydrase II in paraffin-embedded cross-sections (Figs. 4B, 5) showed no obvious difference proximal to the allograft in a PEG-fused animal (G-22) exhibiting excellent SFI behavioral recovery compared to counts for a negative control animal (G-23) showing little or no behavioral recovery. As observed for total axon number in the pilot study, the number of viable sensory axons was greater for the allograft and distal cross sections of a PEG-fused sciatic nerve compared to a negative control; the number of sensory axons decreased in the allograft and further decreased distal to the allograft, but the decrease was less in all cases for the PEG-fused animal (Figs. 4B, 5A, C, E). Comparable results were found for counts of motor axons stained for choline acetyltransferase in paraffin-embedded cross-sections for a PEG-fused animal (G-22) compared to its negative control (G-23) (Figs. 4C, 5B, D, F). As shown in Figure 6A, SFI scores of individual animals at 1wk postoperatively (Fig. 3B) had a significant correlation (R^2 >0.995, $p < 0.05$) to their viable axon counts in the allograft made at 6wk postoperatively (Figs. 2, 4A). As shown in Figure 6B, SFI scores averaged for each animal for all postoperative weeks 1-6 (Fig. 3B) had a positive correlation to viable axon counts in the allograft made at 6wk postoperatively (Figs. 2, 4A).

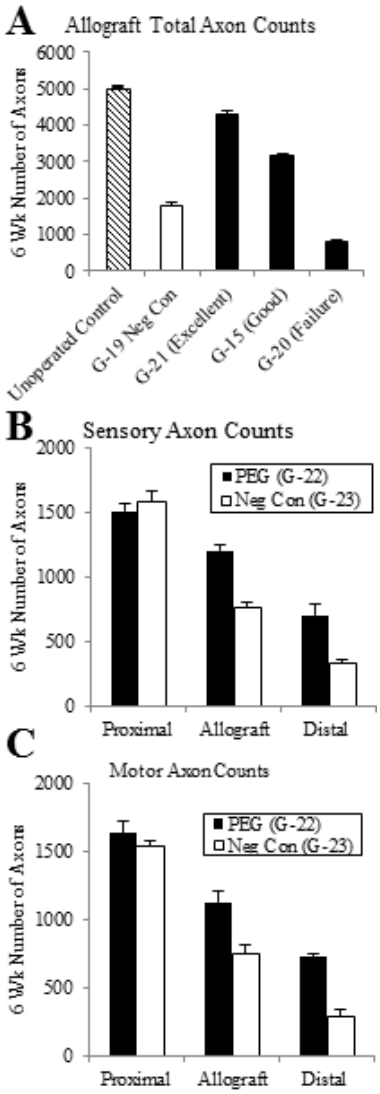

Figure 4. Number of viable myelinated axons with and without allograft PEG-fusion 6w postoperatively.

A. Total viable myelinated axon counts (mean ± SE, n=4) from a representative cross-section of sciatic nerves from the allograft region of un-operated control, negative control, and three PEG-fused allografts showing excellent, good or no SFI behavioral recovery 6wk postoperatively.

B, C. Sensory (**B**) or motor (**C**) viable myelinated axon counts (mean ± SE, n=6) at 6wk post-operatively from a representative cross section from each of proximal, allograft, and distal regions of PEG-fused and negative control animals.

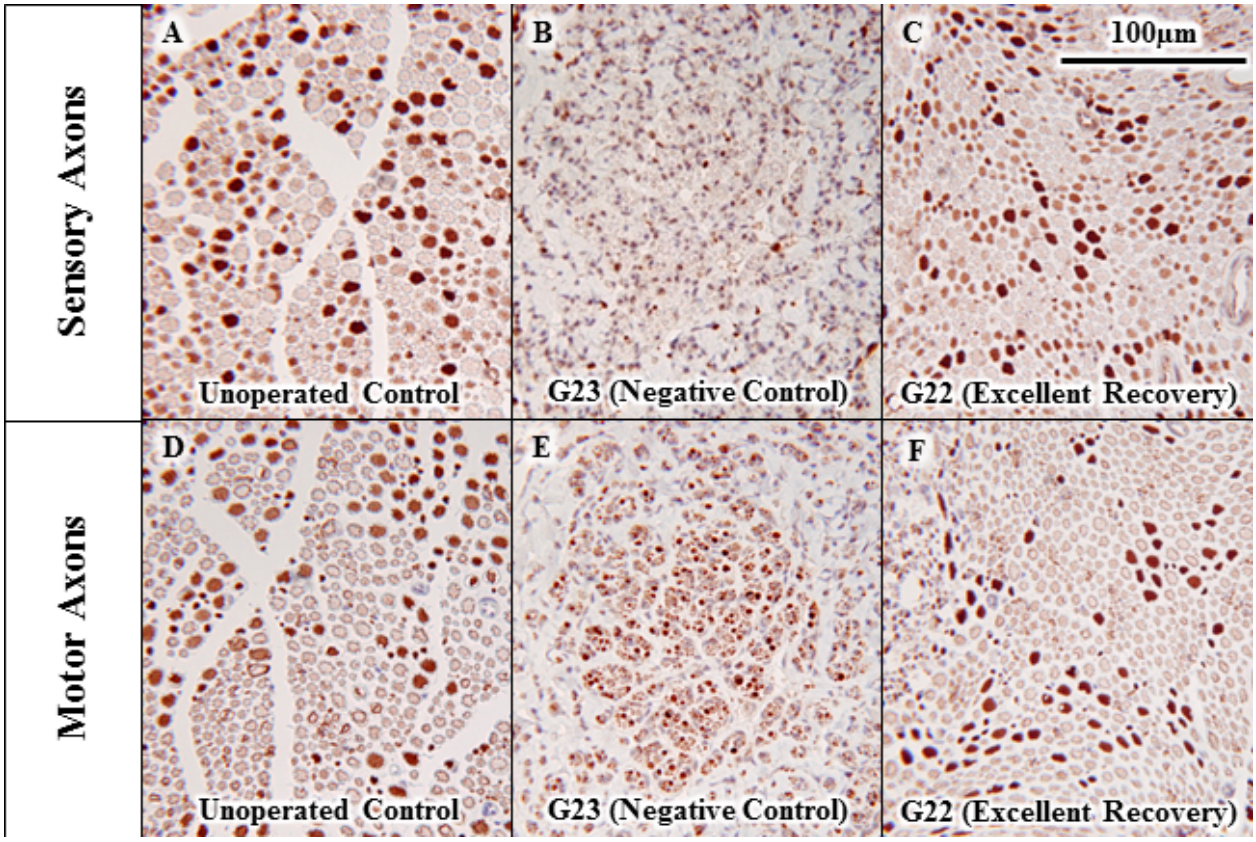

Figure 5. Morphological evidence of myelinated sensory or motor axon viability with and without allograft PEG-fusion 6wk postoperatively

Viable sensory (**A, C, E**) or motor (**B, D, F**) myelinated axons in paraffin-embedded sections of sciatic nerves viewed at 20x stained for carbonic anhydrase II (**A, C, E**) or choline acetyltransferase (**B, D, F**) for an un-operated control (**A, B**) and distal to the allograft 6wk postoperatively for a negative control (**C, D**) and PEG-fused sciatic nerves showing typical (**E, F)** behavioral recovery

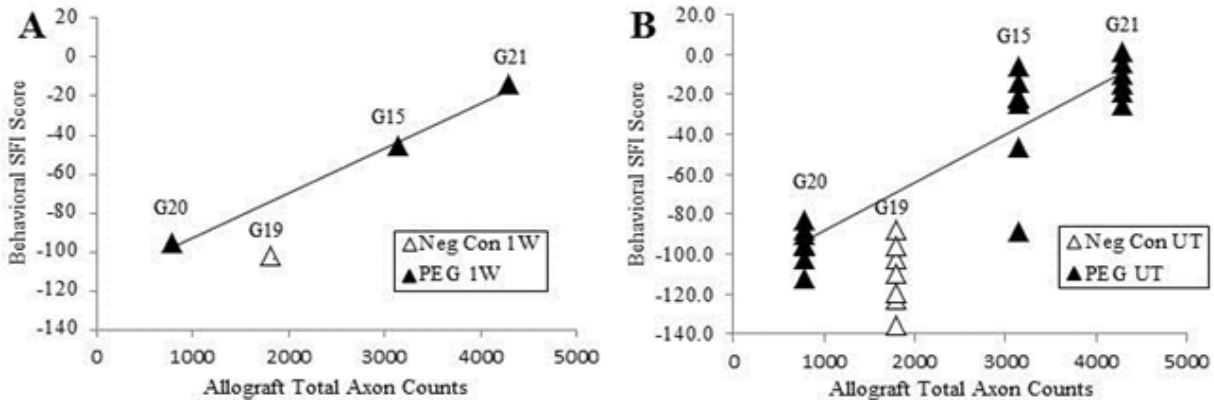

Figure 6. Correlation of behavioral recovery with surviving axons in allografts with and without successful PEG-fusion at UT.

A. SFI scores at 1w for each animal as listed versus number of surviving myelinated axons in allografts at 6wk postoperatively. $R^2 = 0.9946$, $p < 0.05$. G19 = negative control animal not PEG-fused.

B. SFI scores at 1 -6wk individually plotted for each animal as listed versus number of surviving myelinated axons in allografts at 6wk postoperatively.

Discussion

Repair and recovery after clinical repair of peripheral nerve injuries

Peripheral nerve injuries in humans are common and often devastating as they frequently lead to poor recovery of sensory function in the affected extremity. Even worse can be the loss of motor function after proximal injury as axonal outgrowth is slow, and irreversible muscle atrophy often occurs before re-innervation, even with appropriate repair. (Allan, 2000; Campbell, 2008; Williams and Dellon, 2008; Burch, 2011). The cell bodies of PNS nerves lie within the spinal cord or dorsal root ganglion and their axons can extend great lengths (centimeters in rats, meters in humans) to reach their synaptic targets. Transection of these axons leads to distal axonal (Wallerian) degeneration within days (Ramon y Cajal, 1938; Burch, 2011). Functional recovery after nerve injury depends upon slow proximal outgrowth at ~1mm/d, requiring months to years for potentially appropriate re-

innervation to distal-most targets. Since muscles lose the ability to be re-innervated effectively over time, functional recovery has a greatly reduced chance of occurring (Fu and Gordon, 1995). Current clinical nerve repair techniques make no attempt to limit Wallerian degeneration (Burch, 2011; Menorca et al, 2013.

The success of subsequent nerve repair following PNS nerve transection in a human extremity depends on a number of variables such as mechanism of injury, timing of repair, associated muscle, skin, vascular and bone injury, repair technique of the surgeon such as stretching or drying the nerve, postoperative rehabilitation, age of the patient, and patient coping mechanisms (Williams and Dellon, 2008; Farber et al., 2013; Menorca et al., 2013). More-distal nerve injuries have better results than more-proximal injuries, but successful sensory recovery is typically equated only to protective sensation, not full recovery (Bertelli et al., 2009; 2011). The most critical determinants of recovery are distance of the injury site from the target organ, the length of nerve damaged by the injury (defect length or gap), and stretching the nerve during repair. For example, a sharp clean nerve injury with a short nerve defect typically has a better recovery than a severe traction rupture nerve injury that produces a long segment of nerve injury. The outgrowing axons lose their way, or get trapped in scar, preventing proper outgrowth (Menorca et al., 2013). Current strategies use conduits or nerve grafts to bridge nerve gaps (Bertelli et al., 2009, 2011; Farber et al., 2013). These nerve repair strategies often yield poor results and functional recovery can be limited (Bertelli et al., 2009, 2011; Taras et al., 2011; Huag et al., 2013). Nerve autografts have been employed to shorten the effective distance from the re-innervation and/or repair site to the target, but appropriate donor autografts are not always available (Williams and Dellon, 2008: Cho et al., 2012). In brief, current PNS nerve repair techniques often produce very limited functional recovery, especially for more proximal injuries in humans that involve large nerve gaps that cannot be closely apposed without stretching the nerve. For example, the loss of function associated with nerve resection for oncologic purposes can be devastating and prevent limb salvage when tumors involve major peripheral nerves (Campbell, 2008).

Results of PEG-fused sciatic allografts

Our data suggest that PEG-fusion of allograft tissues might greatly reduce many of these problems outlined above and clinically produce nerve recovery within weeks and prevent or retard much Wallerian degeneration. For example, our data reported herein consistently show that action potential (CAP) conduction and dye diffusion in sciatic nerves from upper to lower thigh is much better for PEG-fused that for negative control animals and PEG-fused sciatics are similar to unoperated animals, especially for intraaxonal dye diffusion. are similar to unoperated, intact sciatic axons. Total axon counts in the allograft are higher for PEG-fused animals compared to negative controls at 6wk (main study) and at 1 wk (pilot study), as are counts of sensory and motor axons for the main study for different animals than those used for total axon counts. In brief, the electrophysiological, morphological and behavioral data presented herein are consistent with hypotheses that (**1**) PEG-fusion of allografts rapidly (within minutes) restores electrophysiological, axolemmal, and axoplasmic continuity to many sciatic axons . (**2**) PEG-fusion of allografts maintains the viability of many sciatic axons (motor and sensory) for at least 1hr - 6wk, perhaps permanently, thereby preventing Wallerian degeneration of many of those axons. (**3**) Greater restoration of through-conducting CAPs immediately after PEG-fusion of allografts is associated with greater SFI behavioral recovery at 1wk, but not at 6wk. (**4**) Greater numbers of surviving axons in the allograft are associated with greater SFI behavioral recovery.

Our data from PEG-fused allografts are consistent with previously published data on PEG-fusion of sciatic nerves after a 1mm long crush severance (Britt er al., 2010) or cut-severance (Bittner et al, 2012; Rodriguez-Feo et al., 2013) producing ~ 1mm separation of the cut ends that were then re-apposed by microsutures after which moderate (15 -30 SFI units) but significant SFI-assessed behavioral recovery was noted at 3d – 1wk. Behavioral recovery then greatly increased starting at 2 - 3 wk postoperatively, then plateaus at 4 - 6 postoperative weeks (Britt et al., 2010; Bittner et al, 2012) and is maintained for at least 12 postoperative weeks. PEG-fused autografts also produced moderate but significant behavioral recovery at 1 - 3d (Sexton et al, 2013). The SFI-measured behavioral recovery of 70-80% in two weeks or six weeks for PEG-fused allografts following ablations in calcium-containing salines in the current study is at least as good (in fact, slightly better) than SFI behavioral

recovery at two weeks (40%) or six weeks (50-60%) for PEG-fused sciatic nerves following single cuts or crushes in calcium-free salines. We suspect this enhanced recovery using allografts is due to cleanly re-cutting the cut ends in calcium-free salines and avoiding any stretching of sciatic axons. In any event, our PEG-fusion procedure uses concepts, techniques, and chemical substances that should be readily translatable to clinical procedures.

Morphological data from these previous studies are consistent with the hypothesis that PEG-fusion of cut axonal ends eliminates or retards Wallerian degeneration of some severed axons. In this study,as in a previous study (Sexton et al., 2012), the total number (or number of sensory axons or number of motor axons) of viable myelinated axons in an allograft or autograft is greater for PEG-fused versus negative control animals. The same result holds for the number of viable axons distal to the allograft or autograft.

As described in the Introduction, the cellular/molecular mechanism underlying retardation of Wallerian degeneration and behavioral recovery is rapid fusion-repair of open ends of severed axons produced by a sequence of bioengineered solutions varying in their composition of ionic strength, calcium, PEG, and MB as previously published (Lore et al., 1999; Britt et al., 2010; Bittner et al., 2012; Spaeth et al., 2012; Sexton et al, 2012). However, we do not know how such PEG-fusion mechanisms at the cellular/ molecular level produce such rapid and dramatic behavioral recovery at the systems level. The simplest explanation would be that we are reconnecting appropriate proximal and distal portions of transected sensory and motor axons. However, we recognize that there is no readily-conceivable way that we are selectively reconnecting distal and proximal portions of severed motor or sensory axons, much less individually-identifiable axons, in simple transections, much less for ablations and insertions of donor allografts. For example, we do not know whether (**1**) distal portions of sensory or motor axons are re-specified by the PEG-fused proximal portion; or, (**2**) distal portions of sensory or motor axons re-specify spinal connections made by the PEG-fused proximal segment; or, (**3**) higher CNS sensory or motor centers are highly plastic and can quickly learn how to reuse altered sensory and motor peripheral connections; or (**4**) collateral outgrowths from surviving distal and motor axons rather quickly remake a set of new peripheral connections.

We note that these unanswered questions on behavioral mechanisms at the systems level that are obvious for PEG-fused allografts are also questions that have not been answered (and often not asked) for behavioral recovery by outgrowth from surviving proximal stumps in sciatic and other PNS preparations. That is, unanswered questions for regeneration by outgrowth at the systems level include how many (if any) outgrowing motor axons reinnervate their original muscle fibers, grow down sensory sheaths, the relative importance of collateral sprouting vs spinal or brain plasticities. However, we do attempt to maintain proximal and anatomic orientation during the procedure and we suspect that functional axonal groups/fascicles are typically aligned leading to our observed functional outcomes.

Significance and implications of our data

Whatever the systems-level mechanisms responsible for the behavioral recovery, our data show that PEG-fusion of allografts following ablation of sciatic nerve segments can produce rapid, dramatic, and long-lasting recovery of sciatic nerve function. On a few animals (data not shown), we have also observed that sciatic allografts can be stored for several days at 7ºC and then successfully PEG-fused as measured by CAP through-conduction. These data are consistent with previous findings that Wallerian degeneration of the distal portions of cut-severed sciatic or tail nerves in rats can be retarded for 5 - 7d *in vivo* by cooling the body part to 13 - 25ºC or by cyclosporine injections (Sea et al., 1995; Sunio and Bittner, 1997). Furthermore, rat sciatic or spinal axons can be maintained *ex vivo* for 5 - 7d by cooling to 6-9º C and then successfully PEG-fused (Marzullo et al, 2001). We do not know why non-processed allografts that are successfully PEG-fused as measured by SFI behavioral recovery show no obvious evidence of tissue rejection by six weeks. It is possible that fused cell membranes share MHC I molecules and thus down regulate host recognition of allografted sciatic nerves. We have not yet carefully examined this issue.

Consideration of all these data suggest that a well-specified use of microsutures, allografts, and PEG-fusion

procedures might produce a paradigm shift in the clinical treatment of traumatic injuries to peripheral nerves for which the gold-standard for simple cuts has been microsuturing the severed ends (Allan, 2000; Campbell, 2008; Williams and Dellon, 2008; Menorca et al., 2013). The ability to PEG- fuse severed axons in allografts to restore behavioral deficits within weeks after ablation of long segments of major peripheral nerves might dramatically alter functional outcomes for patients with mutilated extremity injuries and potentially even change the types of injuries for which salvage is attempted after extensive traumatic injury or oncologic resection. It is perhaps even reasonable to consider the future establishment of tissue banks for peripheral nerve allografts. Finally, since the loss of function following traumatic injury to spinal cords is primarily due to loss of axonal continuity within spinal white matter (Bittner at al., 2000), it might even be possible that PEG-fusion, perhaps combined with peripheral or spinal nerve allografts, would restore behavioral function lost after spinal injury much better than any currently-used procedure.

References

1. Allan CH. 2000. Functional results of primary nerve repair. Hand Clinics. 16:67-71.

2. Bertelli JA, Ghizoni MF. 2009. Results of c5 root grafting to the musculocutaneous nerve using pedicled, vascularized ulnar nerve grafts. J. Hand Surg. 34A:1821–1826 2009.

3. Bertelli JA, Ghizoni MF. 2011. Very distal sensory nerve transfers in high median nerve lesions. J. Hand Surg. 36A:387–393.

4. Birch R, Bonney G, Wynn-Parry CB. 1998. Clinical aspects of nerve injury. Surgical Disorders of the Peripheral Nerves. 2:71-87.

5. Bittner GD, Keating CP, Kane JR, Britt JM, Spaeth CS, Fan JD, Zuzek A, Wilcott RW, Thayer WP,

Winograd JM, Gonzalez-Lima F, Schallert T. 2012. Rapid, effective and long-lasting behavioral recovery produced by microsutures, methylene blue and polyethlene glycol after complete cut of rat sciatic nerves. J Neurosci Res. 90:967-980.

6. Bittner GD, Schallert T, Peduzzi JD. 2000. Degeneration, trophic interactions, and repair of severed axons. The Neuroscientist 6:88-109.

7. Britt JM, Kane JR, Spaeth CS, Zuzek A, Robinson GL, Gbanaglo MY, Estler CJ, Boydston EA, Schallert T, Bittner GD. 2010. Polyethylene glycol rapidly restores axonal integrity and improves the rate of motor behavior recovery after sciatic nerve crush injury. J Neurophysiol. 104:695-703.

8. Burch R. 2011. Nerve repair. Green operative hand surgery. Elsevier Churchill Livingstone. 6:1035-107.

9. Campbell WW. 2008. Evaluation and management of peripheral nerve repair. Clinical Neurophys 119:1951–1965.

10. Cho MS, Rinker BD, Weber RV, Chao JD, Ignari JV, Brooks D, Buncke GM. 2012. Functional outcome following nerve repair in the upper extremity using processed nerve allografts. J Hand Surg. 37A:2340–2349.

11. Farber SJ, Glaus SW, Moore AM, Hunter DA, Mackinnon SE, Johnson PJ. 2013. Supercharge nerve transfer to enhance motor recovery: a laboratory study. J Hand Surg. 38A:466–477.

12. Fu SY, Gordon T. 1995. Contributing factors to poor functional recovery after delayed nerve repair: prolonged denervation. J Neurosci. 15:3886-3895.

13. Haug A, Bartels A, Kotas J, Kunesch E. 2013. Sensory recovery 1 year after bridging digital nerve defects with collagen tubes. J Hand Surg. 38A:90–97.

14. Hoy RR, .Bittner GD, Kennedy D. 1967. Regeneration in Crustacean Motorneurons: Evidence for

Axonal Fusion. *Science.* 156, 251-252.

15. Krause TL, Bittner GD. 1990. Rapid Mophological Fusion of Severed Myelinated Axons by Polyethylene Glycol. *PNAS*. 87, 1471-1475.

16. Krause TL, Fishman HM, Ballinger ML, Bittner GD. 1994. Extent and Mechanism of Sealing in Transected Giant Axons of Squid and Earthworms. *J. Neurosci*. 14, 6638-6651.

17. Lore AB, Hubbell JA, Bobb Jr. DS, Ballinger ML, Loftin KL, Smith JW, Smyers ME, Garcia HD, Bittner GD. 1999. Rapid induction of functional and morphological continuity between severed ends of mammalian or earthworm myelinated axons. J Neurosci. 19:2442–2454.

18. Marzullo TC, Britt JS, Stavisky R, Bittner GD. 2001. Cooling enhances in vitro survival and fusion repair of severed axons taken from the peripheral and central nervous system of rats. Neuroscience Letters. 327:9-12.

19. Medinaceli L, Freed WJ, Wyatt RJ. 1982. An index of the functional condition of rat sciatic nerve based on measurements made from walking tracks. Exp Neurol. 77:634-643.

20. Menorca R, Fussell TS, Elfar JC. 2013. Nerve physiology: mechanisms of injury and recovery. Hand Clin. 29:317-330.

21. Ramon y Cajal S. 1928. Degeneration and regeneration of the nervous system. Translated May RM (Oxford University Press). London.

22. Rodriguez-Feo CL, Sexton KW, Boyer RB, Pollins AC, Cardwell NL, Nanney LB, Shack RB, Mikesh MA, McGill CH, Driscoll CW, Bittner GD, Thayer WP. 2013. Blocking the P2X7 receptor improves outcomes after axonal fusion. J. Surgical. Res. 184:705-13.

23. Sea T, Ballinger ML, Bittner GD. 1995. Cooling of peripheral myelinated axons retards Wallerian degeneration. J Neurophys. 133:85-95.

24. Sexton KW, Pollins AC, Cardwell NL, Del Corral GA, Bittner GD, Shack RB, Nanney LB, Thayer WP. 2012. Hydrophilic polymers enhance early functional outcomes after nerve autografting. J. Surgical Res. 177:392-400.

25. Spaeth CS, Boydston EA, Figard LA, Zuzek A, Bittner GD. 2010. A Model for Sealing Plasmalemmal Damage in Neurons and Other Eukaryotic Cells. *J. Neurosci*. 30, 15790-15800.

26. Spaeth CS, Robinson T, Fan JD, Bittner GD. 2012. Cellular mechanisms of plasmalemmal sealing and axonal repair by polyethylene glycol and methylene blue. J Neursosci Res. 90:955-966.

27. Steinhardt RA, Bi G, Alderton JM. Cell Membrane Resealing by a Vesicular Mechanism Similar to Neurotransmitter Release. *Science*. 263, 390-393 (1994).

28. Sunio A, Bittner GD. 1997. Cyclosporin A retards the Wallerian degeneration of peripheral mammalian axons. Exp. Neurol. 146:46-56.

29. Taras JS, Jacoby SM, Lincoski CJ. 2011. Reconstruction of digital nerves with collagen conduits. J.Hand Surg. 36A:1441–1446.

30. Williams EH, Dellon AL. 2008. Upper extremity nerve repair tips and techniques: a master skills publication. ASSH. 75-88.